EXPERIMENTAL INVESTIGATION OF A SPHERICAL SOLAR COLLECTOR

A THESIS SUBMITTED TO
THE GRADUATE SCHOOL OF NATURAL AND APPLIED SCIENCES
OF
MIDDLE EAST TECHNICAL UNIVERSITY

BY

ÖZTEKİN BAKIR

IN PARTIAL FULFILLMENT OF THE REQUIREMENTS
FOR
THE DEGREE OF MASTER OF SCIENCE
IN
MECHANICAL ENGINEERING

APRIL 2006

Approval of the Graduate School of Natural and Applied Sciences

_____

Prof. Dr. Canan ÖZGEN
Director

I certify that this thesis satisfies all the requirements as a thesis for the degree of Master of Science.

_____

Prof. Dr. S. Kemal İDER
Head of Department

This is to certify that we have read this thesis and that in our opinion it is fully adequate, in scope and quality, as a thesis for the degree of Master of Science

_____

Assoc. Prof. Dr. Cemil YAMALI
Supervisor

Examining Committee Members

Prof. Dr. Kahraman Albayrak	(METU, ME)	_____
Assoc. Prof. Dr. Cemil Yamalı	(METU, ME)	_____
Asst. Prof. Dr. Abdullah Ulaş	(METU, ME)	_____
Asst. Prof. Dr. Derek Baker	(METU, ME)	_____
Prof. Dr. Ö. Ercan Ataer	(Gazi Unv., ME)	_____

I hereby declare that all information in this document has been obtained and presented in accordance with academic rules and ethical conduct. I also declare that, as required by these rules and conduct, I have fully cited and referenced all material and results that are not original to this work.

Öztekin Bakır

ABSTRACT

EXPERIMENTAL INVESTIGATION OF
A SPHERICAL SOLAR COLLECTOR

Bakır, Öztekin
M.S., Department of Mechanical Engineering
Supervisor: Assoc. Prof. Dr. Cemil Yamalı

April 2006, 174 pages

The purpose of this study is to investigate the performance of a spherical solar collector by using numerical and experimental methods. For this analysis, equations were obtained by choosing appropriate control volumes in the system and applying The First Law of Thermodynamics.

The experiments were realized at four different mass flow rates and non-flow situation. For the numerical simulation of the system, a computer program in Mathcad was written. Another computer program in Mathcad was written for the variation of the absorbed solar radiation through out the day.

Finally, the performance of the spherical solar collector is compared theoretically to that of flat plate solar collectors.

Keywords: Solar Collector, Solar Water Heater, Solar Energy

ÖZ

KÜRESEL BİR GÜNEŞ KOLLEKTÖRÜNÜN
DENEYSEL OLARAK İNCELENMESİ

Bakır, Öztekin
Y.Lisans, Makine Mühendisliği Bölümü
Tez Yöneticisi: Doç. Dr. Cemil Yamalı

Nisan 2006, 174 sayfa

Bu çalışmanın amacı, sayısal ve deneysel metotlar kullanarak küresel bir güneş kollektörünün performansını incelemektir. Bu analiz için, sistemde uygun kontrol hacimleri seçerek ve Termodinamiğin Birinci Kanunu'nu uygulayarak eşitlikler elde edilmiştir.

Deneyler 4 kütlesel debide ve akışın olmadığı durum için gerçekleştirilmiştir. Sistemin sayısal simülasyonu için Mathcad'de bir bilgisayar programı yazılmıştır. Absorbe edilen güneş radyasyonunun gün boyunca değişimi için Mathcad'de bir diğer bilgisayar programı yazılmıştır.

Küresel güneş kolektörünün performansı teorik olarak düz kolektörlerinki ile karşılaştırılmıştır.

Anahtar Kelimeler: Güneş Kollektörü, Güneşli Su Isıtıcı, Güneş Enerjisi

To my parents,

who always support me in all aspects of my life

ACKNOWLEDGEMENTS

I would like to thank my supervisor, Assoc. Prof. Dr. Cemil YAMALI for his guidance, support and valuable contribution throughout this study.

I would also like to thank Asst. Prof. Dr. Derek BAKER for his suggestions and comments.

I offer sincere appreciation to my family for their encouragements throughout my education life.

TABLE OF CONTENTS

LIST OF TABLES

TABLES

LIST OF FIGURES

FIGURES

LIST OF SYMBOLS

A	Area, m^2
A_1	Hemispherical absorber surface area, m^2
A_{eff}	Projection area of the hemispherical surface A_1, m^2
A_T	Total surface area of the spherical solar collector, m^2
$c_{p,w}$	Specific heat of water, J/kg^0C
E	Total energy, kJ
F'	Collector efficiency factor
F_R	Heat removal factor
G_0	Extraterrestrial radiation on a horizontal surface, W/m^2
G_{0n}	Extraterrestrial solar radiation at normal incidence, W/m^2
G_{sc}	The solar constant, W/m^2
h	Convection coefficient, $W/m^2\,{}^0C$
H	Enthalpy, kJ
H_0	Daily extraterrestrial radiation on a horizontal surface, J/m^2
I	Total radiation on a horizontal surface for an hour period, J/m^2
I_0	Hourly extraterrestrial radiation on a horizontal surface, J/m^2
I_b	Beam solar radiation on a horizontal surface for an hour period, J/m^2
I_d	Diffuse solar radiation for an hour period, J/m^2
I_T	Total solar radiation on a sloped surface for an hour period, J/m^2
G_b	Beam solar radiation on a horizontal surface, W/m^2
G_d	Diffuse solar radiation, W/m^2
G_T	Total solar radiation on a sloped surface, W/m^2
G_{Ths}	Total solar radiation on a horizontal plane, W/m^2

G_{Tsph}	Total solar radiation incident on the spherical solar collector per unit surface area, W/m^2
k	Thermal conductivity, $W/m\,^0C$
K	Extinction coefficient, m^{-1}
k_T	Hourly clearness index
K_T	Daily clearness index
$\overline{K}_T$	Monthly average clearness index
L	Longitude
m	Air mass
m_{tank}	Mass of water stored in the tank, kg
$\dot{m}$	Mass flow rate through the collector, kg/s
N	Number of daylight hours
Q	Total amount heat transfer, kJ
Q_u	Useful energy collected by the solar collector, W/m^2
R	Geometric factor for total solar radiation
R_b	Geometric factor for beam solar radiation
R_c	Radius of the spherical cover, m
R_p	Radius of the spherical absorber, m
$\dot{S}$	Solar radiation absorbed by the spherical solar collector per unit surface area, W/m^2
T_a	Ambient temperature, ^0C
$T_{c,i}$, T_{in}	Water temperature at collector inlet, ^0C
$T_{c,o}$, T_{out}	Water temperature at collector outlet, ^0C
T_f	Mean water temperature within the spherical collector, ^0C
T_p	Absorber temperature, ^0C
U	Internal energy, kJ
U_L	Overall heat loss coefficient, $W/m^2\,^0C$
V	Volume, m^3

V_T	Storage volume of the spherical solar collector, m^3
α	Absorptance
α_n	Absorptance at normal incidence
α_s	Solar altitude angle
β	Slope
γ	Surface azimuth angle
γ_s	Solar azimuth angle
δ	Declination
δ_p	Thickness of the absorber, m
δ_c	Thickness of the cover, m
η	Efficiency
θ	Angle of incidence
θ_z	Zenith angle
ρ_g	Diffuse reflectance of the ground
ρ_w	Density of water, kg/m^3
τ	Transmittance
ϕ	Latitude
ω	Hour angle

CHAPTER 1

INTRODUCTION

Solar energy is energy that comes from the sun. The sun generates energy in its core in a process called nuclear fusion. During a nuclear fusion, four hydrogen nuclei fuse to become one helium atom. The helium atom weighs less than the four nuclei that combined to form it. Energy equivalent of this mass defect is emitted into space. A small part of the solar radiation reaches the earth.

Today, solar energy is used in many areas such as heating water for domestic use, space heating of buildings, lumber drying, agricultural products drying, cooking, electricity production and water distillation. Heating water for domestic use is the most economical way of solar energy utilization.

There are three advantages of solar energy. First of all, it is free. We do not pay for this energy. Secondly, it is clean. It does not create pollution. It does not produce harmful waste products to the environment. Third, it is renewable. The sun will keep making energy for millions of years.

Basically, solar energy is converted into heat using solar collectors and converted into electricity using solar cells. In solar collectors, a fluid is heated using solar energy. According to the type of the fluid used, solar collectors can be also named as solar water heater or solar air heater.

We can divide solar water heaters into two categories according to water storage structure of the heaters :

a) Solar water heaters which have collection and storage in separate units.

b) Solar water heaters which have collection and storage in a single unit. (Built-in-storage)

Built-in-storage solar water heaters are an alternative to conventional solar water heaters which have a separate storage tank. Combining the collector and the storage tank into one unit has following advantages:

a) Better heat transfer since there are no pipes, no fin, and no bonding resistance.

b) Lower flow resistance.

c) Simplified construction.

On the other hand, built-in-storage solar water heaters suffer big energy losses at night or at low radiation periods due to the absence of a separate fully insulated storage tank. This loss of energy can be minimized by some techniques. One of them is to use two covers instead of one. The second is use of an insulation cover during the night hours. The third one is use of a transparent insulation between the absorber and the cover. The fourth method employs an insulating baffle plate inside the storage tank such that this plate divides the depth of the tank in a certain ratio. During the night hours, this baffle plate protects the water in the lower column of the tank from the cold sky. The fifth method uses a phase changing material (PCM) within the tank. During the sunshine hours, the stored water transfers an amount of its heat to the PCM. The PCM collects this energy in the form of latent heat and melts. During off-sunshine hours, on the contrary, the PCM gives its energy to the water and changes its phase from liquid to solid.

Several experimental and theoretical studies have been made about rectangular, triangular and trapezoidal shaped built-in-storage solar

collectors. As far as the author's knowledge is concerned, there is only one limited study for a spherical solar collector in literature.

In this study, performance of a stationary spherical solar collector with built-in-storage water heater was investigated experimentally. In addition, a numerical model was developed for transient simulation of the system and performance of the system was compared with that of flat plate solar collectors.

The main advantage of the system is that there is no need for a special orientation and any tracking mechanism for this collector to receive maximum solar energy. Because of its spherical shape, all orientations have the same effect. Furthermore, its spherical shape provides low resistance to wind.

CHAPTER 2

REVIEW OF PREVIOUS STUDIES

It is seen in the literature that adequacy of built-in-storage solar water heaters have been investigated under various conditions and some improvement studies have been made by studying the factors affecting the performance of the system. Some of the studies based on experimental and theoretical approaches are mentioned briefly below.

Chinnappa and Gnanalingam [1] tested a solar water heater combining collection and storage in Ceylon. The heater consisted of a square coil of 3 in diameter pipe, 13.5 m (44.3 ft) in length, in a wooden box with heat insulation at the bottom and two glass covers. The water heater was connected directly to the mains. The tests were made under two modes of operation. In the first mode warm water was drawn off as soon as the temperature reached 49°C (120 ^{0}F). Warm water was drawn off until all the warm water was replaced by a fresh charge of cold water, and the number of such draw-offs noted. In the second mode no water was drawn off until the water reached the highest possible temperature. The authors found that If water is drawn off whenever the water reaches 49°C (120 ^{0}F), it is possible to obtain 114-189 L (30-50 gal) of water a day, the first draw-off being made about noon. The efficiency of collection based on the exposed glass area on top of the box was around 46 percent. An equation for the performance of the heater over the day was devised and this was applied by means of a computer program to solar radiation data for the whole year. The results showed that no heat could be collected for less then 10 percent of the year. The total energy collection for the year was about 1250 kWh. Another computer program compared the

performance of the heaters made up of 2, 2½, 3, 3½ and 4 in diameter pipes respectively. This study indicated that a heater of 2½ to 3½ in diameter pipe obtains the best performance.

Garg [2] designed and tested a built-in storage type solar water heater with a capacity of 90 L. It consisted of a rectangular, 20 gauge galvanized iron tank measuring 112x80x10 cm. This tank was contained in a mild steel sheet box with 5 cm layer of fiber glass insulation below it and one glass cover on the top. The hot water was taken from the heater outlet pipe at the top. The heater was inclined at 43^0 from the horizontal and was oriented due south to collect maximum solar radiation during the winter season at Jodhpur. The solar water heater was filled daily at 8:00am with fresh water. For one complete year the storage water temperature was noted. He found that in winter months (December, January and February) hot water from 50 to 60^0C can be obtained, and in summer and monsoon months (except on few rainy days) hot water from 50 to 75^0C can be obtained. In order to asses the performance or efficiency of the heater, He devised a testing program in which a number of practical domestic conditions were simulated by drawing off various quantities of water at different times during the day. He observed that maximum efficiency is obtained if the water is drawn off at short intervals without allowing the temperature of the water to raise much in excess of the outdoor air temperature, i.e. heat losses are restricted to a minimum. His second observation is the night cooling problem in the system. Because of the night cooling the heater could not be provide hot water in the early mornings. He reduced heat losses by two alternative ways. First was covering the heater with an insulation material over the night, and the second was storing hot water in an insulated tank. For optimum performance the gap depth was found as 10 cm.

Chauhan and Kadambi [3] studied a collector/storage type of solar water heater with a capacity of 70 L. The unit was enclosed in a wooden box with 1.5 m^2 blackened plate area, 10 cm thick glass wool insulation at the bottom and one glass cover at the top. Experiments were carried out under

four different modes of operation. In the first mode, the water in the collector was circulated with a small pump and allowed to reach the highest possible temperature. In the second mode, the heater was filled with water in the morning and allowed to reach the highest possible temperature under natural convection conditions. In the third mode, the water was drawn off as soon as the temperature reached 50-60 ^{0}C. Then a fresh charge of water was introduced. In the fourth mode, tests made for continuous flow of water throughout the day with flow rates of 38, 60 and 75.9 kg/h. No appreciable difference in the efficiency was observed under the first two modes of testing. The day-long collection efficiency under the first two modes was ascertained to be around 50-53 percent for a rise in water temperature of 50-57 ^{0}C. The average collection efficiency under the third mode of testing was found to be 64.8 percent with 202.6 l of water heated from 38.5 to 58 ^{0}C. In the tests for continuous flow of water, maximum collection efficiency of 71.8 percent was achieved with a flow rate of 75.9 kg/h.

A study similar to that of Garg was made by Sodha, Nayak, Kaushik, Sabberwal and Malik [4]. In this study, a rectangular, 18 gauge galvanized iron tank was encased in a wooden box (122x90x20 cm). A layer of glass wool insulation of 5 cm thickness was used between the walls of the tank and the wooden box. The top blackened surface of the tank was covered by a common window glass piece (122 x 90 cm, 3 mm thick) at a distance of 4 cm. The heater was kept inclined at the optimum angle and was oriented due south to collect maximum solar radiation during May at New Delhi. It was filled with water at about 8:30 a.m. and the unit was left exposed to solar radiation. The change of temperature of water and the shade-ambient air temperature was measured at hourly intervals. The intensity of solar radiation on the glazing was calculated from the solar irradiation data. When the solar intensity was significantly diminished, the top glass was covered by a 5 cm layer of insulation. Also, they made an improved numerical analysis for the variation of water temperature using the parameters of their experiment as well as those corresponding to Garg's experiment. As a conclusion, their

numerical results showed same behavior with those of Garg's, but their results were in much better agreement with both the experimental studies.

Sodha, Bansal and Kaushik [5] presented a simple transient thermal model, which includes solutions for off-sunshine hours, for predicting the time dependence of water temperature for the cases non withdrawal of hot water and withdrawal of hot water at constant flow rate. The results of this model were compared with earlier models as well as experimental observations. For certain applications, it is desirable to extract hot water at constant temperature. For this case one has to vary the flow rate hour to hour. The authors concluded that the required variability is less for higher temperatures than for lower ones. Subsequent calculations were made for arbitrary demand pattern characteristics of industrial applications and rural hospitals of India. In a later study [6], similar investigations were made for generalized demand patterns.

Garg and Rani [7] investigated night cooling drawback of built-in-storage solar water heater. They made studies by covering the collector system by an insulation cover during cooling hours and also by using an insulated baffle plate inside the tank adjacent to the absorber plate. It was observed that by using the insulation cover, the collector performance can be improved by 70 percent. Use of baffle plate improved the performance during day as well as night time.

Use of a baffle plate inside built-in-storage water heater was also investigated by Tiwari and Dhiman [8], and its significance was emphasized in this study.

Sokolov and Vaxman [9] made a comparative study in which a rectangular shaped tank and a triangular shaped tank were investigated. Although both systems showed similar efficiencies, temperature gradient in the rectangular system was larger in the experiments. Also in this article, the

authors suggested that to prevent energy losses during periods of insufficient radiation the entrance and/or exit of the absorbing channel should be closed by means of valves.

Vaxman and Sokolov [10] also made a detailed experimental analysis of a system including baffle plate. In this study it was seen that in periods of no radiation a reverse flow region is developed, resulting in increased heat loss. To prevent this, use of nonreturning valves in the system was suggested.

In a later study, Mohamad [11] investigated a system contained a thermal diode to prevent reverse circulation at night-time. Thus, heat losses were significantly reduced at night-time. It was observed that a thermal diode provides an increase of 10% in the storage tank efficiency.

Prakash, Garg and Datta [12] investigated the performance of a built-in-storage type water heater containing a layer of PCM-filled capsules at the bottom. Main idea of this study was to keep the temperature difference between the water and the surroundings as low as possible at off-sunshine hours. The heater consisted of a rectangular galvanized iron tank of 9 cm depth and 1 m^2 exposed surface area. The top surface of the tank was coated with ordinary black paint. A glass cover 3 mm thick was placed over the black surface of the tank with an air gap of 2.5 cm. The whole system was fixed at an angle of 45^0 to the horizontal and faced south to collect maximum solar radiations in Delhi. Paraffin wax was selected as the PCM (Phase Changing Material). The bottom and the sides of the heater were insulated with a 5 cm thick layer of fiber-glass insulation. In this study temperatures during the day were higher for the conventional water heater, but the temperatures after 22:00 were about the same for all the three designs of water heaters. The authors concluded that the PCM layered system is not recommended for day-time hot water requirements, but more suitable for hot water requirements during off-sunshine hours. Also, effect of

the PCM was compared with that of night insulation and it was seen that PCM storage without night insulation is almost as effective as conventional built-in-storage type water heaters with night insulation.

A built-in-storage type water heater with same construction (without PCM) also analysed by Prakash, Garg and Hrishikesan [13] in a later study. Aim of this study was to determine effect of tracking on the performance. At the end of the calculations the authors concluded that the performance of the system could be improved by employing a tracking device so as to follow the direction of the sun. But in this analysis, double axis tracking did not improve the performance of the system substantially more than the single axis tracking.

Another study for the same construction was made to determine effect of transparent insulation [14]. In this study, the air gap between the plate and the glazing is replaced by a transparent insulation of honeycomb (hexagonal PS) structure of 4.3 cm thickness. As a result, the storage potential of the water heater was observed to be higher than that of a system with movable insulation.

Muneer [15] investigated experimentally the effect of storage volume / collector area ratio, number of glazing and mode of operation on the heaters performance. The work involved the construction of three box type built-in-storage water heaters, two of which had depths of 8 cm and the third heater having a depth of 6 cm. A galvanized steel sheet of 2 mm thickness painted with ordinary blackboard paint was used as the absorber plate. The dimensions were 144 x 72 cm, resulting in an absorber area of approximately 1 m^2. The storage tank was wrapped with 10 cm of fiber glass wool insulation on all sides and bottom. Each heater was mounted to face south at an angle of 30^0 to the horizontal. The capacity of the 8 cm depth heater was 80 l, while that of the 6 cm depth heater was 60 l. The three heaters were operated side-by-side during the period August-December. The heaters were filled with

water at 8:00 in the morning, and emptied at 16:00 in the evening. The effect of depth of storage tank on the performance was studied by making side-by-side tests on the 6 cm and 8 cm heaters. The maximum and minimum temperatures recorded for the 6 cm heater were 76 and 46^{0}C, respectively. The maximum average daily efficiencies of the 6 cm and 8 cm heaters were 65 and 73 percent, respectively. The study of stratification on the two heaters showed no significant influence of the depth. The effect of the number of glass covers on the performance was studied by making side-by-side tests on two heaters, both of 80 l capacity, one of which had a singe glass cover of thickness 3 mm and the other with two glass covers of the same thickness. The double-glazed heater performed better with a difference of 1-10^{0}C in water temperature. To see effect of mode of operation on two heaters of 80 l capacity, he devised a testing program in which a number of practical domestic conditions were simulated by drawing off various quantities of water at different times during the day. The results showed that best performance could be obtained by drawing of all heated water into a separate storage as soon as it reached a pre-set temperature level (in this study 35^{0}C).

Ecevit, Al-Shariah and Apaydın [16] proposed a triangular built-in-storage solar water heater for improving the performance by natural convection, leading to better heat transfer between the absorbing surface and the water stored in the heater.

Kaushik, Kumar, Garg and Prakash [17] presented a mathematical model for a triangular built-in-storage type solar water heater. In this analysis, the performance of the system was found to be better than that of a rectangular built-in-storage water heater under various operating conditions. Also, effect of angle of inclination on water temperature was investigated for 11.5^0, 30^0, 45^0 and 60^0. It was observed that the water temperature was higher at 45^0.

In a later study [18], the authors analysed a triangular built-in-storage type solar water heater with transparent insulation on the top and sides. Performance of the system with transparent insulation was compared with a conventional water heater with movable insulation. Consequently, effect of the transparent insulation was found to be better.

Kaptan [19] made theoretical and experimental investigations for a built-in-storage type solar water heater of 87 l capacity. The solar water heater which performs the dual function of absorbing and storing hot water was made of 5 pipes. A baffle plate was placed inside each pipe. The experiments were performed during 4 hours inside a laboratory using an artificial sun consisting of 27 lamps of 250W each. At the end of the 4 hours, the efficiency was found as 55%.

Cruz, Hammond and Reis [20] proposed a simple, low-cost solar water heater for the climate in Portugal and Mediterranean Europe. The heater was in the form of a trapezoidal–shaped water store in direct contact with an inclined flat-plate solar collector assembly. In this design, the inclination angle of the absorber plate was 45^0 and the other sides were well insulated. Both theoretical and experimental studies were made, and the authors observed that the system provides sufficient energy store to meet typical daily domestic hot-water demands.

Joudi, Hussein and Farhan [21] investigated numerically the performance of a prism shaped storage solar collector with a right cross sectional area. Calculations were carried out using the finite element method and the ANSYS software was used for this purpose. In the calculations, while the horizontal and vertical walls were insulated, the inclined wall was subjected to a heat flux of incoming solar radiation. After calculations, temperature distribution and velocity distribution inside the storage solar collector, stored energy and mean tank temperature was determined. Effect of using a horizontal adiabatic partition inside the tank was also investigated.

The length of the partition and its location along the height of the storage collector was analyzed to give optimum stored energy and maximum possible mean tank temperature. The results showed that the performance of the storage collector could be improved by using the partition.

Samanta and Balushi [22] proposed a stationary spherical solar collector which consists of a spherical body with a cover, an absorbing surface and the working fluid in the annular space. Expressions for incident radiation for a spherical collector were derived from the corresponding relations for a stationary flat-plate collector taking into account the self-tracking ability of the spherical collector. Results for Dhahran, Saudi Arabia and Seeb, Sultanate of Oman were chosen to test the applicability of the proposed spherical solar collector. Results showed that the annual average of the daily incident solar irradiation on spherical collector is about 21% higher than on the flat-plate collector for these locations.

CHAPTER 3

SOLAR RADIATION

The sun has a spherical shape with a diameter of 1.39×10^9 m. It is, on the average, 1.5×10^{11}m from the earth and has an effective blackbody temperature of 5777 K [23].

The sun is major energy source of the earth and generates its energy in a process called nuclear fusion. During a nuclear fusion, four hydrogen nuclei fuse to become one helium atom. Mass of the helium atom is less than the four hydrogen nuclei and energy equivalent of this mass defect is emitted into space.

At the outside of earth's atmosphere a constant called as "solar constant" is defined for solar energy applications. The solar constant, G_{sc}, is the energy from the sun, per unit time, received on a unit area of surface perpendicular to the direction of propagation of the radiation, at mean earth-sun distance, outside of the atmosphere. There are several studies to measure the solar constant with different results. The value of 1367 W/m^2 is used in this thesis.

The earth moves around the sun on an elliptical orbit. The variation of the earth-sun distance due to earth's orbit causes variable extraterrestrial radiation. The dependence of extraterrestrial radiation on time of year is indicated by below equation [23]:

$$G_{0n} = G_{sc}(1 + 0.033\cos\frac{360n}{365}) \quad (3.1)$$

where G_{0n} is the extraterrestrial radiation, measured on the plane normal to the radiation on the nth day of the year.

Solar radiation at normal incidence received at the surface of the earth is subject to variations due to atmospheric scattering and atmospheric absorption [23]. Scattering of radiation as it passes through the atmosphere is caused by interaction of the radiation with air molecules, water (vapor and droplets), and dust. Absorption of radiation in the atmosphere in the solar energy spectrum is due largely to ozone in the ultraviolet and to water vapor and carbon dioxide in bands in the infrared.

There are several studies in literature to estimate solar radiation taking into account the time, measured radiation data, climate types, and location.

3.1. Definitions

Some definitions used in solar energy applications are listed below [23]:

Air Mass (m) : The ratio of the mass of atmosphere through which beam radiation passes to the mass it would pass through if the sun were at the zenith. Thus at sea level, m=1 when the sun is at the zenith, and m=2 for a zenith angle θ_z of 60^0. For zenith angles from 0^0 to 70^0 at sea level, to a close approximation,

$$m = 1/\cos\theta_z \quad (3.2)$$

For higher zenith angles, the effect of the earth's curvature becomes significant and must be taken into account.

Beam Radiation : The solar radiation received from the sun without having been scattered by the atmosphere.

Diffuse Radiation: The solar radiation received from the sun after its direction has been changed by scattering by the atmosphere.

Total Solar Radiation : The sum of the beam and diffuse solar radiation on a surface

Irradiance, W/m^2 : The rate at which radiant energy is incident on a surface, per unit area of surface. The symbol G is used for solar irradiance.

Irradiation, J/m^2 : The incident energy per unit area on a surface, found by integration of irradiance over a specified time, usually an hour or a day. Insolation is a term applying specifically to solar energy irradiation. The symbol H is used for insolation for a day. The symbol I is used for insolation for an hour (or other period if specified).

Solar Time : Solar time in minutes is

$$\text{solar time} = \text{standard time} + 4(L_{st} - L_{loc}) + E \tag{3.3}$$

where L_{st} is the standard meridian for the local time zone, L_{loc} is the longitude of the location in question (in degrees west) and E is the equation of time (in minutes). E is calculated using below equation [23]:

$$\begin{aligned} E = 229.2(&0.000075 + 0.001868\cos\beta - 0.032077\sin\beta \\ &- 0.014615\cos(2\beta) - 0.04089\sin(2\beta) \end{aligned} \tag{3.4}$$

where $\beta = (n-1)\frac{360}{365}$, n is the day of the year and can be obtained using Table 3.1.

Table 3.1 Average Days for Months and Values of n by Months [23]

		For the Average Day of the Month		
Month	n for ith Day of Month	Date	n, Day of Year	δ, Declination
January	i	17	17	-20.9
February	31+i	16	47	-13.0
March	59+i	16	75	-2.4
April	90+i	15	105	9.4
May	120+i	15	135	18.8
June	151+i	11	162	23.1
July	181+i	17	198	21.2
August	212+i	16	228	13.5
September	243+i	15	258	2.2
October	273+i	15	288	-9.6
November	304+i	14	318	-18.9
December	334+i	10	344	-23.0

Hour Angle (ω) : The angular displacement of the sun east or west of the local meridian due to rotation of the earth on its axis. (It is negative in the morning, positive in the afternoon and zero at noon). Hour angle is calculated using below equation [23]:

$$\omega = (\text{ solar time - noon time}) \times 15^{\circ} \tag{3.5}$$

where solar time and noon times are in hours (noon time is 12:00).

Declination (δ) : The angular position of the sun with respect to the equatorial plane at solar noon. Declination is in the range $-23.45^{0} < \delta < 23.45^{0}$. (North is the positive direction.) and below equation is used to calculate it [23]:

$$\delta = 23.45 \ \sin\left(360\frac{284+n}{365}\right) \tag{3.6}$$

Latitude (ϕ) : The angular distance from equator plane. Latitude is given in the range $-90^0 < \phi < 90^0$. (North is the positive direction.)

Longitude (L) : The angular distance from prime meridian. Longitude ranges from 0° to 180°, either east or west.

Slope (β) : The angle between the plane of the surface in question and the horizontal. It is in the range $0^0 \leq \beta \leq 180^0$. ($\beta > 90^0$ means that the surface has a downward facing component).

Surface azimuth angle (γ) : The angle between south and the projection of normal of the surface on the horizontal ground plane. Direction of an angular displacement from south to west of south is positive. It is in the range $-180^0 \leq \gamma \leq 180^0$.

Angle of incidence (θ) : The angle between the beam radiation on a surface and the normal to that surface. Equations relating the angle of incidence of beam radiation on a surface to the other angles are

$$\begin{aligned}\cos\theta = {} & \sin\delta\sin\phi\cos\beta - \sin\delta\cos\phi\sin\beta\cos\gamma + \cos\delta\cos\phi\cos\beta\cos\omega \\ & + \cos\delta\sin\phi\sin\beta\cos\gamma\cos\omega + \cos\delta\sin\beta\sin\gamma\sin\omega\end{aligned} \tag{3.7}$$

and $$\cos\theta = \cos\theta_z\cos\beta - \sin\theta_z\sin\beta\cos(\gamma_s - \gamma) \tag{3.8}$$

Zenith angle (θ_z) : The angle between normal of the ground plane and the line to the sun, ie. , the angle of incidence of beam radiation on a horizontal surface. Equation for zenith angle is below [23]:

$$\cos\theta_z = \cos\phi\cos\delta\cos\omega + \sin\phi\sin\delta \tag{3.9}$$

<u>Solar altitude angle</u> (α_s) : It is the vertical angle between the horizontal ground plane and the line to the sun. It is complement of the zenith angle and given in the range $0^0 < \alpha_s < 90^0$.

$$\alpha_s = 90 - \theta_z \tag{3.10}$$

<u>Solar azimuth angle</u> (γ_s) : The angle between south and the projection of beam radiation on the horizontal ground plane. Direction of an angular displacement from south to west of south is positive.

A general formulation for solar azimuth angle is below [23] :

$$\gamma_s = C_1\ C_2\ \gamma_s' + C_3\left(\frac{1 - C_1\ C_2}{2}\right)180 \tag{3.11a}$$

where;

$$\sin\gamma_s' = \frac{\sin\omega\cos\delta}{\sin\theta_z} \tag{3.11b}$$

or $$\tan\gamma_s' = \frac{\sin\omega}{\sin\delta\cos\omega - \cos\phi\tan\delta} \tag{3.11c}$$

$$C_1 = \begin{cases} 1 \text{ if } |\omega| \le \omega_{ew} \\ -1 \text{ if } |\omega| > \omega_{ew} \end{cases} \tag{3.11d}$$

$$C_2 = \begin{cases} 1 \text{ if } (\phi - \delta) \ge 0 \\ -1 \text{ if } (\phi - \delta) < 0 \end{cases} \tag{3.11e}$$

$$C_3 = \begin{cases} 1 & \text{if } \omega \geq 0 \\ -1 & \text{if } \omega < 0 \end{cases} \tag{3.11f}$$

$$\cos\omega_{ew} = \frac{\tan\delta}{\tan\phi} \tag{3.11g}$$

Solar altitude angle, solar azimuth angle, zenith angle and surface azimuth angle are shown by Figure 3.1 and Figure 3.2 on the following page.

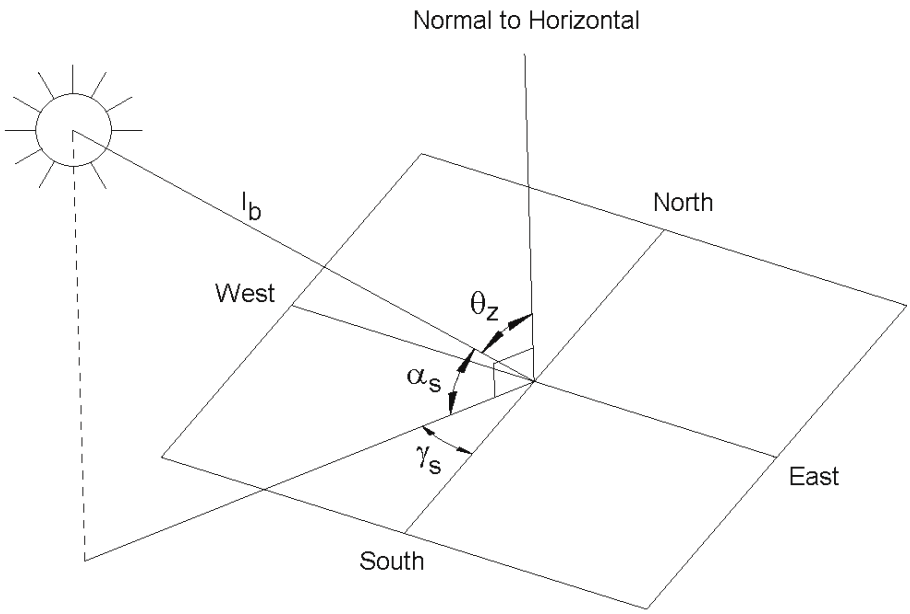

Figure 3.1 Solar Altitude Angle, Solar Azimuth Angle and Zenith Angle

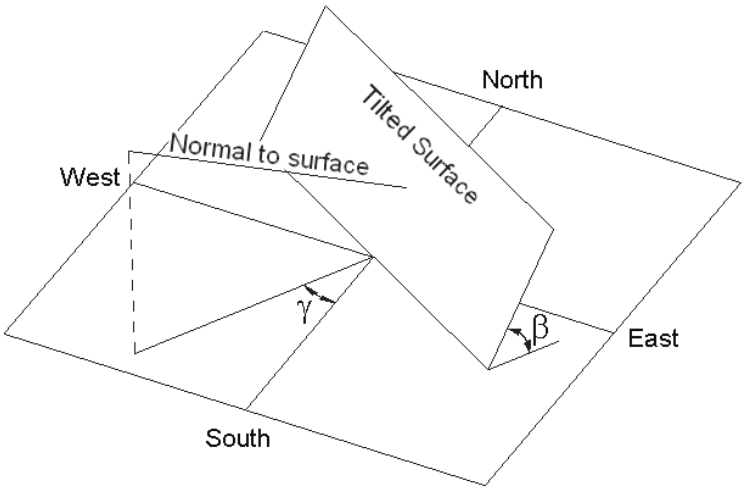

Figure 3.2 Surface Azimuth Angle and Slope

3.2 Extraterrestrial Radiation on a Horizontal Surface

The extraterrestrial radiation on a horizontal surface at any time is

$$G_0 = G_{0n} \cos\theta_z \tag{3.12}$$

(Figure 3.3a and Figure 3.3b).

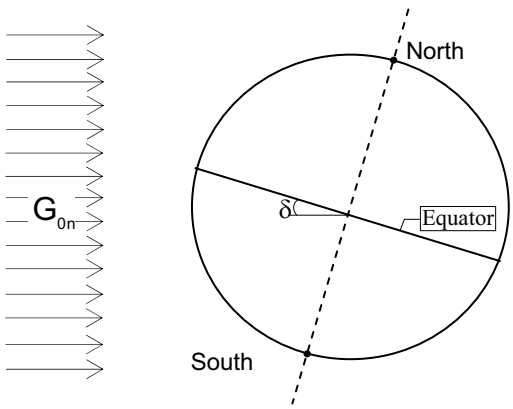

Figure 3.3a Schematic of the Sun Rays Coming to Earth's Atmosphere

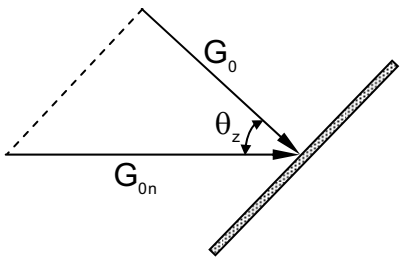

Figure 3.3b Extraterrestrial Radiation on a Horizontal Surface Outside of The Atmosphere

If Equation 3.1 for G_{0n} and Equation 3.9 for $\cos\theta_z$ are substituted in this equation, below equation is obtained for the extraterrestrial radiation on a horizontal surface.

$$G_0 = G_{sc}(1 + 0.033\cos\frac{360n}{365})(\cos\phi\cos\delta\cos\omega + \sin\phi\sin\delta) \tag{3.13}$$

where G_{sc} is the solar constant and n is the day of the year.

Integration of this equation over the period from sunrise to sunset, gives daily extraterrestrial radiation on a horizontal surface.

$$H_0 = \frac{24x3600G_{sc}}{\pi}(1 + 0.033\cos\frac{360n}{365})x(\cos\phi\cos\delta\sin\omega_s + \frac{\pi\omega_s}{180}\sin\phi\sin\delta) \tag{3.14}$$

where ω_s is the sunset hour angle, in degrees. When we solve Equation 3.9 for ω using the value θ_z=90^0, ω_s is obtained as below :

$$\cos\omega_s = -\frac{\sin\phi\sin\delta}{\cos\phi\cos\delta} = -\tan\phi\tan\delta \tag{3.15}$$

It must be noted here that, sunset and sunrise hour angles have the same value ($\omega_s = \omega_{sr}$) and they are also used to calculate number of daylight hours, N.

$$N = (\omega_s + \omega_{sr})\ x\ \frac{1h}{15\deg}$$

$$N = \frac{2}{15}\cos^{-1}(-\tan\phi\tan\delta) \tag{3.16}$$

Also, integration of Equation 3.13 for an hour period gives us hourly extraterrestrial radiation on a horizontal surface.

$$I_0 = \frac{12x3600G_{sc}}{\pi}(1+0.033\cos\frac{360n}{365})x\left[\cos\phi\cos\delta(\sin\omega_2 - \sin\omega_1) + \frac{\pi(\omega_2-\omega_1)}{180}\sin\phi\sin\delta\right] \tag{3.17}$$

The limits ω_1 and ω_2 may define a time other than an hour. Therefore this equation can also be used for any time difference.

As a simplification, the hourly extraterrestrial radiation can be approximated by writing Equation 3.13 in terms of I, evaluating ω at the midpoint of the hour.

$$I_0 \cong G_{0,\ \text{at}\ (t_1+t_2)/2}\ x\ (1\ \text{hour})$$

$$I_0 \cong 3600G_{sc}(1+0.033\cos\frac{360n}{365})(\cos\phi\cos\delta\cos\omega + \sin\phi\sin\delta) \tag{3.18}$$

where $\omega=(\omega_1+\omega_2)/2$.

3.3 Radiation on Sloped Surfaces

Incident solar radiation on earth surface has three components. These are beam, diffuse and ground reflected radiations. Also, diffuse component has three parts. The first is isotropic part, received uniformly from all of the sky dome. The second is circumsolar diffuse, resulting from forward scattering of solar radiation and concentrated in the part of the sky around the sun. The third is concentrated near the horizon, and is most pronounced in clear skies [23].

The total incident radiation on a sloped surface is given by

$$I_T = I_b R_b + I_{d,iso} F_{c-s} + I_{d,cs} R_b + I_{d,hz} F_{c-hz} + I \rho_g F_{c-g} \tag{3.19}$$

In this equation, the first term is the beam contribution, the second is the isotropic diffuse term, the third is the circumsolar diffuse term, the fourth term is the contribution of the diffuse from the horizon from a band, and the fifth term is the reflected radiation from the ground. The ground surface is assumed to be a diffuse reflector.

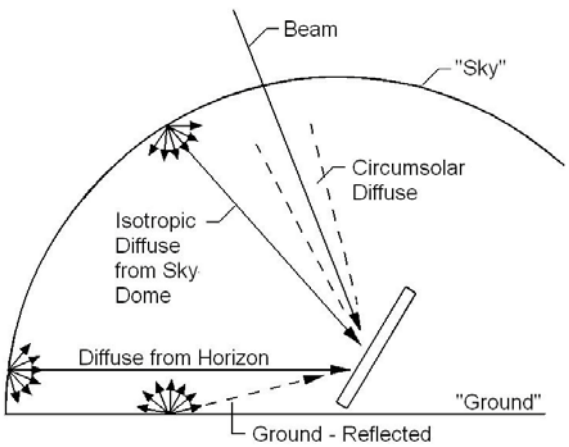

Figure 3.4 Beam, Diffuse and Ground-Reflected Radiation on a Tilted Surface [23]

Other symbols in this equation are as follows :

$F_{c\text{-}s}$: Radiation view factor from the sloped surface to the sky

$F_{c\text{-}hz}$: Radiation view factor from the sloped surface to the horizon

$F_{c\text{-}g}$: Radiation view factor from the sloped surface to the ground

I : Total radiation on a horizontal surface ($I = I_b + I_d$)

ρ_g : Diffuse reflectance of the ground.

R_b : The geometric factor. It is the ratio of beam radiation on the tilted surface to that on a horizontal surface at any time.

$$R_b = \frac{\text{Beam radiation on the tilted surface}}{\text{Beam radiation on a horizontal surface}} = \frac{G_{b,T}}{G_b} = \frac{G_{b,n}\cos\theta}{G_{b,n}\cos\theta_z}$$

$$R_b = \frac{\cos\theta}{\cos\theta_z} \tag{3.20}$$

The geometric factor for total radiation is obtained by below definition :

$$R = \frac{\text{Total radiation on the tilted surface}}{\text{Total radiation on a horizontal surface}} = \frac{I_T}{I} \tag{3.21}$$

Preferred methods for calculation of I_T are given in the following sections [23].

3.3.1 The Isotropic Diffuse Model

In this model, all diffuse radiation is assumed to be isotropic. As a result of this assumption, Equation 3.22 takes following form :

$$I_T = I_b R_b + I_d F_{c-s} + I\rho_g F_{c-g} \tag{3.22}$$

For a surface tilted at slope β, the view factor to the sky F_{c-s} and the view factor to the ground F_{c-g} are given by (1+ cosβ)/2 and (1 - cosβ)/2 respectively.

If the surroundings have a diffuse reflectance of ρ_g for the total solar radiation, the reflected radiation from the surroundings on the surface will be $I\rho_g(1 - \cos\beta)/2$.

Consequently, below equation is obtained for the total solar radiation on the tilted surface for an hour :

$$I_T = I_b R_b + I_d \left(\frac{1+\cos\beta}{2} \right) + I\rho_g \left(\frac{1-\cos\beta}{2} \right) \tag{3.23}$$

The geometric factor for total radiation is

$$R = \frac{I_b}{I} R_b + \frac{I_d}{I} \left(\frac{1+\cos\beta}{2} \right) + \rho_g \left(\frac{1-\cos\beta}{2} \right) \tag{3.24}$$

3.3.2 The HDKR Model

In this model, circumsolar diffuse and horizon brightening components are taken into account and the diffuse radiation on a tilted collector is calculated as below :

$$I_{d,T} = I_d \left\{ (1 - A_i) \left(\frac{1+\cos\beta}{2} \right) \left[1 + f \sin^3 \left(\frac{\beta}{2} \right) \right] + A_i R_b \right\} \tag{3.25}$$

where A_i is an anisotropy index which is a function of the transmittance of the atmosphere for beam radiation

$$A_i = \frac{I_{bn}}{I_{0n}} = \frac{I_b}{I_0} \tag{3.26}$$

and f is a modulating factor to account for cloudiness

$$f = \sqrt{I_b / I} \tag{3.27}$$

Consequently, the total radiation on the tilted surface is

$$I_T = \left(I_b + I_d A_i\right) R_b + I_d \left(1 - A_i\right)\left(\frac{1+\cos\beta}{2}\right)\left[1 + f\sin^3\left(\frac{\beta}{2}\right)\right] + I\rho_g\left(\frac{1-\cos\beta}{2}\right) \tag{3.28}$$

The geometric factor for total radiation is

$$R = \left(\frac{I_b}{I} + \frac{I_d}{I}A_i\right)R_b + \frac{I_d}{I}\left(1 - A_i\right)\left(\frac{1+\cos\beta}{2}\right)\left[1 + f\sin^3\left(\frac{\beta}{2}\right)\right] + \rho_g\left(\frac{1-\cos\beta}{2}\right) \tag{3.29}$$

3.3.3 The Perez Model

This model has more detailed analysis and the diffuse radiation on a tilted collector is calculated as below :

$$I_{d,T} = I_d\left[\left(1 - F_1\right)\left(\frac{1+\cos\beta}{2}\right) + F_1\frac{a}{b} + F_2\sin\beta\right] \tag{3.30}$$

where F_1 and F_2 are circumsolar and horizon brightness coefficients and depend on the zenith angle θ_z, a clearness ε, and a brightness Δ.

$$F_1 = \max\left[0, \left(f_{11} + f_{12}\Delta + \frac{\pi\theta_z}{180} f_{1,3}\right)\right] \tag{3.31}$$

$$F_2 = \left(f_{21} + f_{22}\Delta + \frac{\pi\theta_z}{180} f_{23}\right) \tag{3.32}$$

In the equations above f_{11}, f_{12}, f_{13}, f_{21}, f_{22} and f_{23} are statistically derived coefficients for ranges of values of ε.

$$\varepsilon = \frac{\frac{I_d + I_n}{I_d} + 5.535\text{x}10^{-6}\theta_z^{\ 3}}{1 + 5.535\text{x}10^{-6}\theta_z^{\ 3}} \tag{3.33}$$

where θ_z is in degrees. A recommended set of these coefficients is shown in Table 3.2.

Δ is found by

$$\Delta = m\frac{I_d}{I_{0n}} \tag{3.34}$$

where m is the air mass, I_{0n} is the extraterrestrial normal incidence radiation.

Table 3.2 Brightness Coefficients for The Perez Model [23]

Range of ε	f_{11}	f_{12}	f_{13}	f_{21}	f_{22}	f_{23}
0 – 1.065	-0.196	1.084	-0.006	-0.114	0.180	-0.019
1.065 – 1.230	0.236	0.519	-0.180	-0.011	0.020	-0.038
1.230 – 1.500	0.454	0.321	-0.255	0.072	-0.098	-0.046
1.500 – 1.950	0.866	-0.381	-0.375	0.203	-0.403	-0.049
1.950 – 2.800	1.026	-0.711	-0.426	0.273	-0.602	-0.061
2.800 – 4.500	0.978	-0.986	-0.350	0.280	-0.915	-0.024
4.500 – 6.200	0.748	-0.913	-0.236	0.173	-1.045	0.065
6.200 – ↑	0.318	-0.757	0.103	0.062	-1.698	0.236

a and b are terms that account for the angles of incident of the cone of circumsolar radiation on the tilted and horizontal surfaces. The circumsolar radiation is considered to be from a point source at the sun. The terms a and b are given by

$$\begin{aligned} a &= \max\ [0,\ \cos\theta] \\ b &= \max\ [\cos 85,\ \cos\theta_z] \end{aligned} \tag{3.35}$$

Consequently, the total radiation on the tilted surface is

$$I_T = I_b R_b + I_d\left(1-F_1\right)\left(\frac{1+\cos\beta}{2}\right) + I_d F_1 \frac{a}{b} + I_d F_2 \sin\beta + I\rho_g\left(\frac{1-\cos\beta}{2}\right) \tag{3.36}$$

The geometric factor for total radiation is

$$R = \frac{I_b}{I} R_b + \frac{I_d}{I}\left(1-F_1\right)\left(\frac{1+\cos\beta}{2}\right) + \frac{I_d}{I} F_1 \frac{a}{b} + \frac{I_d}{I} F_2 \sin\beta + \rho_g\left(\frac{1-\cos\beta}{2}\right) \tag{3.37}$$

When these three models are compared, it is evident that the isotropic model and the HDKR model are simpler than the Perez model. Furthermore, the HDKR model produces results that are closest to measured values [23]. The Isotropic and the HDKR models are suggested for surfaces sloped toward the equator, and the Perez model is suggested for surfaces with γ far from 0^0 in the northern hemisphere or 180^0 in the southern hemisphere [23].

3.4. Calculation of Beam and Diffuse Components of the Total Radiation Measured on a Horizontal Surface

Clearness of the sky have an important role in determination of beam and diffuse components of the total radiation, and it is expressed by a ratio

named as “clearness index”. Three clearness indices are defined. These are hourly clearness index (k_T), daily clearness index (K_T) and monthly average clearness index ($\overline{K}_T$).

The ratio of a particular hour’s radiation on a horizontal surface to the extraterrestrial radiation for that hour is defined as hourly clearness index.

$$k_T = \frac{I}{I_0} \tag{3.38}$$

The ratio of a particular day’s radiation on a horizontal surface to the extraterrestrial radiation for that day is defined as daily clearness index.

$$K_T = \frac{H}{H_0} \tag{3.39}$$

The ratio of monthly average daily radiation on a horizontal surface to the monthly average daily extraterrestrial radiation is defined as monthly average clearness index.

$$\overline{K}_T = \frac{\overline{H}}{\overline{H}_0} \tag{3.40}$$

The data $\overline{H}$, H and I are from measurements of total solar radiation on a horizontal surface, that is, the commonly available pyranometer measurements. Values $\overline{H}_0$, H_0 and I_0 can be calculated by the methods of Section 3.2..

To obtain diffuse and beam components of measured total solar radiation on a horizontal surface, below correlations are suggested by [23] for hourly, daily and monthly radiation, respectively :

$$\frac{I_d}{I} = \begin{cases} 1.0 - 0.09k_T & \text{for } k_T \le 0.22 \\ 0.9511 - 0.1604k_T + 4.388k_T^2 - 16.638k_T^3 + 12.336k_T^4 & \text{for } 0.22 < k_T \le 0.80 \\ 0.165 & \text{for } k_T > 0.80 \end{cases} \tag{3.41}$$

$$\frac{H_d}{H} = \begin{cases} 1.0 - 0.2727K_T + 2.4495K_T^2 - 11.9514K_T^3 + 9.3879K_T^4 & \text{for } K_T < 0.715 \text{ and } \omega_s < 81.4^0 \\ 0.143 & \text{for } K_T \ge 0.715 \text{ and } \omega_s < 81.4^0 \end{cases} \tag{3.42.a}$$

$$\frac{H_d}{H} = \begin{cases} 1.0 + 0.2832K_T - 2.5557K_T^2 + 0.8448K_T^3 & \text{for } K_T < 0.722 \text{ and } \omega_s \ge 81.4^0 \\ 0.175 & \text{for } K_T \ge 0.722 \text{ and } \omega_s \ge 81.4^0 \end{cases} \tag{3.42.b}$$

$$\frac{\overline{H}_d}{\overline{H}} = \begin{cases} 1.391 - 3.560\overline{K}_T + 4.189\overline{K}_T^2 - 2.137\overline{K}_T^3 & \text{for } 0.3 \le \overline{K}_T \le 0.8 \text{ and } \omega_s \le 81.4^0 \\ 1.311 - 3.022\overline{K}_T + 3.427\overline{K}_T^2 - 1.821\overline{K}_T^3 & \text{for } 0.3 \le \overline{K}_T \le 0.8 \text{ and } \omega_s > 81.4^0 \end{cases} \tag{3.43}$$

Using the correlations above, diffuse component of the measured total radiation on a horizontal surface is calculated. Then, beam component is found by subtracting the diffuse radiation from the total radiation.

3.5. Absorbed Solar Radiation

Absorbed solar radiation, S, can be obtained by multiplying each term of Equation (3.23), Equation (3.28) and Equation (3.36) by the appropriate transmittance-absorptance product [23]. So, S is calculated as below according to the isotropic diffuse, HDKR and Perez models, respectively :

$$S = I_b R_b (\tau\alpha)_b + I_d (\tau\alpha)_d \left(\frac{1+\cos\beta}{2}\right) + I\rho_g (\tau\alpha)_g \left(\frac{1-\cos\beta}{2}\right) \tag{3.44}$$

$$\begin{aligned} S = {} & (I_b + I_d A_i) R_b (\tau\alpha)_b + I_d (1 - A_i)(\tau\alpha)_d \left(\frac{1+\cos\beta}{2}\right)\left[1 + f\sin^3\left(\frac{\beta}{2}\right)\right] \\ & + I\rho_g (\tau\alpha)_g \left(\frac{1-\cos\beta}{2}\right) \end{aligned} \tag{3.45}$$

$$\begin{aligned} S = {} & I_b R_b (\tau\alpha)_b + I_d (1 - F_1)(\tau\alpha)_d \left(\frac{1+\cos\beta}{2}\right) + I_d F_1 \frac{a}{b} (\tau\alpha)_d + I_d F_2 (\tau\alpha)_d \sin\beta \\ & + I\rho_g (\tau\alpha)_g \left(\frac{1-\cos\beta}{2}\right) \end{aligned} \tag{3.46}$$

In these equations $(\tau\alpha)_b$, $(\tau\alpha)_d$ and $(\tau\alpha)_g$ are transmittance-absorptance products for beam, diffuse and ground reflected radiation.

$(\tau\alpha)_b$ is obtained by ray-tracing techniques as below

$$(\tau\alpha)_b = \frac{\tau\alpha}{1-(1-\alpha)\rho_d} \tag{3.47}$$

where τ and α are transmittance of the cover and absorptance of the absorber, ρ_d refers to the reflectance of the cover for diffuse radiation incident from the absorber. Although ρ_d is a constant, τ and α are angle of

incidence dependent variables. Therefore, $(\tau\alpha)_b$ is also an angle of incidence dependent variable.

Transmittance of the cover is calculated using below equation [23] :

$$\tau = \frac{\tau_a}{2}\left[\frac{1-r_\perp}{1+r_\perp} x \frac{1-r_\perp{}^2}{1-(r_\perp\tau_a)^2} + \frac{1-r_{||}}{1+r_{||}} x \frac{1-r_{||}{}^2}{1-(r_{||}\tau_a)^2}\right] \tag{3.48}$$

where;

$$\tau_a = \exp\left(-\frac{KL}{\cos\theta_2}\right) \tag{3.49}$$

$$\theta_2 = \sin^{-1}\left(\frac{n_1}{n_2}\sin\theta\right) \tag{3.50}$$

$$r_\perp = \frac{\sin^2(\theta_2-\theta)}{\sin^2(\theta_2+\theta)} \tag{3.51}$$

$$r_{||} = \frac{\tan^2(\theta_2-\theta)}{\tan^2(\theta_2+\theta)} \tag{3.52}$$

n_1 and n_2 are the refractive indices ($n_1 = 1$ for air and $n_2 = 1.526$ for glass), and K is the extinction coefficient ($K = 0.3\text{cm}^{-1}$ for windows glass).

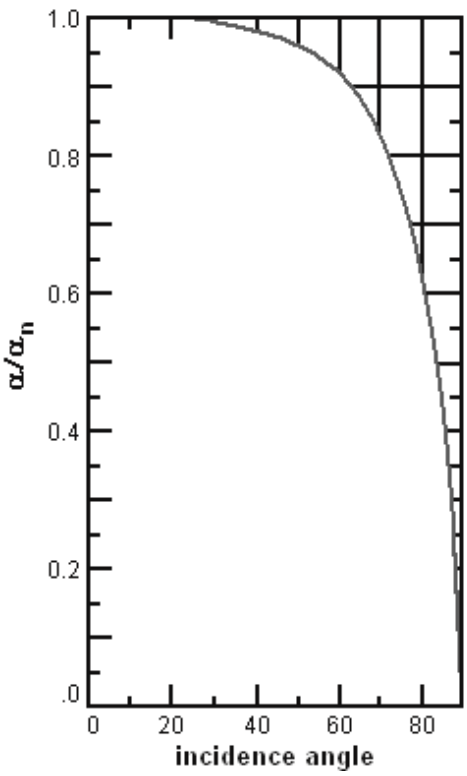

Figure 3.5 Change of Absorptivity by Incidence Angle [23]

Change of absorptivity is given by following equation for $0 \leq \theta \leq 80^0$ [23] :

$$\alpha = \alpha_n(1 + 2.0345 \times 10^{-3}\theta - 1.990 \times 10^{-4}\theta^2 + 5.324 \times 10^{-6}\theta^3 - 4.799 \times 10^{-8}\theta^4) \quad (3.53.a)$$

where α_n is absorptivity of the absorber at normal incidence.

Using Figure 3.5 and assuming linear changes for α in the ranges $80 \leq \theta \leq 86^0$ and $86 \leq \theta \leq 90^0$, we can write below equations :

$$\alpha = \alpha_n(-\frac{1}{24}\theta + \frac{239}{60}) \qquad (80^0 \leq \theta \leq 86^0) \qquad (3.53.b)$$

$$\alpha = \alpha_n(-\frac{1}{10}\theta + 9) \qquad (86^0 \le \theta \le 90^0) \tag{3.53.c}$$

ρ_d is estimated as reflectance for beam radiation incident at an angle of 60^0 [23].

$$\rho_d = \frac{1}{2}\left[r_\perp\left(1+\tau_a r_\perp\right) \; + \; r_{||}\left(1+\tau_a r_{||}\right)\right]_{\theta=60^\circ} \tag{3.54}$$

All of the diffuse radiation can be treated as having a single equivalent angle of incidence for the calculation of $(\tau\alpha)_d$, and all of the ground reflected radiation can be treated as having another equivalent angle of incidence for the calculation of $(\tau\alpha)_g$ [23]. These equivalent angles are given for ground reflected radiation by

$$\theta_e = 90 - 0.5788\beta + 0.002693\beta^2 \tag{3.55}$$

and for diffuse radiation by

$$\theta_e = 59.7 - 0.1388\beta + 0.001497\beta^2 \tag{3.56}$$

Then $(\tau\alpha)_d$ and $(\tau\alpha)_g$ are calculated using Equations from (3.47) to (3.54) for these equivalent angles of incidence.

CHAPTER 4

MATHEMATICAL MODELLING OF THE SYSTEM

4.1. Description of the Spherical Collector

The solar collector used in this analysis was constructed in Mechanical Engineering Department of METU. No specially produced equipment was purchased and therefore all the equipment used in construction was provided from the department and also from the market. The collector has a spherical absorber and a spherical glass cover. Water enters at the bottom and leaves at the top of the collector. Heating of water occurs in the absorber which has 113 L control volume (Figure 4.1).

The absorber is 60cm in diameter and made of two hemispheres. Each hemisphere was constructed by bending and welding of steel sheets, which are 3mm in thickness (Figure 4.2).

The glass cover is 68cm in diameter and produced from specially cut glass pieces, which are 3mm in thickness, which are sealed by silicon on two hemispherical frames (Figure 4.3).

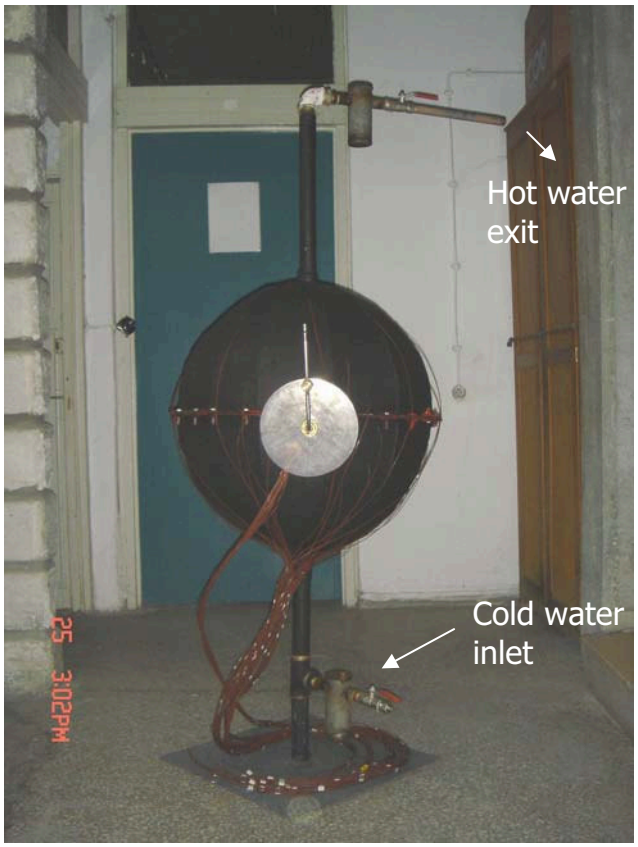

Figure 4.1 A General View of The Collector without Glass Covers

Figure 4.2 Bottom and Top Pieces of The Absorber

Figure 4.3 Bottom and Top Pieces of The Cover

4.2. Heat Transfer Mechanisms

When the solar radiation reaches the glass cover, some is reflected back to the environment, some is absorbed by the glass cover and the remaining part is transmitted through the cover and reaches to the absorber surface. This radiation is absorbed by the absorber and some of the heat is transferred to water store as useful energy by convection; the remaining part is transferred to glass cover and from there to the environment as a loss by convection and radiation mechanisms (Figure 4.4).

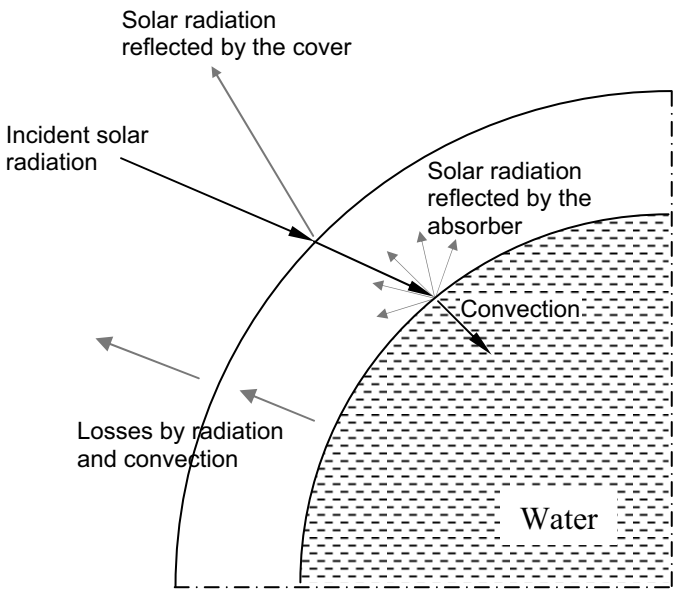

Figure 4.4 Heat Transfer Mechanisms

4.3. Energy Balance

Following assumptions are made in the analysis of the mathematical modeling of the spherical solar collector :

1- Thermal conductivity of steel is high and the absorber is sufficiently thin. Therefore, temperature variation across the thickness is neglected.
2- Heat capacities of the absorber plate and the glass cover are neglected in performance calculations.
3- Specific heat and density of water are constant everywhere.

When the energy balance is expressed for the fluid in the tank, Equation (4.1) is obtained to determine the useful energy (Figure 4.5) :

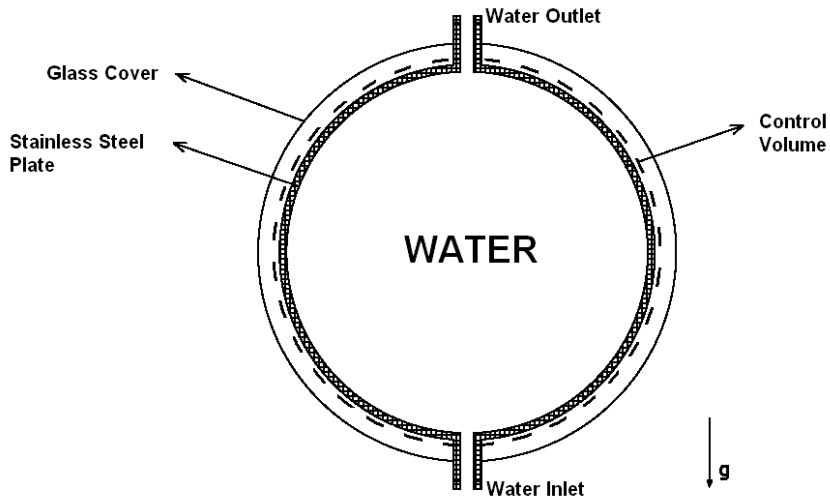

Figure 4.5 Control Volume

$$\dot{E}_{IN} - \dot{E}_{OUT} = \frac{dE}{dt}$$

$$\begin{bmatrix}\text{Absorbed}\\ \text{solar energy}\end{bmatrix} + \begin{bmatrix}\text{Energy carried by}\\ \text{the mass of water}\\ \text{entering the system}\end{bmatrix} - \begin{bmatrix}\text{Heat loss from the system}\\ \text{by convection and radiation}\\ \text{to the environment}\end{bmatrix}$$

$$- \begin{bmatrix}\text{Energy carried by}\\ \text{the mass of water}\\ \text{leaving the system}\end{bmatrix} = \begin{bmatrix}\text{Rate of change of}\\ \text{total energy in}\\ \text{the system}\end{bmatrix}$$

$$(\dot{S} A_T + \dot{H}_{IN}) - (\dot{Q}_{OUT} + \dot{H}_{OUT}) = \frac{dU}{dt}$$

$$\left[\dot{S} A_T + \dot{m} c_{p,w} T_{c,i}\right] - \left[A_T U_L (T_{p,ave} - T_a) + \dot{m} C_{p,w} T_{c,o}\right] = m_{tank} c_{p,w} \frac{dT_f}{dt}$$

$$\dot{S}A_T - A_T U_L (T_{p,ave} - T_a) = \dot{m} c_{p,w} (T_{c,o} - T_{c,i}) + m_{tank} c_{p,w} \frac{dT_f}{dt} = \dot{Q}_u \quad (4.1)$$

where A_T is total surface area of the spherical solar collector, U_L is overall heat loss coefficient, $T_{p,ave}$ is average absorber temperature, T_a is the ambient temperature, $\dot{S}$ is solar radiation absorbed by the spherical solar collector per unit surface area. $\dot{S}$ is calculated by

$$\dot{S} = G_{Tsph} (\tau\alpha)_{ave} \quad (4.2)$$

In Equation (4.2), G_{Tsph} is solar radiation incident on the spherical solar collector per unit surface area and per unit time. $(\tau\alpha)_{ave}$ is average transmittance-absorptance product for the absorber-cover system.

For a flat plate collector, incident solar radiation can be measured directly using a pyranometer parallel to the surface of the collector, or it can be calculated by any method mentioned in Section 3.3. For the spherical solar collector, there is no specific method to calculate G_{Tsph}. However, an estimation can be made by considering the spherical collector surface made of small flat surfaces. For this aim, surface area, surface azimuth angle and tilt angle of each of the small flat pieces are calculated by using the methods of chapter 6. Then, solar radiation incident on each small flat piece is estimated by one of the methods in Section 3.3 and adding them together will give $G_{Tsph}A_T$ product.

$\dot{S}A_T$ product can be also estimated in the same way for the spherical solar collector, and ratio of $\dot{S}A_T$ to $G_{Tsph}A_T$ will give $(\tau\alpha)_{ave}$ for the absorber-

cover system. For the calculation of $\dot{S}A_T$, $G_{Tsph}A_T$ and $(\tau\alpha)_{ave}$ a computer program in Mathcad software was written [Appendix F].

Collector efficiency is defined as the ratio of the useful energy collected to the solar energy reaching to the surface. So, instantaneous efficiency can be written as follows:

$$\eta = \frac{\dot{Q}_U}{G_{Tsph}A_T} = \frac{\dot{m}c_{p,w}(T_{c,o} - T_{c,i}) + m_{tank}c_{p,w}\left.\frac{dT_f}{dt}\right|_t}{G_{Tsph}A_T} \tag{4.4}$$

Note that, second term in the numerator indicates heat storage.

Hourly and daily efficiencies are calculated by integration of both numerator and denominator of Equation 4.4 :

$$\eta = \frac{\dot{m}c_{p,w}\int_{t_{initial}}^{t_{final}}(T_{c,o} - T_{c,i})dt + m_{tank}c_{p,w}(T_{f,final} - T_{f,initial})}{\int_{t_{initial}}^{t_{final}} G_{Tsph}A_T dt} \tag{4.5}$$

It is also possible to define heat removal factor and collector efficiency factor.

The useful energy is expressed in terms of the fluid inlet temperature. For this purpose, *heat removal factor* is defined which is the ratio of the actual useful energy gain to the useful energy gain if the whole collector surface were at the fluid inlet temperature. Thus,

$$F_R = \frac{\dot{Q}_U}{\dot{S} A_T - A_T U_L (T_{c,i} - T_a)} \tag{4.6}$$

Then useful energy equation becomes

$$\dot{Q}_U = F_R \left[\dot{S} A_T - A_T U_L (T_{c,i} - T_a) \right] \tag{4.7}$$

Maximum possible useful energy gain in a solar collector occurs when the whole collector is at the fluid inlet temperature.

When a least squares fit is applied to experimental data, a linear relation between η and $(T_{c,i} - T_a)/G_{Tsph}$ is obtained. Using this linear fit and equation below for collector efficiency, heat removal factor is obtained.

$$\eta = F_R (\tau\alpha)_{ave} - F_R U_L \left(\frac{T_{c,i} - T_a}{G_{Tsph}} \right) \tag{4.8}$$

Collector efficiency factor is the ratio of the actual useful energy gain to the useful energy gain if the whole collector surface were at the mean fluid temperature in the collector. Thus,

$$F' = \frac{Q_U}{\dot{S} A_T - A_T U_L (T_f - T_a)} \tag{4.9}$$

Then useful energy equation becomes

$$Q_U = F' \left[\dot{S} A_T - A_T U_L (T_f - T_a) \right] \tag{4.10}$$

Collector efficiency factor is obtained using a least squares fit, which is applied to experimental data for η - $(T_f - T_a)/G_{Tsph}$ relation, and equation below for collector efficiency.

$$\eta = F'(\tau\alpha)_{ave} - F'U_L\left(\frac{T_f - T_a}{G_{Tsph}}\right) \tag{4.11}$$

4.4. Mathematical Analysis of the Temperature Distribution on the Spherical Cover, on the Spherical Absorber and in the Water

This analysis can be made by choosing a differential element on the absorber and on the cover, and determining heat transfer mechanisms on these elements (Figure 4.6).

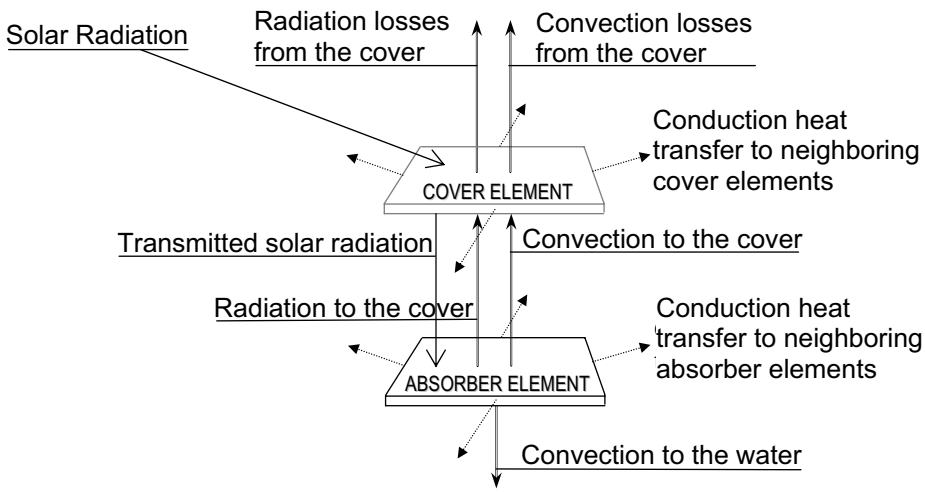

Figure 4.6 Heat Transfer Mechanisms on the Cover and the Absorber

Assumptions used in this analysis are as follows:

(1) Temperature gradient across the thickness of the absorber is ignored

(2) Temperature gradient across the thickness of the cover is ignored.

(3) For the flow situation water flow is laminar and one dimensional. For the non-flow situation the water is stagnant.

For a differential element of the absorber, energy balance can be defined as below with the help of Figure 4.7 and 4.8.

$$
\begin{aligned}
&-k(r\sin\theta d\phi\delta_p)\frac{\partial T_p}{\partial\theta}\bigg|_{\theta} + k(r\sin\theta d\phi\delta_p)\frac{\partial T_p}{\partial\theta}\bigg|_{\theta+d\theta} - k(rd\theta\delta_p)\frac{\partial T_p}{\partial\phi}\bigg|_{\phi} + k(rd\theta\delta_p)\frac{\partial T_p}{\partial\phi}\bigg|_{\phi+d\phi} \\
&-h_w(r^2\sin\theta d\phi d\theta)(T_p - T_w) + G(r^2\sin\theta d\phi d\theta)(\tau\alpha) \\
&-(h_{pc} + h_{rpc})(r^2\sin\theta d\phi d\theta)(T_p - T_c) \\
&= \rho(r^2\sin\theta d\phi d\theta\delta_p)c_p\frac{\partial T_p}{\partial t}
\end{aligned}
\tag{4.12}
$$

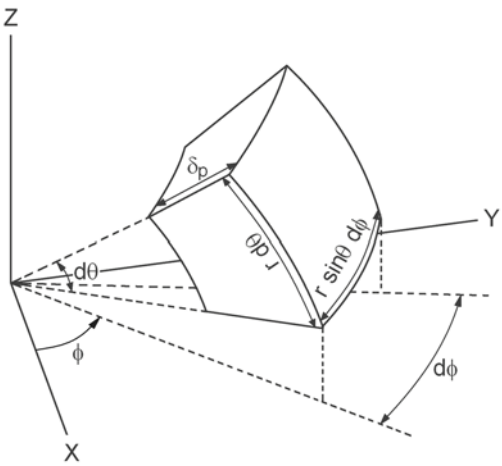

Figure 4.7 Dimensions of a Differential Absorber Element in Spherical Coordinates

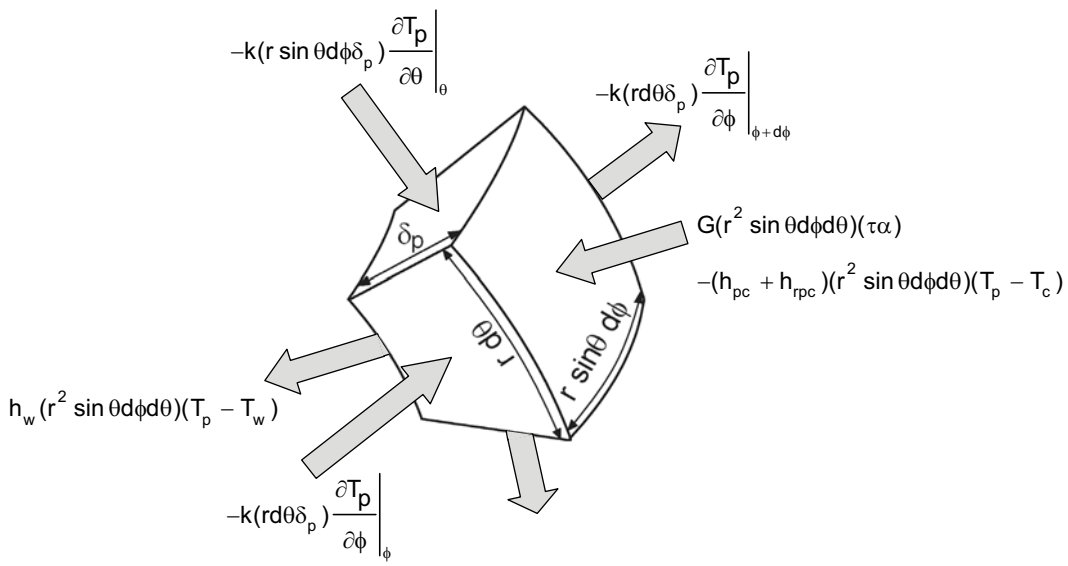

Figure 4.8 Mathematical Expressions of Heat Transfer Mechanisms on a Differential Absorber Element

Using the first two terms of Taylor series expansion, Equation 4.12 is transferred to Equation 4.13 shown below.

$$k\left[\frac{1}{r^2\sin\theta}\frac{\partial}{\partial\theta}\left(\sin\theta\frac{\partial T_p}{\partial\theta}\right)+\frac{1}{r^2\sin^2\theta}\frac{\partial^2 T_p}{\partial\phi^2}\right]+\frac{G(\tau\alpha)-h_w(T_p-T_w)-(h_{pc}+h_{rpc})(T_p-T_c)}{\delta_p} = \rho c_p\frac{\partial T_p}{\partial t} \tag{4.13}$$

where;

$$h_{rpc}=\frac{\sigma(T_p+T_c)(T_p^2+T_c^2)}{\frac{1}{\varepsilon_p}+\frac{1}{\varepsilon_c}-1} \tag{4.14}$$

δ_p is thickness of the absorber , ε_p and ε_c are emissivities of the absorber and the cover, respectively.

This equation gives temperature distribution on the spherical plate with following boundary conditions :

1- $T_p\big|_{\phi} = T_p\big|_{\phi+2\pi}$

2- $\left.\dfrac{\partial T_p}{\partial \phi}\right|_{\phi} = \left.\dfrac{\partial T_p}{\partial \phi}\right|_{\phi+2\pi}$

3- At water inlet, $\left.\dfrac{\partial T_p}{\partial \theta}\right|_{\theta=\pi} = 0$

4- At water outlet, $\left.\dfrac{\partial T_p}{\partial \theta}\right|_{\theta=0} = 0$

Using similar calculations, Equation (4.15) is obtained for the temperature distribution on the spherical cover.

$$k\left[\frac{1}{r^2 \sin\theta}\frac{\partial}{\partial\theta}\left(\sin\theta\frac{\partial T_c}{\partial\theta}\right)+\frac{1}{r^2\sin^2\theta}\frac{\partial^2 T_c}{\partial\phi^2}\right]$$

$$+\frac{G\alpha_c+(h_{pc}+h_{rpc})(T_p-T_c)-(h_{ca}+h_{rca})(T_c-T_a)}{\delta_c} \tag{4.15}$$

$$=\rho c_c\frac{\partial T_c}{\partial t}$$

where;

$$h_{rca}=\frac{\sigma\varepsilon_c(T_c+T_s)(T_c^{\,2}+T_s^{\,2})(T_c-T_s)}{(T_c-T_a)} \tag{4.16}$$

and δ_c is thickness of the cover.

Boundary conditions are as follows :

1- $T_c\big|_{\phi} = T_c\big|_{\phi+2\pi}$

2- $\left.\dfrac{\partial T_c}{\partial \phi}\right|_{\phi} = \left.\dfrac{\partial T_c}{\partial \phi}\right|_{\phi+2\pi}$

3- At water inlet, $\left.\dfrac{\partial T_c}{\partial \theta}\right|_{\theta=\pi} = 0$

4- At water outlet, $\left.\dfrac{\partial T_c}{\partial \theta}\right|_{\theta=0} = 0$

For a differential element of the water in the tank, energy balance can be defined as below with the help of Figure 4.9 and 4.10.

$$\begin{aligned} &\dot{m}cT_w\Big|_z + \int_{\phi=0}^{2\pi} h_w\left[\left(R_p \sin\theta d\phi\right)ds\right](T_p - T_w) - \dot{m}cT_w\Big|_{z+dz} \\ &= \rho\left[\pi\left(R_p \sin\theta\right)^2 dz\right]c_w \frac{\partial T_w}{\partial t} \end{aligned} \tag{4.17}$$

where;

$$ds = \frac{dz}{\sin\theta} \tag{4.18}$$

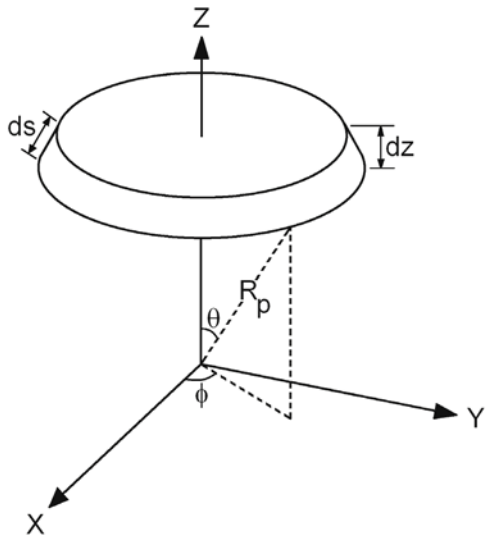

Figure 4.9 Dimensions of a Differential Water Element in Spherical Coordinates

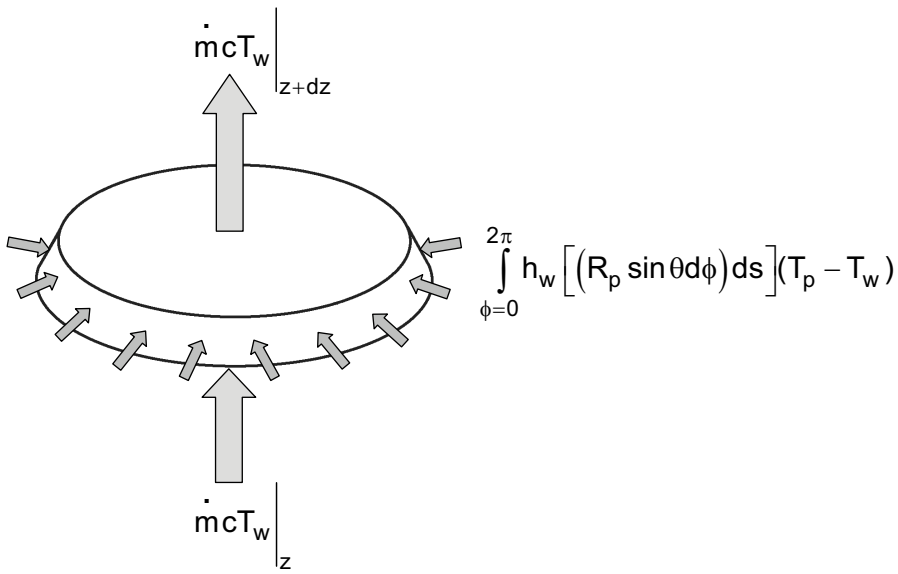

Figure 4.10 Mathematical Expressions of Heat Transfer Mechanisms on a Differential Water Element

Using the first two terms of Taylor series expansion, Equation 4.17 is transferred to Equation 4.19 shown below.

$$R_p \int_{\phi=0}^{2\pi} h_w (T_p - T_w) d\phi - \dot{m} c \frac{\partial T_w}{\partial z} = \rho \pi R_p^{\ 2} \sin^2 \theta c_w \frac{\partial T_w}{\partial t} \tag{4.19}$$

This equation gives water temperature distribution inside the tank with following boundary conditions :

1- $T_w \big|_{z=-R_p} = T_{in}$

2- $T_w \big|_{z=R_p} = T_{out}$

CHAPTER 5

EXPERIMENTAL WORK

5.1. The Measuring and Recording Instruments

Instruments below were used in the experiments:

- Copper-constantan thermocouples in connection with two “Elimko Model E680” data loggers to measure temperature distribution inside the water, on the absorber plate, on the cover and water temperatures at the inlet and at the exit of the collector.
- Glass thermometers to measure ambient air temperature and water inlet and exit temperatures. In order to obtain a uniform temperature, water is stirred in metallic boxes placed at the collector inlet and outlet pipes. Also, the pipes between the collector and the metallic boxes were well insulated.
- An Eppley type pyranometer to measure total solar radiation on horizontal is used.
- A hand-held wind speed indicator to measure instantaneous wind speeds is employed.

The measuring and recording instruments are shown by Figure 5.1 to Figure 5.4.

The mass flow rate of the water through the collector was measured by measuring the amount of water collected in a container of given size in a measured period of time.

Figure 5.1 “Elimko Model E680” Type Data Loggers

Figure 5.2 “Keithley Instruments Model 160” Type Digital Multimeter

Figure 5.3 Eppley Pyronometer

Figure 5.4 “Davis Instruments Wind Wizard Model 0281” Type Wind Speed Indicator

5.2. Description of the Experimental Setup

The experiments were carried out at four different mass flow rates (0.0023, 0.0055, 0.0077 and 0.011kg/s) and for non-flow situation.

The experimental solar collector consists of three parts:

First of all a spherical glass cover made of two pieces as top and bottom hemispheres is designed and manufactured. On the inner side of this glass cover, 12 thermocouples were located and fixed by silicon close to some thermocouple locations on the absorber. (6 thermocouples are placed on the top hemisphere and the remaining 6 thermocouples are placed on the bottom hemisphere). In Figure 5.5 how a thermocouple is fixed on a glass and locations of some of the thermocouples are shown.

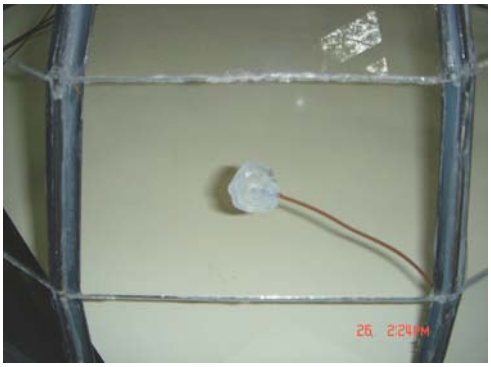

(a)

(b)

Figure 5.5 (a) Fixing of a Thermocouple on Glass Cover, (b) Thermocouple Locations on the Cover

The second important piece of the collector is a spherical absorber surface with two pieces as top and bottom hemispheres inside the spherical cover. These two pieces were assembled by bolt and nuts and to prevent leakage of water a rubber gasket was placed with silicon between them. On outer surface of the absorber 42 thermocouples were located by a metallic epoxy adhesive. Locations of the thermocouples are shown in Figure 5.6.

Figure 5.6 Thermocouple Locations on the Absorber

The third important piece of the setup is a semicircular frame made of stainless steel placed inside the absorber. Rotating this frame 360^0 with 30^0 increments, local water temperatures are measured inside the spherical tank. 12 thermocouples were located on the frame. The aim of using the semicircular construction is to reduce number of thermocouples used to measure the temperature distribution inside the spherical volume. 5 of the 12 thermocouples were located on the centerline of rotation and temperatures at these 5 points are taken (Figure 5.7). Remaining 7 thermocouples are used to measure water temperatures at 7 x 12 = 84 points inside the tank (360^0 / 30^0 = 12). Consequently, water temperatures at 84 + 5 = 89 points inside the tank are used to obtain 3D temperature distribution. Locations of the thermocouples on the frame and location of the frame in the tank are shown in Figures 5.7 to 5.9. To prevent mixing that might result from the rotation of the frame in the tank, the frame was constructed as simply as possible and rotations of the frame was made slowly in the experiments.

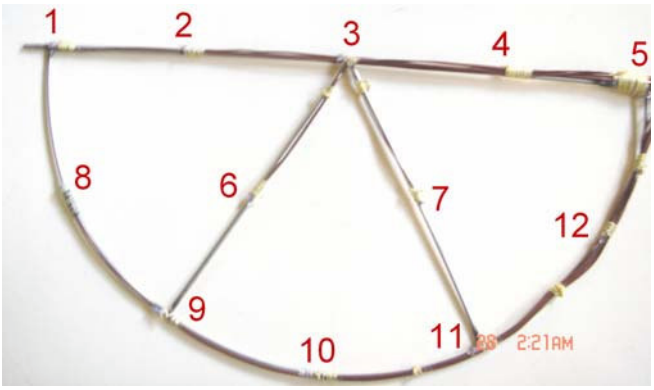

Figure 5.7 Frame Used to Measure Water Temperatures (Numbers Show Thermocouple Locations)

Figure 5.8 Location of the Frame in the System

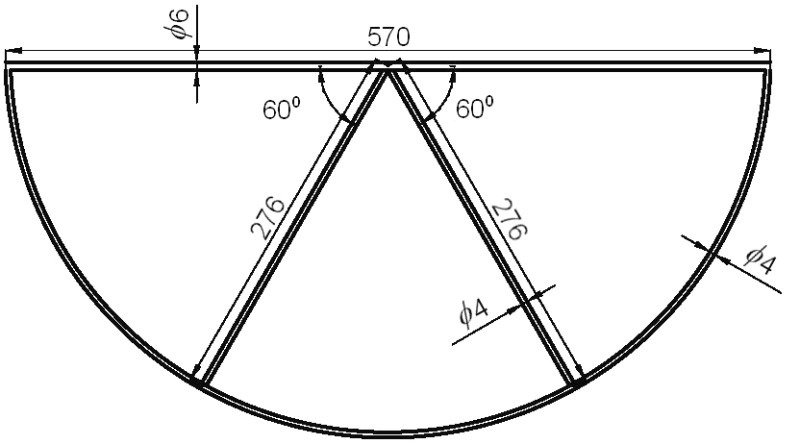

Figure 5.9 Dimensions of the Frame at Inner Side of the Absorber
(Dimensions are in mm)

Dimensions of the spherical solar collector, schematic drawing of the experimental setup and different views of the test stand are given by Figures 5.10, 5.11 and 5.12 on the following pages. The descriptive data is given by Table 5.1 on page 57.

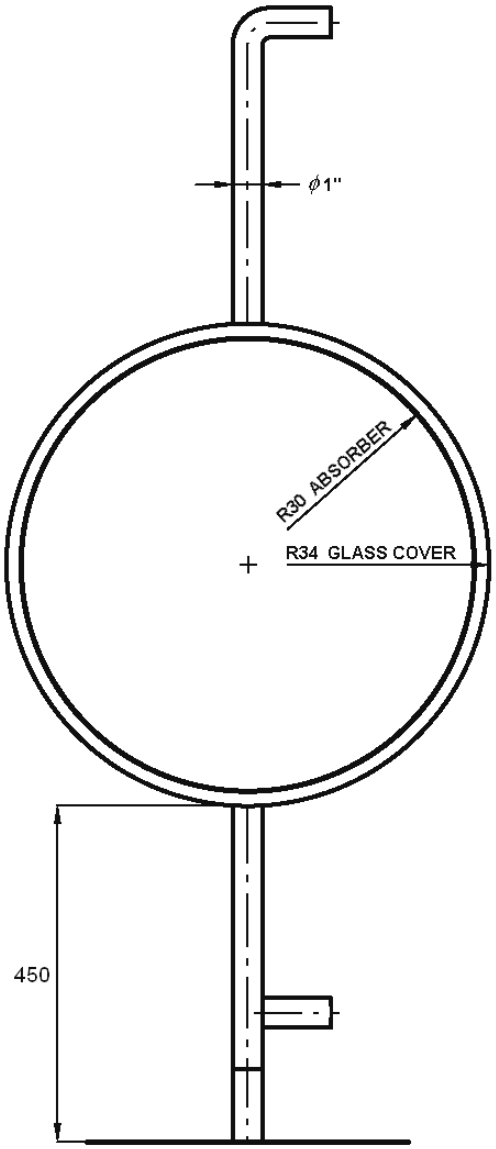

Figure 5.10 Dimensions of the Spherical Solar Collector

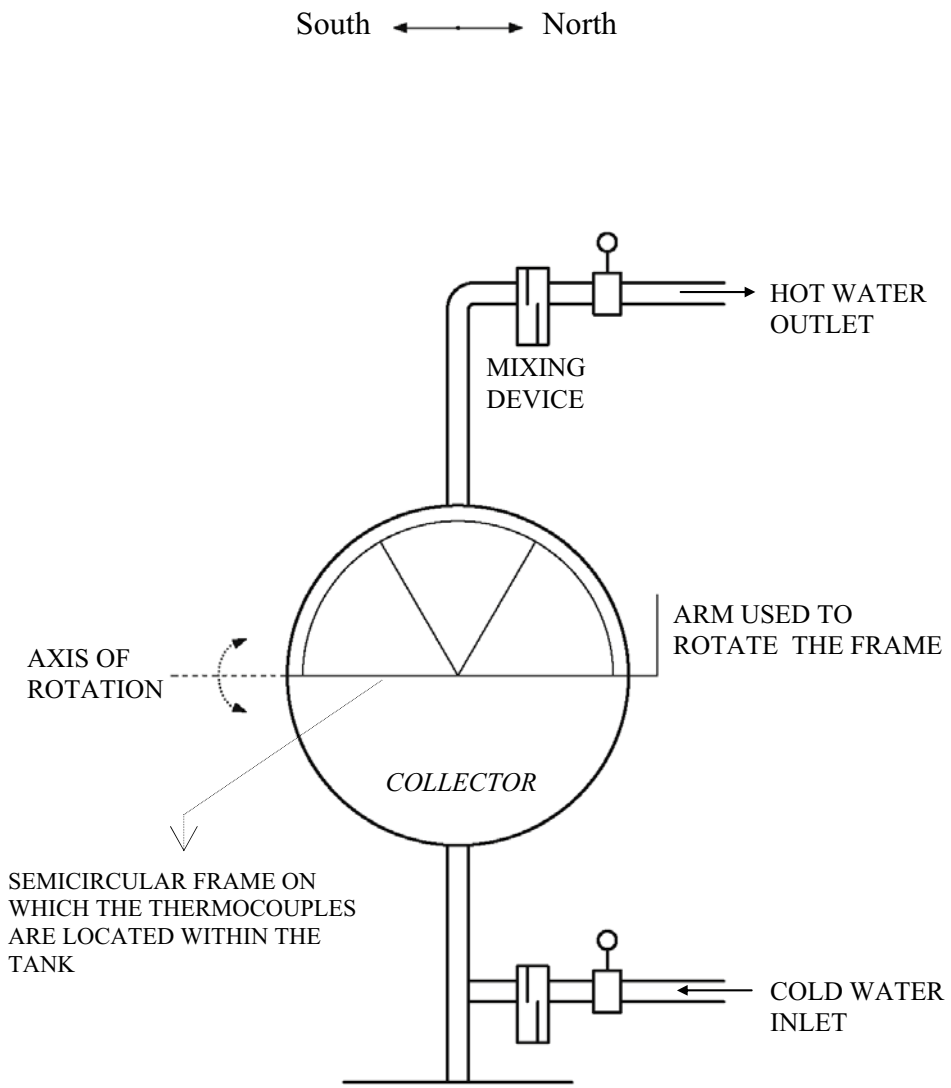

Figure 5.11 Schematic View of the Experimental Setup

Figure 5.12 Different Views of the Test Stand

Table 5.1 Descriptive Data for the Spherical Solar Collector

Dimensions	Radius of the cover	34 cm
	Radius of the absorber	30 cm
Glazing	Material	Window glass
	Thickness	3 mm
	Conductivity	1.12 W/m.C^0
	Specific heat	670 J/kg.C^0
	Total reflectance ($\theta = 0^0$)	0.0794
	Total absorptance ($\theta = 0^0$)	0.0386
	Index of refraction	1.526
Absorber	Material	Stainless steel
	Thickness	3 mm
	Conductivity	15.1 W/m.C^0
	Specific heat	480 J/kg.C^0
	Coating	Matt black paint
	Absorptivity	0.9 (assumed)

CHAPTER 6

NUMERICAL SIMULATION OF THE SYSTEM

The numerical modeling of the spherical collector is made by imagining longitudes and latitudes on its spherical surface. In this approach, the spherical absorber and the spherical cover are divided by K number of longitudes and L number of latitudes. Assuming that; each piece remaining between two neighboring longitudes and latitudes can be considered as a flat trapezoidal surface. This is done to simplify the analysis. Water in the tank is divided into L+1 number of control volumes such that each control volume in the tank remains between two adjacent latitudes and enclosed by K number of absorber elements. (Figure 6.1)

Assumptions used in the numerical solutions are as follows:

(1) Temperature gradient across the thickness of the absorber is ignored
(2) Temperature gradient across the thickness of the cover is ignored.
(3) For the flow situation water flow is laminar and one dimensional. For the non-flow situation the water is stagnant.
(4) Each piece of the absorber and cover that remain between neighboring longitudes and latitudes is assumed to be at a uniform temperature.
(5) Each control volume in the water is assumed to be at a uniform temperature. Note that in the experiments T gradients of 2-8 °C were measured, but for modeling simplicity were ignored.
(6) Because of low thermal conductivity of glass, thermal conduction in the glass cover in the direction normal to the radial direction is ignored.

6.1. Energy Balance Equations for the Water in the Tank

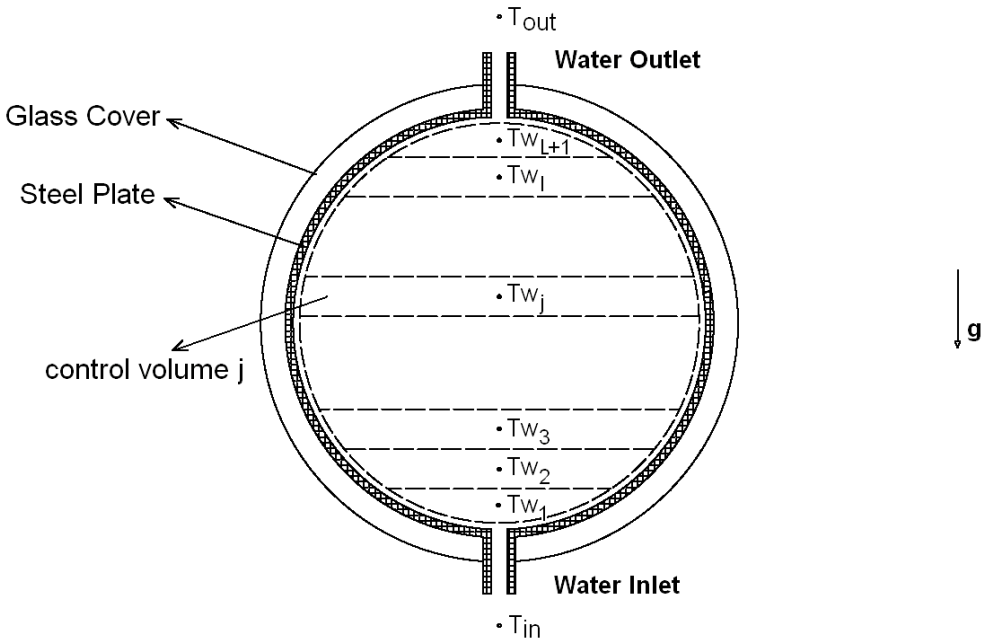

Figure 6.1 Open System Analysis

From the conservation of energy and energy balance, equation below is obtained for a control volume j :

$$\begin{bmatrix}\text{Energy carried by the}\\ \text{mass coming from the}\\ j-1^{\,th}\text{ control volume}\end{bmatrix}+\begin{bmatrix}\text{Heat transfer from}\\ \text{the absorber by}\\ \text{convection}\end{bmatrix}-\begin{bmatrix}\text{Energy carried by}\\ \text{the mass leaving the}\\ j^{\,th}\text{ control volume}\end{bmatrix}$$

$$=\begin{bmatrix}\text{Rate of change of}\\ \text{total energy in the}\\ j^{\,th}\text{ control volume}\end{bmatrix}$$

$$\dot{m}c_{w_j}(Tw_{j-1} - Tw_j) + A_j\sum_{i=1}^{K}\left[h_{w_{i,j}}(Tp_{i,j} - Tw_j)\right] = \rho_{w_j}V_jc_{w_j}\frac{dTw_j}{dt} \quad , \ (1 \le j \le L+1) \qquad (6.1)$$

where;

$\dot{m}$: mass flow rate of the water [kg/s]

c_{w_j}: Specific heat of water in the control volume j [J/kg^{0}C]

ρ_{w_j}: Density of water in the control volume j [kg/m^3]

A_j: Surface area of each enclosing absorber elements of the control volume j [m^2]

V_j: Volume of the control volume j [m^3]

Tw_{j-1}: Mean water temperature of the control volume (j-1) [^{0}C]

Tw_j: Mean water temperature of the control volume j [^{0}C]

$Tp_{i,j}$: Temperature of the absorber element i,j [^{0}C]

$h_{w_{i,j}}$: Convection coefficient at waterside of the absorber element i,j [W/m^2 ^{0}C]

Equation 6.1 is transformed to finite difference form as shown below

$$\left[\dot{m}c_{w_j}(Tw_{j-1} - Tw_j) + A_j\sum_{i=1}^{K}\left[h_{w_{i,j}}(Tp_{i,j} - Tw_j)\right]\right]^p = V_j\left(\rho_{w_j}c_{w_j}\right)^p\frac{Tw_j^{p+1} - Tw_j^p}{\Delta t} \qquad (6.2)$$

By rearranging the equation above, temperature after a time interval Δt for the control volume j is obtained :

$$Tw_j^{p+1} = Tw_j^p + \frac{\Delta t}{V_j\left(\rho_{w_j}c_{w_j}\right)^p}\left[\dot{m}c_{w_j}(Tw_{j-1} - Tw_j) + A_j\sum_{i=1}^{K}\left[h_{w_{i,j}}(Tp_{i,j} - Tw_j)\right]\right]^p \qquad (6.3)$$

where thermodynamical properties of water are calculated using equations below derived from tables in Referance [24].

$$c_w = 3.178x10^{-6}Tw^4 - 7.791x10^{-4}Tw^3 + 0.076Tw^2 - 2.963Tw + 4.217x10^3 \quad (6.4)$$

$$\rho_w = -1.768x10^{-7}Tw^4 + 5.061x10^{-5}Tw^3 - 8.13x10^{-3}Tw^2 + 0.065Tw + 999.784 \quad (6.5)$$

(Temperatures are in ^0C)

Initial conditions for the temperature distribution in plate and water are stated below :

$Tw_j = Tp_{i,j} = T_{in} = T_{out}$ (p = 0)

In these statements, the subscript i takes all values between 1 and K and the subscript j takes all values between 1 and L+1. In addition, definitions below are made to use in the computer program :

$Tw_0 = T_{in}$

$Tw_{L+1} = Tw_{L+2} = T_{out}$

6.2. Energy Balance Equations for the Absorber

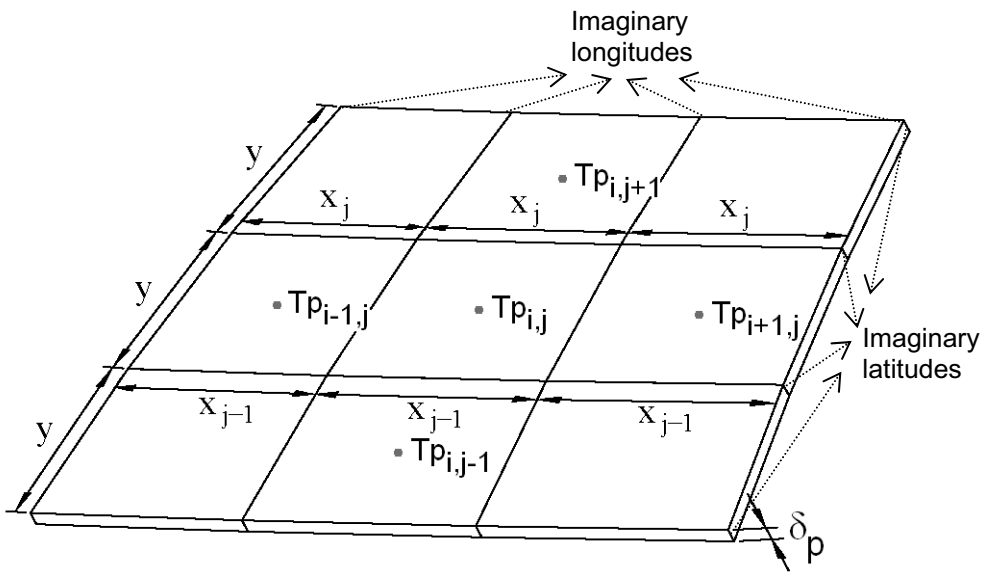

Figure 6.2 Finite Differences Model for the Absorber Plate

In Figure 6.2, y is distance between the imaginary latitudes on the spherical absorber surface and x is the distance between the imaginary longitudes. Although the distance between the latitudes is fixed, distance between the longitudes changes. Therefore a subscript is used for x and its value is determined as a function of location on the spherical surface.

In order to simplify the analysis, view factor is chosen as one.

Starting from the conservation of energy, energy balance for the absorber element i,j on Figure 6.2 is found as below (Figure 6.3) :

$$\begin{bmatrix}\text{Solar energy}\\ \text{absorbed by}\\ \text{the absorber}\end{bmatrix} - \begin{bmatrix}\text{Convection and}\\ \text{radiation losses}\\ \text{to the cover}\end{bmatrix} - \begin{bmatrix}\text{Convection}\\ \text{heat transfer}\\ \text{to the water}\end{bmatrix} - \begin{bmatrix}\text{Conduction}\\ \text{heat transfer}\\ \text{to neighboring}\\ \text{elements}\end{bmatrix} = \begin{bmatrix}\text{Rate of change of}\\ \text{total energy in the}\\ \text{absorber element}\end{bmatrix}$$

$$\begin{aligned}
&A_j G_{i,j}(\tau\alpha)_{i,j} - (h_{pc_{i,j}} + h_{rpc_{i,j}})A_j(Tp_{i,j} - Tc_{i,j}) - h_{w_{i,j}}A_j(Tp_{i,j} - Tw_j)\\
&-k(x_j\delta_p)\frac{Tp_{i,j} - Tp_{i,j+1}}{y} - k(x_{j-1}\delta_p)\frac{Tp_{i,j} - Tp_{i,j-1}}{y}\\
&-k(y\delta_p)\frac{Tp_{i,j} - Tp_{i+1,j}}{\left(\frac{x_{j-1} + x_j}{2}\right)} - k(y\delta_p)\frac{Tp_{i,j} - Tp_{i-1,j}}{\left(\frac{x_{j-1} + x_j}{2}\right)} = \rho_a V_{i,j} c_a \frac{dTp_{i,j}}{dt}
\end{aligned} \tag{6.6}$$

$(1 \le i \le K \;,\; 1 \le j \le L+1 \;)$

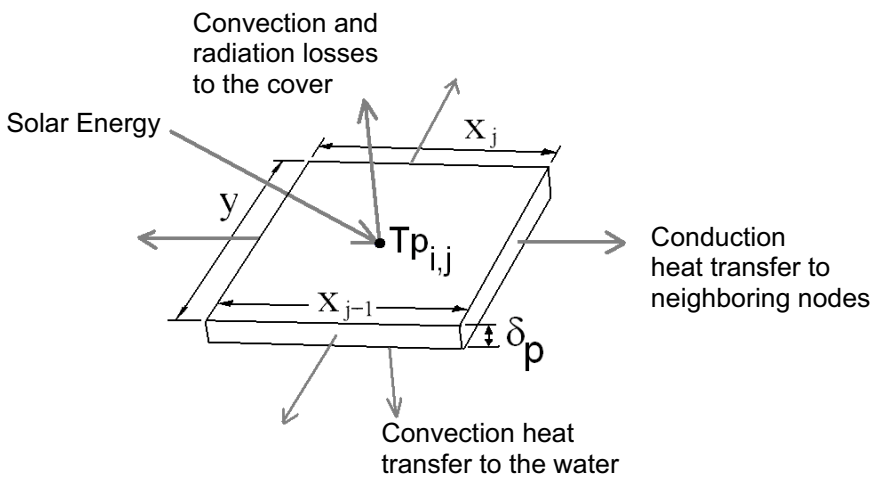

Figure 6.3 Heat Transfers at Absorber Element i,j

where;

A_j : Surface area of each enclosing absorber elements of the control volume j [m^2]

$V_{i,j}$: Volume of each enclosing absorber elements of the control volume j [m^3]

$G_{i,j}$: Solar energy incident on glass cover element i,j [W/m^2]

$(\tau\alpha)_{i,j}$: Transmittance-absorptance product for the absorber-cover elements i,j

$h_{pc_{i,j}}$: Convection coefficient between the absorber-cover elements i,j [$W/m^2\,{}^0C$]

$h_{rpc_{i,j}}$: Radiation coefficient between the absorber-cover elements i,j [$W/m^2\,{}^0C$]

$Tp_{i,j}$: Temperature of the absorber element i,j [^0C]

$Tc_{i,j}$: Temperature of the cover element i,j [^0C]

$h_{w_{i,j}}$: Convection coefficient at waterside of the absorber element i,j [$W/m^2\,{}^0C$]

Tw_j : Mean water temperature of the control volume j [^0C]

k_a : Thermal conductivity of absorber material [$W/m\,{}^0C$]

c_a : Specific heat of the absorber material [$J/kg\,{}^0C$]

ρ_a : Density of the absorber material [kg/m^3]

x_j , x_{j+1} : Latitudinal dimensions of the absorber element I,j [m]

y : Longitudinal dimension of each absorber element [m]

δ_p : Thickness of the absorber [m]

Equation 6.6 is transferred to finite difference form as below :

$$\left[A_j G_{i,j}(\tau\alpha)_{i,j} - (h_{pc_{i,j}} + h_{rpc_{i,j}}) A_j (Tp_{i,j} - Tc_{i,j}) - h_{w_{i,j}} A_j (Tp_{i,j} - Tw_j) \right.$$
$$-k(x_j \delta_p) \frac{Tp_{i,j} - Tp_{i,j+1}}{y} - k(x_{j-1}\delta_p) \frac{Tp_{i,j} - Tp_{i,j-1}}{y} \tag{6.7}$$
$$\left. -k(y\delta_p) \frac{Tp_{i,j} - Tp_{i+1,j}}{(x_{j-1} + x_j)/2} - k(y\delta_p) \frac{Tp_{i,j} - Tp_{i-1,j}}{(x_{j-1} + x_j)/2} \right]^p = \rho_a V_{i,j} c_a \frac{Tp_{i,j}^{p+1} - Tp_{i,j}^{p}}{\Delta t}$$

Temperature of the plate element after a time interval Δt can be obtained as below :

$$Tp_{i,j}^{p+1} = Tp_{i,j}^{p} + \frac{\Delta t}{\rho_a V_{i,j} c_a} \left[A_j G_{i,j}(\tau\alpha)_{i,j} - (h_{pc_{i,j}} + h_{rpc_{i,j}}) A_j (Tp_{i,j} - Tc_{i,j}) \right.$$
$$-h_{w_{i,j}} A_j (Tp_{i,j} - Tw_j) - k(x_j \delta_p) \frac{Tp_{i,j} - Tp_{i,j+1}}{y} - k(x_{j-1}\delta_p) \frac{Tp_{i,j} - Tp_{i,j-1}}{y} \tag{6.8}$$
$$\left. -k(y\delta_p) \frac{Tp_{i,j} - Tp_{i+1,j}}{(x_{j-1} + x_j)/2} - k(y\delta_p) \frac{Tp_{i,j} - Tp_{i-1,j}}{(x_{j-1} + x_j)/2} \right]^p$$

$(1 \le i \le K \;,\; 1 \le j \le L+1 \;)$

where;

$$h_{rpc_{i,j}} = \frac{\sigma (Tp_{i,j} + Tc_{i,j})(Tp_{i,j}^{2} + Tc_{i,j}^{2})}{\frac{1}{\varepsilon_p} + \frac{1}{\varepsilon_c} - 1} \tag{6.9}$$

ε_p and ε_c are emissivities of the plate and the cover, σ is the Stefan-Boltzmann constant.

$$\sigma = 5.67\ 10^{-8}\ \frac{W}{m^2K^4}$$

Initial condition for the temperature distribution in cover is stated below :

$$T_{c_{i,j}} = T_a \quad (p = 0)$$

In this statement, the subscript i takes all values between 1 and K and the subscript j takes all values between 1 and L+1. In addition, assumptions below are defined :

$$Tp_{i,0} = T_{in}$$

$$Tp_{i,L+1} = T_{out}$$

Because of the spherical geometry, $Tp_{K+1,j} = Tp_{1,j}$

6.3. Energy Balance Equations for the Cover

Energy balance equations for the cover are obtained by making calculations similar to that of the absorber. But, due to low thermal conductivity of glass, thermal conduction heat transfer between the neighboring glass pieces are ignored.

$$\begin{bmatrix}\text{Solar energy}\\ \text{absorbed by}\\ \text{the cover}\end{bmatrix} - \begin{bmatrix}\text{Convection and}\\ \text{radiation losses}\\ \text{to environment}\end{bmatrix} + \begin{bmatrix}\text{Convection and}\\ \text{radiation heat transfer}\\ \text{from the absorber}\end{bmatrix} = \begin{bmatrix}\text{Rate of change of}\\ \text{total energy in the}\\ \text{cover element}\end{bmatrix}$$

Energy balance for the cover element becomes :

$$A_j G_{i,j} \alpha_{c_{i,j}} - (h_{ca_{i,j}} + h_{rca_{i,j}}) A_j (Tc_{i,j} - Ta) + (h_{pc_{i,j}} + h_{rpc_{i,j}}) A_j (Tp_{i,j} - Tc_{i,j}) = \rho_c V_{i,j} c_c \frac{dTc_{i,j}}{dt} \quad (6.10)$$

$(1 \le i \le K \;,\; 1 \le j \le L+1 \;)$

where;

A_j : Surface area of each enclosing cover elements of jth control volume (For simplicity, it is taken as equal to that of enclosing absorber elements) $[m^2]$

$V_{i,j}$: Volume of each enclosing cover elements of jth control volume (For simplicity, it is taken as equal to that of enclosing absorber elements) $[m^3]$

$G_{i,j}$: Solar energy incident on the glass cover element i,j $[W/m^2]$

$\alpha_{c_{i,j}}$: Absorptance of the cover element i,j

$h_{pc_{i,j}}$: Convection coefficient between the absorber-cover elements i,j $[W/m^2\,{}^0C]$

$h_{rpc_{i,j}}$: Radiation coefficient between the absorber-cover elements i,j $[W/m^2\,{}^0C]$

$h_{ca_{i,j}}$: Convection coefficient at outer surface of the cover $[W/m^2\,{}^0C]$

$h_{rca_{i,j}}$: Radiation coefficient between the cover element i,j and sky $[W/m^2\,{}^0C]$

$Tp_{i,j}$: Temperature of the absorber element i,j $[{}^0C]$

$Tc_{i,j}$: Temperature of the cover element i,j $[{}^0C]$

T_a : Ambient temperature $[{}^0C]$

c_c : Specific heat of glass $[J/kg\,{}^0C]$

ρ_c : Density of glass [kg/m^3]

Finite difference form of this equation and the temperature after a time interval of Δt becomes :

$$\left[A_j G_{i,j}\alpha_{c_{i,j}} - (h_{ca_{i,j}} + h_{rca_{i,j}})A_j(Tc_{i,j} - Ta) + (h_{pc_{i,j}} + h_{rpc_{i,j}})A_j(Tp_{i,j} - Tc_{i,j})\right]^p = \rho_c V_{i,j} c_c \frac{Tc_{i,j}^{p+1} - Tc_{i,j}^{p}}{\Delta t} \tag{6.11}$$

$$Tc_{i,j}^{p+1} = Tc_{i,j}^{p} + \frac{\Delta t}{\rho_c V_{i,j} c_c}\left[A_j G_{i,j}\alpha_{c_{i,j}} - (h_{ca_{i,j}} + h_{rca_{i,j}})A_j(Tc_{i,j} - Ta) + (h_{pc_{i,j}} + h_{rpc_{i,j}})A_j(Tp_{i,j} - Tc_{i,j})\right]^p \tag{6.12}$$

$(1 \le i \le K \;,\; 1 \le j \le L+1)$

where;

$$h_{rca_{i,j}} = \frac{\sigma\varepsilon_c(Tc_{i,j} + T_s)(Tc_{i,j}^{2} + T_s^{2})(Tc_{i,j} - T_s)}{(Tc_{i,j} - T_a)} \tag{6.13}$$

For the temperature of sky, assumption below is defined [20] :

$$T_s = T_a - 6$$

Calculation of temperature distribution of the water, absorber and cover are made by using the finite difference equations obtained above. In addition to these, calculation of the solar energy incident on each cover element is also made. One of the important parameters in this analysis is tilt angle of an

absorber element and the cover element, which is not fixed but varies over the spherical surface. To calculate the incident radiation, each absorber-cover element pair is considered as a flat collector. Then, the solar radiation incident on each can be calculated according to the models given in Section 3.3. Another important parameter for incident solar radiation is the surface azimuth angle. Calculations of the tilt angles, the surface azimuth angles and surface areas are presented below.

6.4. Calculation of Surface Area of the Absorber and the Cover Elements

This analysis can be made by choosing a spherical coordinate system at the center of the spherical absorber, and defining the angles below in the coordinate system (Figure 6.5) :

$$\Delta\varphi = \frac{360°}{K} \tag{6.14}$$

$$\varphi = \left(\frac{2i-1}{2}\right)\Delta\varphi \quad , \quad (1 \leq i \leq K) \tag{6.15}$$

$$\Delta\xi = \frac{180°}{L+1} \tag{6.16}$$

$$\xi = 180° - j\Delta\xi \quad , \quad (1 \leq j \leq L+1) \tag{6.17}$$

where φ is in x-y plane and it is the angle defined from positive x-axis to positive y-axis, and ξ is the angle defined from positive z-axis to x-y plane (Figure 6.4).

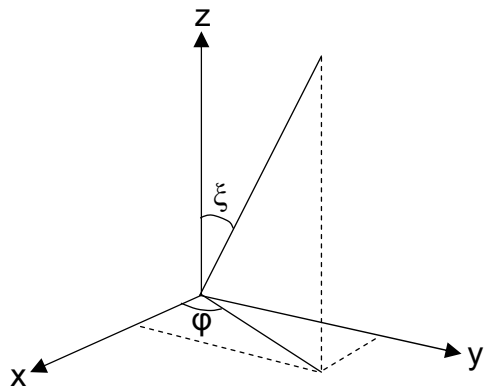

Figure 6.4 Spherical Coordinate System

An absorber element has a flat and trapezoidal shape. Therefore its area is found by using the following equation.

$$A_j = \frac{x_{j-1} + x_j}{2} h_j \tag{6.18}$$

x_{j-1} , x_j and y are edges and h_j is height of the absorber element i,,j (Figure 6.5). The edges can be calculated using related coordinates of the absorber element and law of cosines and h_j is calculated using Pythagorean theorem as follows :

$$x_{j-1} = \sqrt{2}\ R_p \sin(\xi + \Delta\xi)\sqrt{(1 - \cos\Delta\varphi)} \tag{6.19}$$

$$x_j = \sqrt{2}\ R_p \sin\xi\sqrt{(1 - \cos\Delta\varphi)} \tag{6.20}$$

$$y = \sqrt{2}\ R_p\sqrt{(1 - \cos\Delta\xi)} \tag{6.21}$$

$$h_j = \sqrt{y^2 - \left(\frac{x_{j-1} - x_j}{2}\right)^2} \tag{6.22}$$

Surface area of the cover element i,j , above the absorber element i,j , is found by

$$A_{c_j} = \frac{R_c}{R_p} A_j \tag{6.23}$$

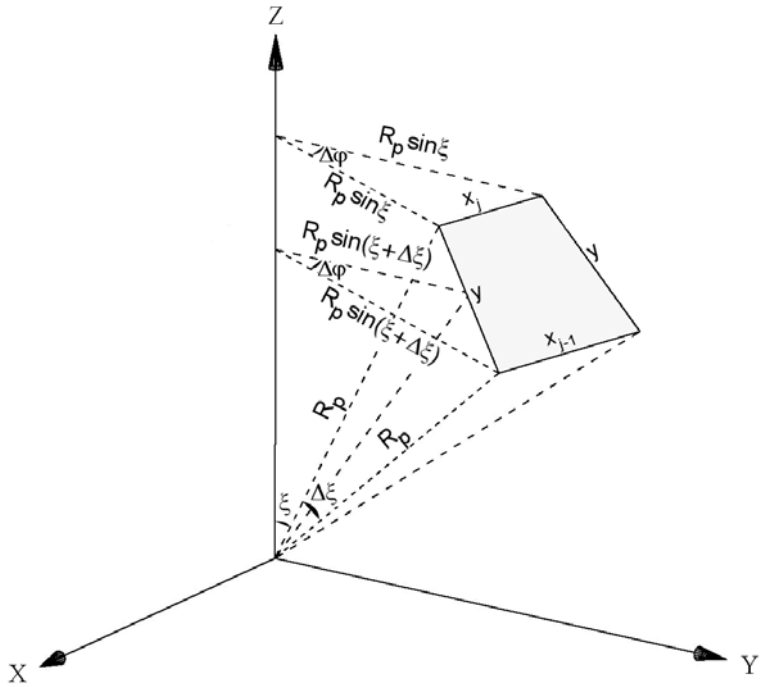

Figure 6.5 Dimensions of an Absorber Element

6.5. Calculation of Tilt Angle of the Absorber and the Cover Elements

Tilt angle of absorber-cover element pair i,j , which is an important parameter in solar energy calculations, can be calculated with the help of Figure 6.6 , Figure 6.7.a and Figure 6.7.b. We can determine the tilt angles using only geometrical parameters of absorber elements

In the Figures, h_j is height of an absorber element and a_j is distance in z-direction between x_{j-1} and x_j. a_j is calculated as

$$a_j = R_p\left[\cos\xi - \cos\left(\xi + \Delta\xi\right)\right] \tag{6.24}$$

An absorber element has a trapezoidal shape. Therefore h_j is height of a trapezoid and calculated by using Equation (6.22) .

Tilt angle of the absorber-cover element pair i,j is calculated considering its location at upper side and lower side of the spherical collector:

At upper side, the tilt angle is found as below by using Figure 6.6.

$$\beta_j = \sin^{-1}\left(\frac{a_j}{h_j}\right) \tag{6.25}$$

At lower side, the tilt angle is found as below using Figure 6.7.b.

$$\beta_j = 180° - \sin^{-1}\left(\frac{a_j}{h_j}\right) \tag{6.26}$$

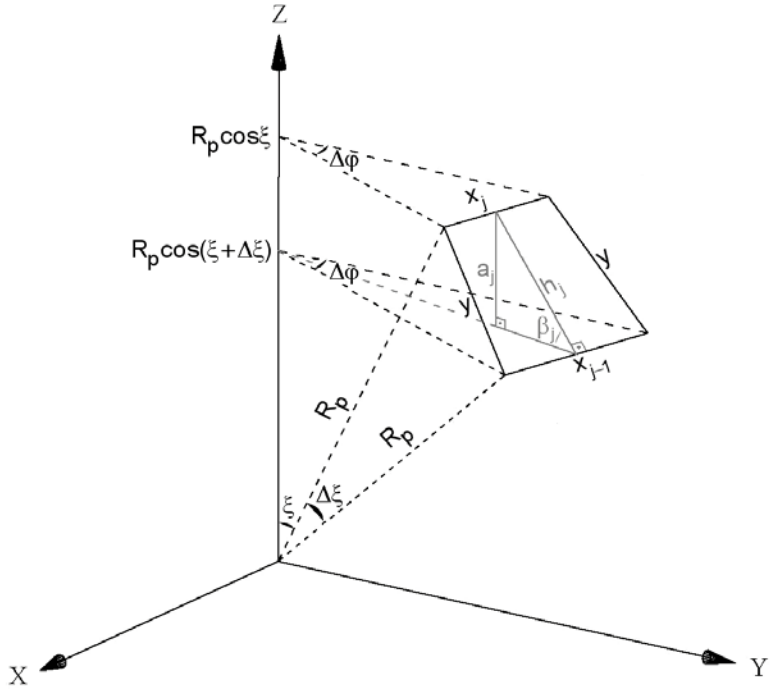

Figure 6.6 Tilt Angle at upper Hemispherical Volume

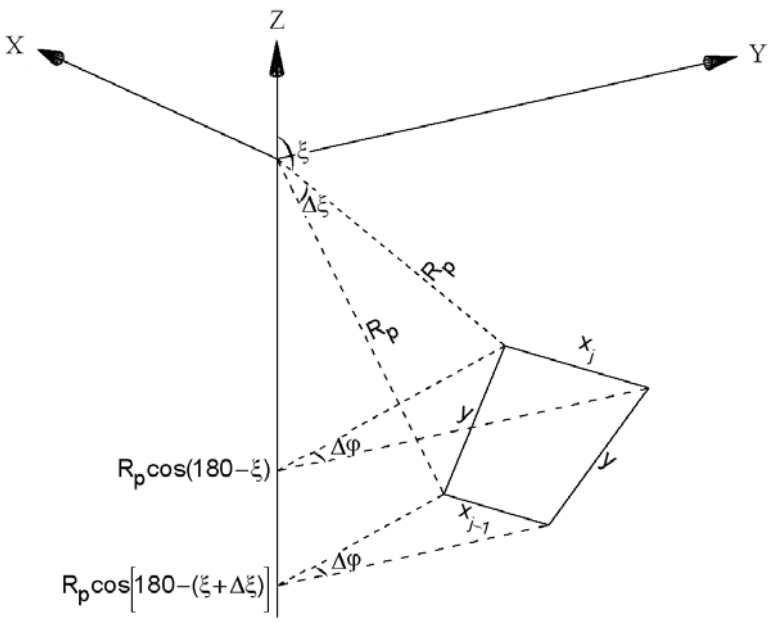

Figure 6.7.a Location of an Absorber Element at lower Hemispherical Volume

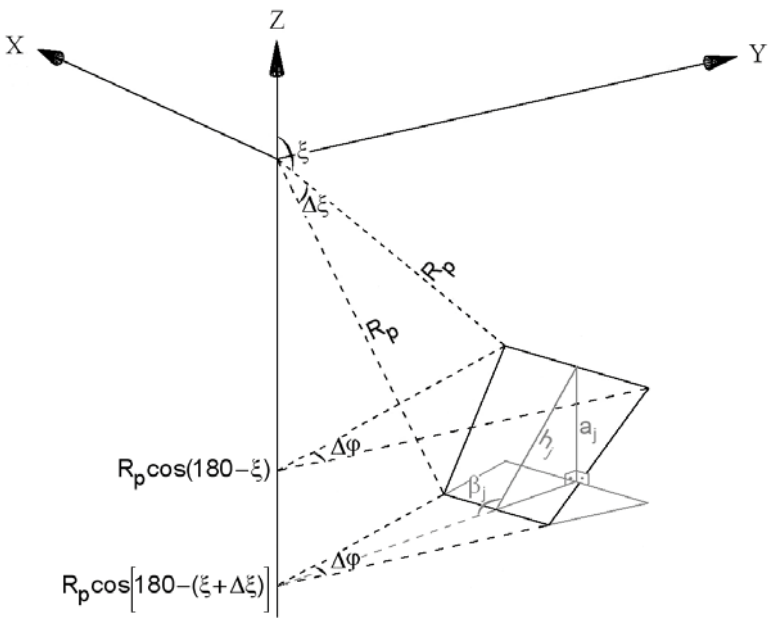

Figure 6.7.b Tilt Angle at lower Hemispherical Volume

In summary, tilt angle of the absorber-cover element pair i,j becomes

$$\beta_j = \begin{cases} \sin^{-1}\left(\dfrac{a_j}{h_j}\right) & , \quad \cos\xi \geq 0 \\ 180° - \sin^{-1}\left(\dfrac{a_j}{h_j}\right) & , \quad \cos\xi < 0 \end{cases} \tag{6.27}$$

6.6. Calculation of Control Volumes and Calculation of Volume of the Tank

Volume of the absorber element i,j is calculated as

$$V_{i,j} = A_j \ \delta_p \tag{6.28}$$

Volume of the cover element i,j is calculated as

$$V_{c_{i,j}} = A_{c_j} \ \delta_c \tag{6.29}$$

Volume of the control volume j in water is calculated at upper hemisphere and lower hemisphere of the tank. For this analysis, each control volume is divided into smaller volumes as shown in Figure 6.8 and Figure 6.9.

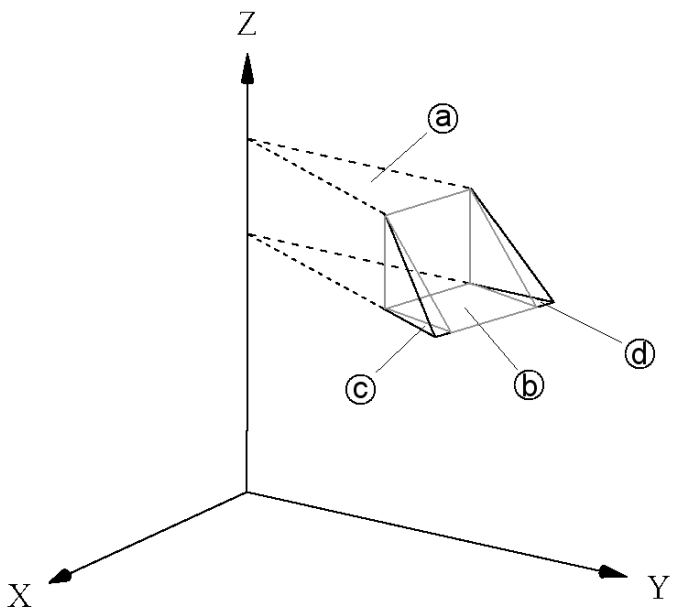

Figure 6.8 The Control Volume j at upper Hemispherical Volume

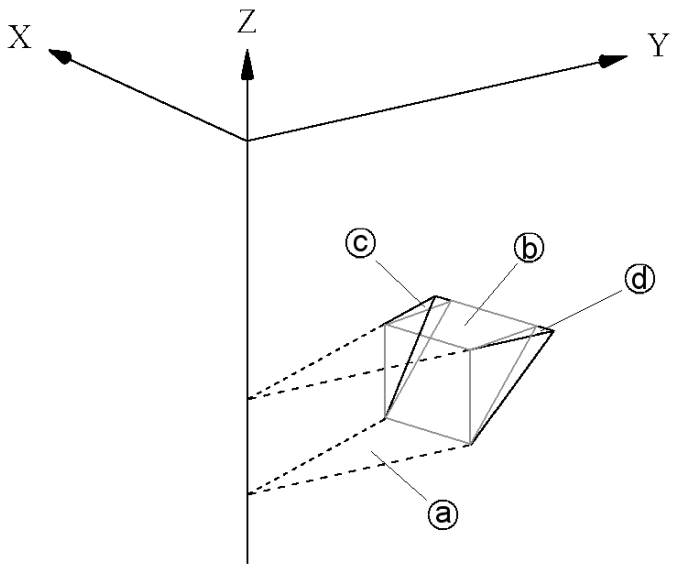

Figure 6.9 The Control Volume j at lower Hemispherical Volume

According to these figures, each control volume is divided into smaller volumes such that

$$V_j = \frac{360}{\Delta\phi}\left(V_a + V_b + V_c + V_d\right) \tag{6.30}$$

where V_a, V_b, V_c and V_d are sub-volumes of each control volume, V_j.

Equations that give the sub-volumes are summarized in Table 6.1.

Table 6.1 Equations to Calculate the Sub-Volumes of Each Control Volume In the Tank

	at upper hemispherical volume ($\cos\xi \geq 0$)	at lower hemispherical volume ($\cos\xi < 0$)
V_a	$\left[\frac{1}{2}\left(R_p \sin\xi\right)^2 \sin(\Delta\varphi)\right]a_j$	$\left[\frac{1}{2}\left(R_p \sin(\xi+\Delta\xi)\right)^2 \sin(\Delta\varphi)\right]a_j$
V_b	$\left(\frac{a_j\sqrt{h_j^2 - a_j^2}}{2}\right)\left(x_j\right)$	$\left(\frac{a_j\sqrt{h_j^2 - a_j^2}}{2}\right)\left(x_{j-1}\right)$
V_c	$\frac{\left(\frac{1}{2}\left[R_p\left(\sin\left(\xi+\Delta\xi\right)-\sin\xi\right)\right]^2 \sin(\Delta\varphi)\right)a_j}{6}$	$\frac{\left(\frac{1}{2}\left[R_p\left(\sin\left(\xi+\Delta\xi\right)-\sin\xi\right)\right]^2 \sin(\Delta\varphi)\right)a_j}{6}$
V_d	$V_d = V_c$	$V_d = V_c$

Consequently, size of the control volume j can be expressed as follows:

$$V_j = \begin{cases} \frac{360°}{\Delta\varphi}\left[\left[\frac{1}{2}\left(R_p \sin\xi\right)^2 \sin(\Delta\varphi)\right]a_j + \left(\frac{a_j\sqrt{h_j^2 - a_j^2}}{2}\right)x_j \right. \\ \left. \quad + \left(\frac{1}{6}\left[R_p\left(\sin\left(\xi+\Delta\xi\right)-\sin\xi\right)\right]^2 \sin(\Delta\varphi)\right)a_j\right] \quad , \quad \cos\xi \geq 0 \\ \frac{360°}{\Delta\varphi}\left[\left[\frac{1}{2}\left(R_p \sin\left(\xi+\Delta\xi\right)\right)^2 \sin(\Delta\varphi)\right]a_j + \left(\frac{a_j\sqrt{h_j^2 - a_j^2}}{2}\right)x_{j-1} \right. \\ \left. \quad + \left(\frac{1}{6}\left[R_p\left(\sin\left(\xi+\Delta\xi\right)-\sin\xi\right)\right]^2 \sin(\Delta\varphi)\right)a_j\right] \quad , \quad \cos\xi < 0 \end{cases} \tag{6.31}$$

Volume of the tank, then, becomes

$$V_{tank} = \sum_{j=1}^{L} V_j \tag{6.32}$$

6.7. Results of the Numerical Simulation

For the numerical simulation, a computer program in Mathcad was written [Appendix C]. In this program, measured values of solar radiation on horizontal surface, ambient temperature and water inlet temperature were used as input data. For comparison purpose, change of mean tank temperature and hot water outlet temperature with time were simulated.

In this program, time step was chosen as 1 s and for the input data between measurement times linear interpolation was used. The solar radiation absorbed by the collector was calculated using Equation (3.45). For the calculation of convection heat transfers at water side of the absorber, between the absorber and the cover and between the outer surface of the cover and the ambient the following heat transfer coefficients are used in the computer program.

$$h_w = 300 \ \frac{watt}{m^2K} \tag{6.33}$$

$$h_{pc} = 7 \ \frac{watt}{m^2K} \tag{6.34}$$

$$h_{ca} = 5 \ \frac{watt}{m^2K} \tag{6.36}$$

Results of the program are shown in Figures 6.9 to 6.13. It is seen from these graphs and from Table 6.2 that, the numerically obtained results are sufficiently close to the experimental data.

Table 6.2 Error Analysis Results for the Numerical Simulation

Mass flow rate	Maximum error [°C]	Average error [°C]	Standard error [°C]
Non-flow	3.742	1.086	1.343
0.0023 kg/s	2.186	0.980	1.120
0.0055 kg/s	1.466	0.599	0.719
0.0077 kg/s	3.223	0.958	1.238
0.011 kg/s	1.109	0.573	0.650

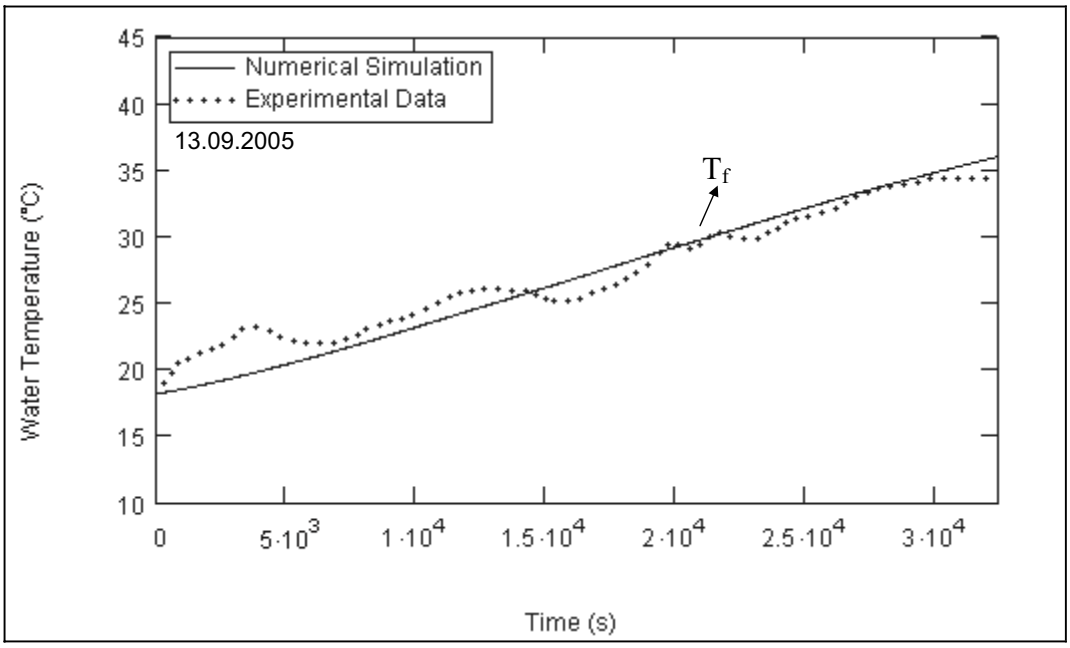

Figure 6.10 Mean Water Temperature Versus Time at Non-flow Situation

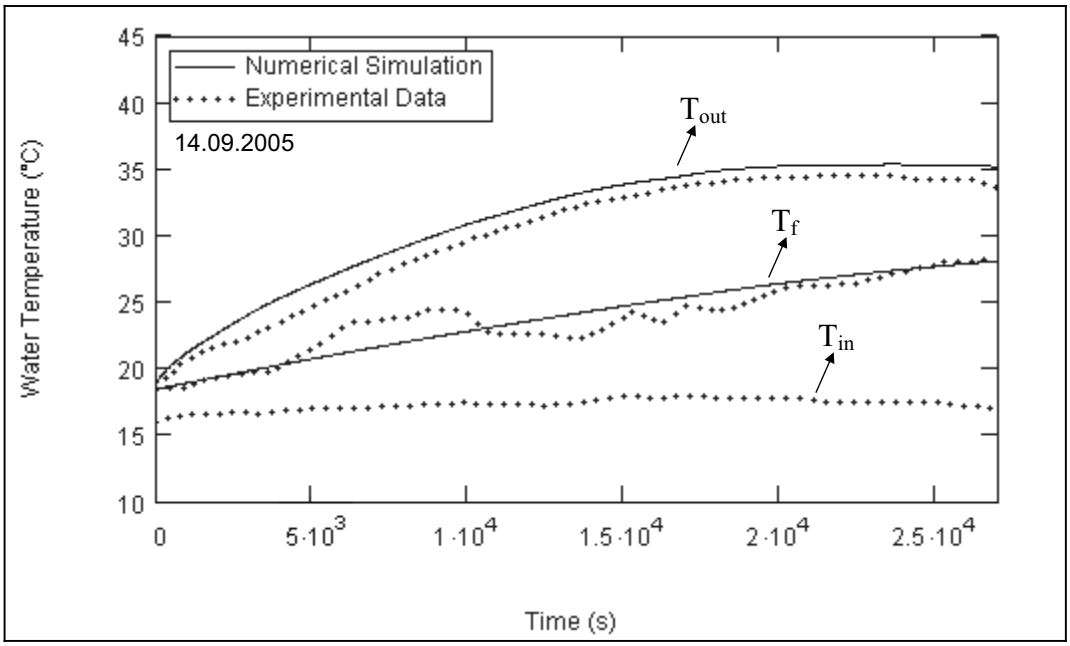

Figure 6.11 Water Temperature Versus Time at Water Mass Flow Rate of 0.0023 kg/s

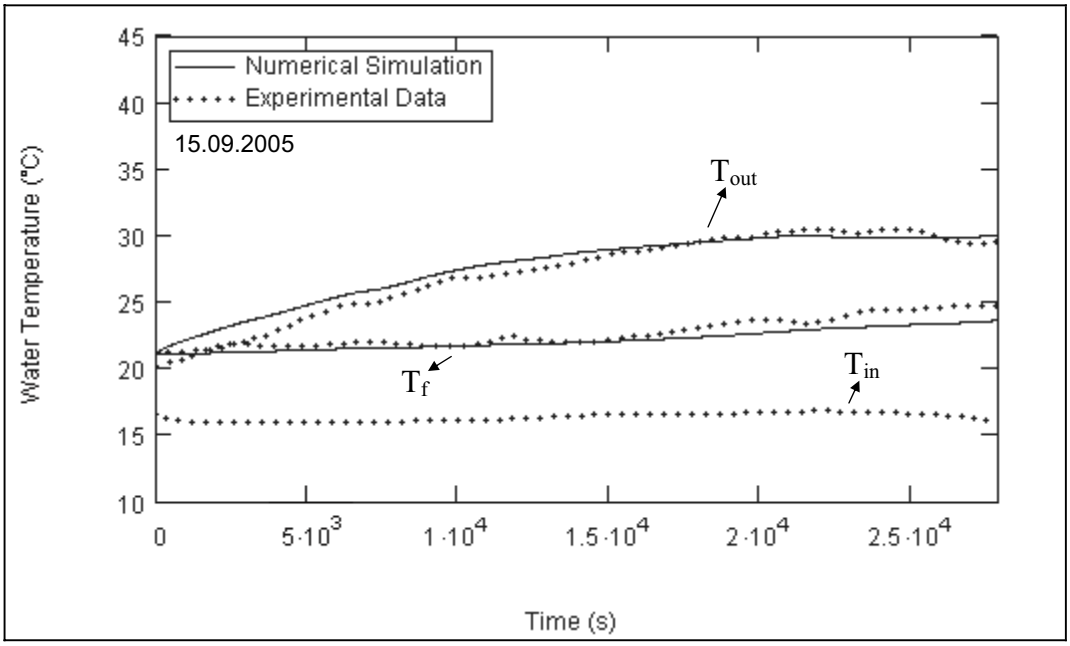

Figure 6.12 Water Temperature Versus Time at Water Mass Flow Rate of 0.0055 kg/s

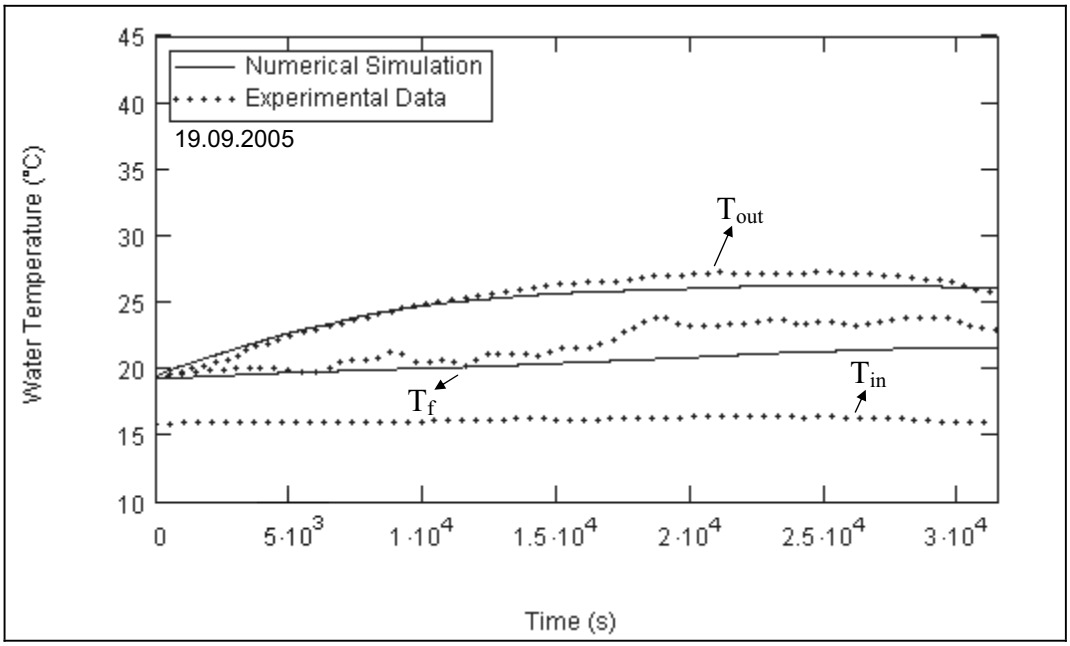

Figure 6.13 Water Temperature Versus Time at Water Mass Flow Rate of 0.0077 kg/s

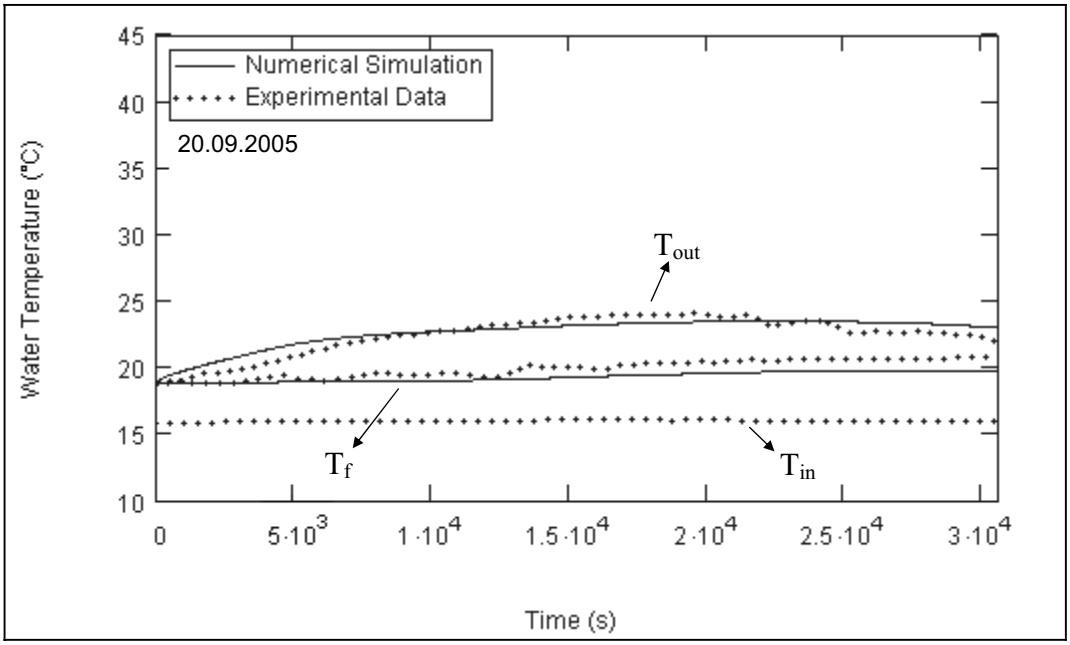

Figure 6.14 Water Temperature Versus Time at Water Mass Flow Rate of 0.011 kg/s

CHAPTER 7

EVALUATION OF THE EXPERIMENTAL RESULTS

The experiments were performed in the months of August, September and October. The tests were made with the flow rates of 0.0023 kg/s, 0.0055 kg/s, 0.0077 kg/s, 0.011 kg/s and for non-flow situation under various ambient temperatures and insolation rates. The range of wind speed was varied between 0 to 2 m/s.

Because of the difficulties which encountered, the data obtained in August were annulled. Thus, only data taken in September and October are taken into account in the analysis. Since the experiments were carried out at small flow rates, it was observed that temperature of the water increased considerably from the mains to the inlet of the collector due to heat gain from the environment. This situation could not previously be controlled. But before the experiments in September, it was thought that if the water mass flow rate in the hose could be increased, the water temperature at collector inlet would be fixed at low temperature. For this purpose a second tap was placed on the hose near the collector inlet. So, mass flow rate within the hose increased and the waste water was drained by this second tap.

During each experiment, local temperatures on the absorber surface and on the cover surface, water temperature at collector inlet and collector outlet, ambient temperature and solar radiation intensity were measured and recorded with a time interval of 15 mins. To measure absorber and cover temperatures a data logger – computer system was used, and to measure water inlet-outlet temperatures and ambient temperature mercury-in-glass

thermometers were employed. Solar radiation intensity was measured using a pyranometer. Local water temperatures within the tank were also measured by the data logger – computer system.

Before the experiments, the spherical collector filled with fresh water and measurements started after the first 30 minutes.

Experimental data are given in Appendix B, and the experimental data are presented in Figures from 7.1 to 7.9.

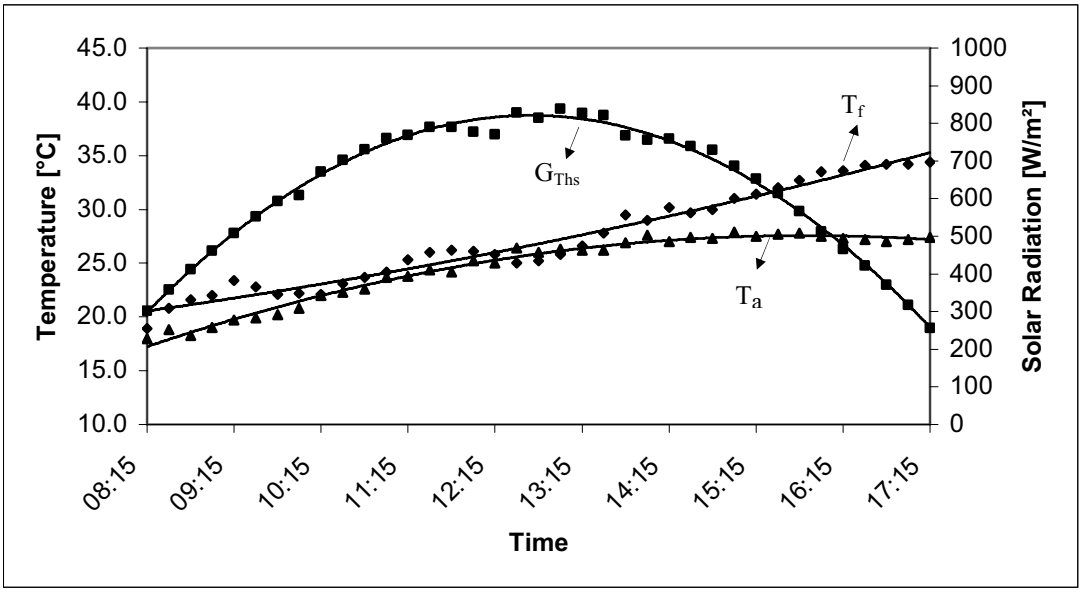

Figure 7.1 Change of Ambient Temperature, Mean Tank Temperature and Solar Radiation on 13 September 2005 (No Flow)

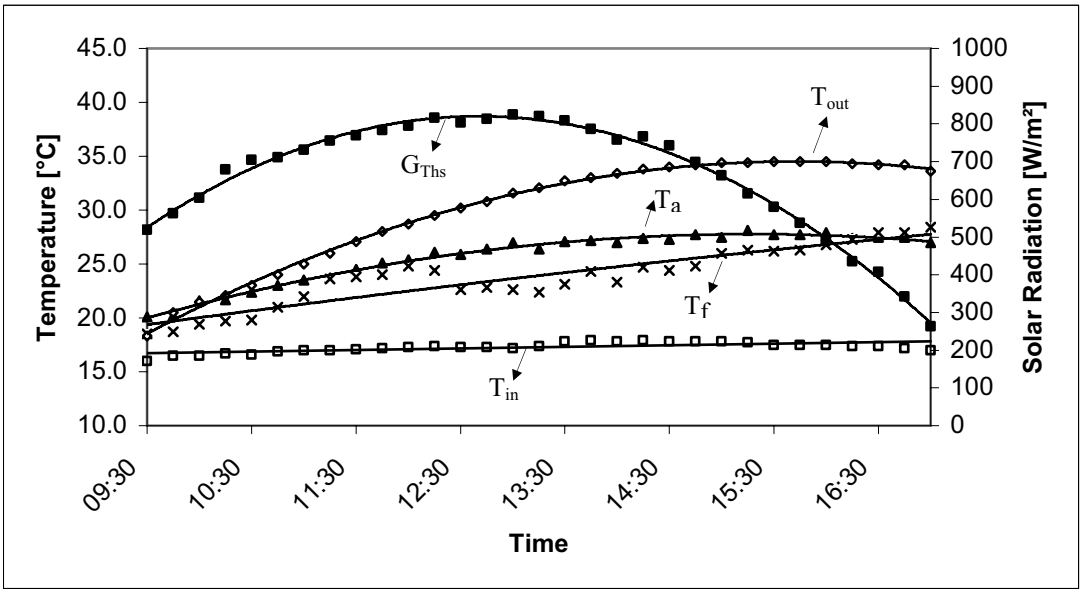

Figure 7.2 Change of Ambient Temperature, Mean Tank Temperature, Inlet Water Temperature, Outlet Water Temperature and Solar Radiation on 14 September 2005 ($\dot{m} = 0.0023 kg/s$)

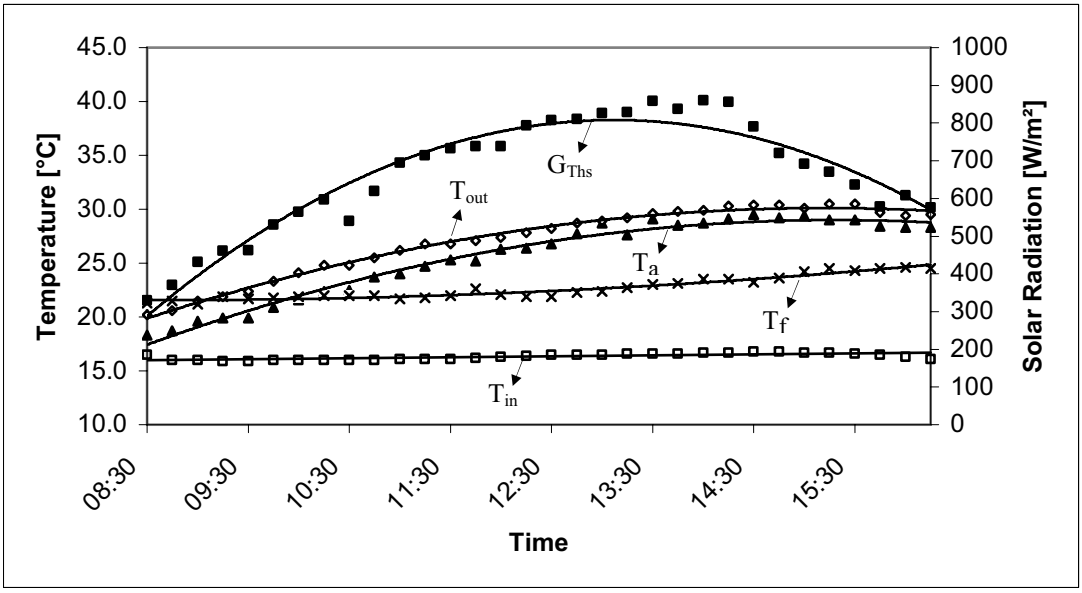

Figure 7.3 Change of Ambient Temperature, Mean Tank Temperature, Inlet Water Temperature, Outlet Water Temperature and Solar Radiation on 15 September 2005 ($\dot{m} = 0.0055 kg/s$)

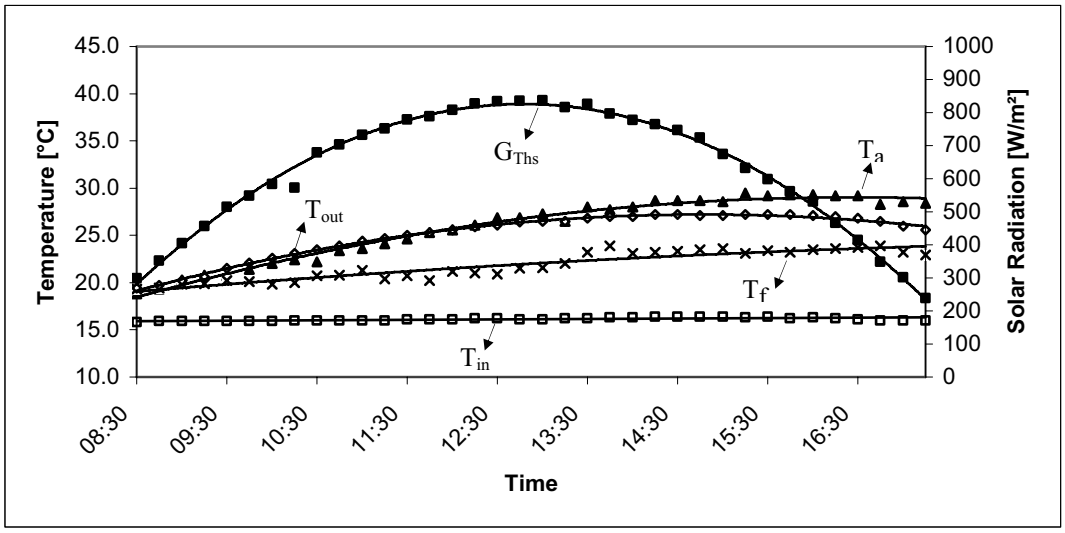

Figure 7.4 Change of Ambient Temperature, Mean Tank Temperature, Inlet Water Temperature, Outlet Water Temperature and Solar Radiation on 19 September 2005 ($\dot{m} = 0.0077 kg/s$)

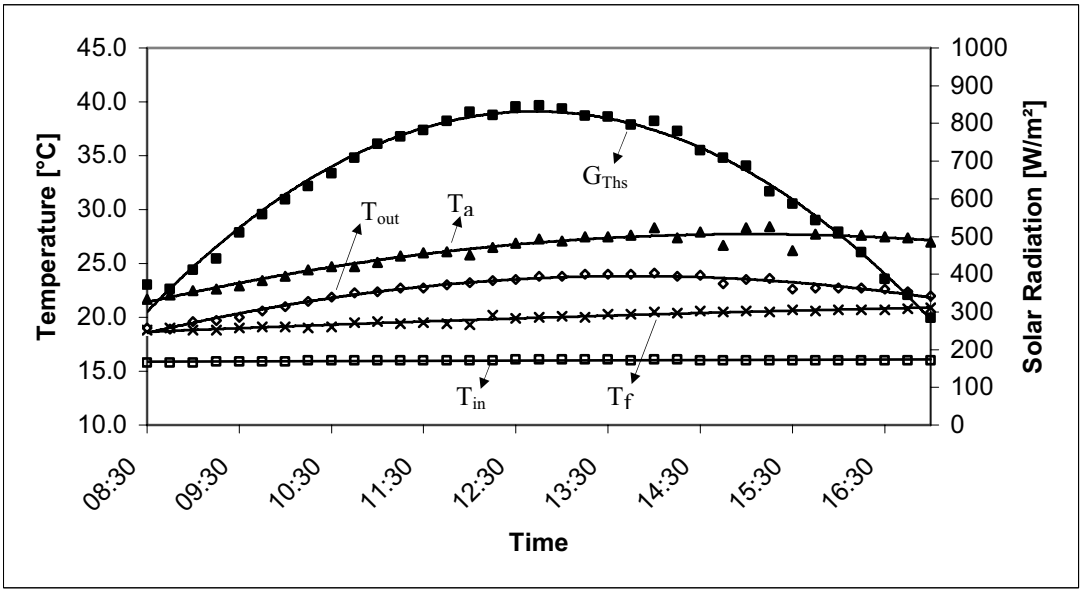

Figure 7.5 Change of Ambient Temperature, Mean Tank Temperature, Inlet Water Temperature, Outlet Water Temperature and Solar Radiation on 20 September 2005 ($\dot{m} = 0.011 kg/s$)

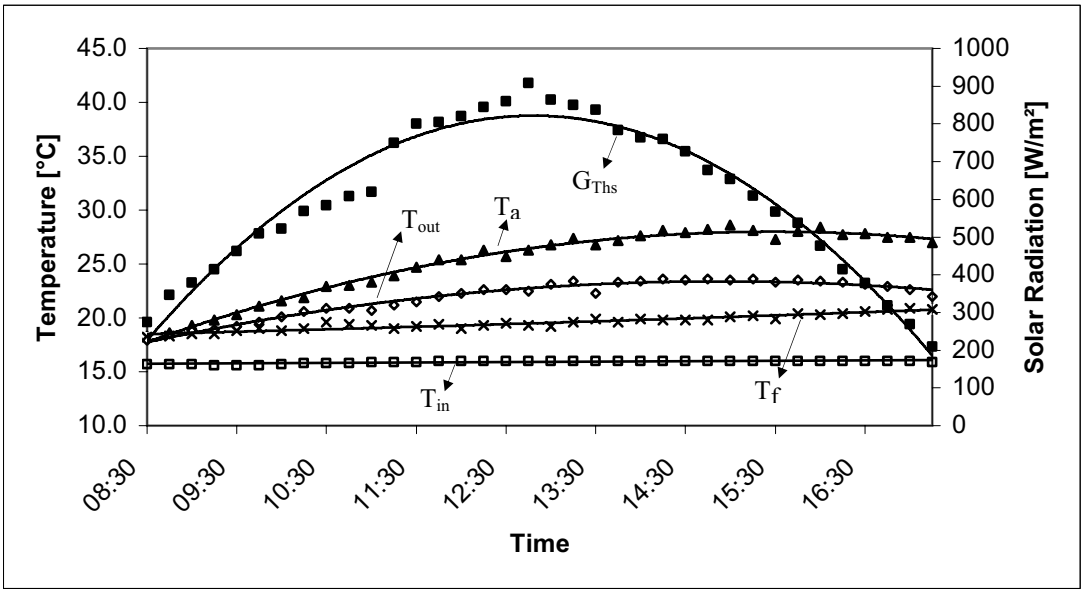

Figure 7.6 Change of Ambient Temperature, Mean Tank Temperature, Inlet Water Temperature, Outlet Water Temperature and Solar Radiation on 21 September 2005 ($\dot{m} = 0.011$kg/s)

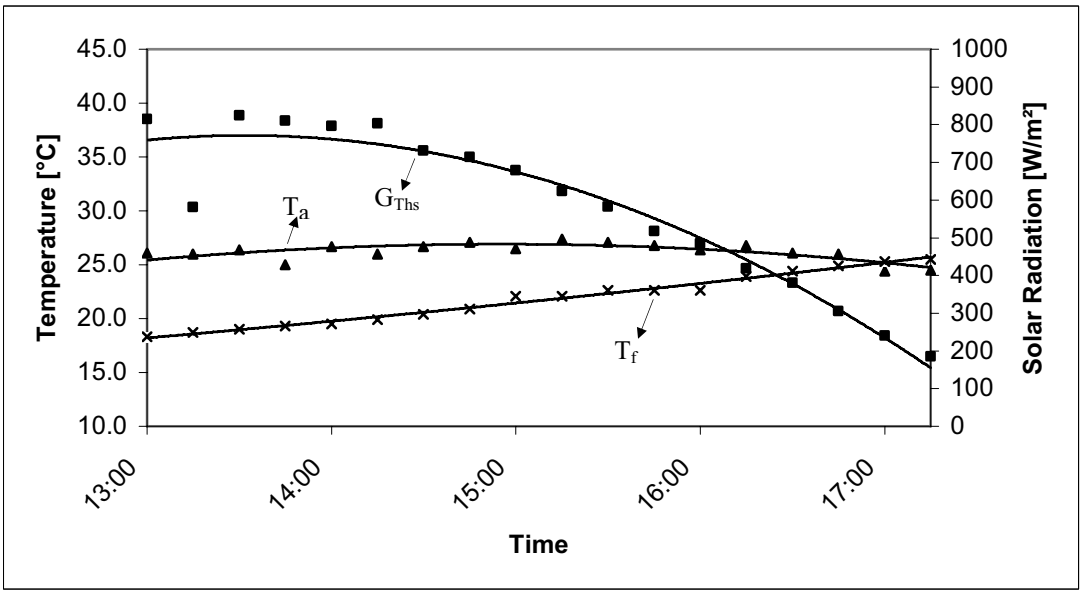

Figure 7.7 Change of Ambient Temperature, Mean Tank Temperature and Solar Radiation on 22 September 2005 (No Flow)

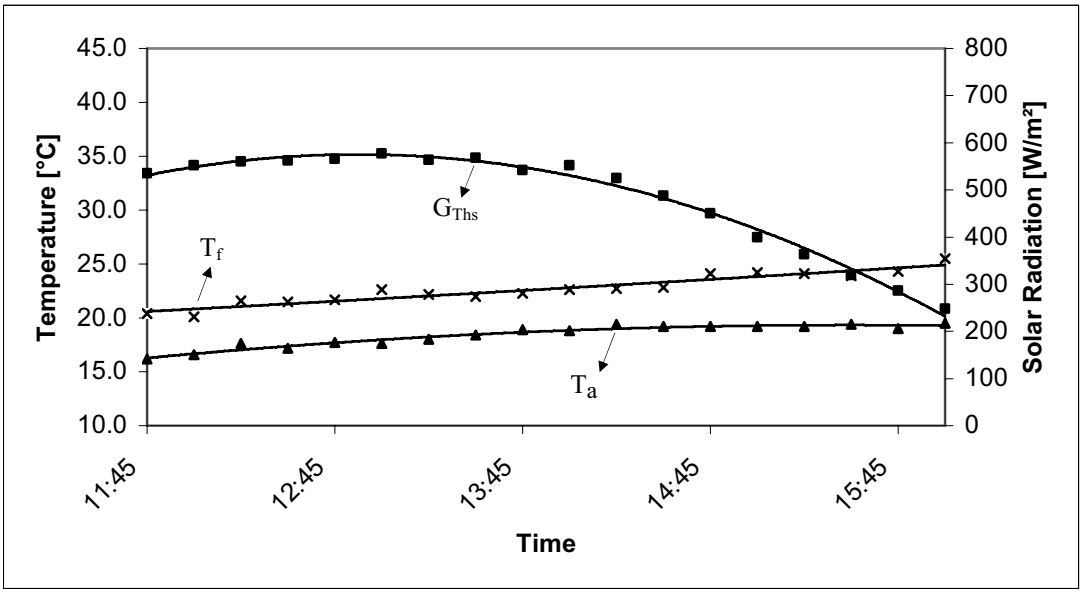

Figure 7.8 Change of Ambient Temperature, Mean Tank Temperature and Solar Radiation on 26 October 2005 (No Flow)

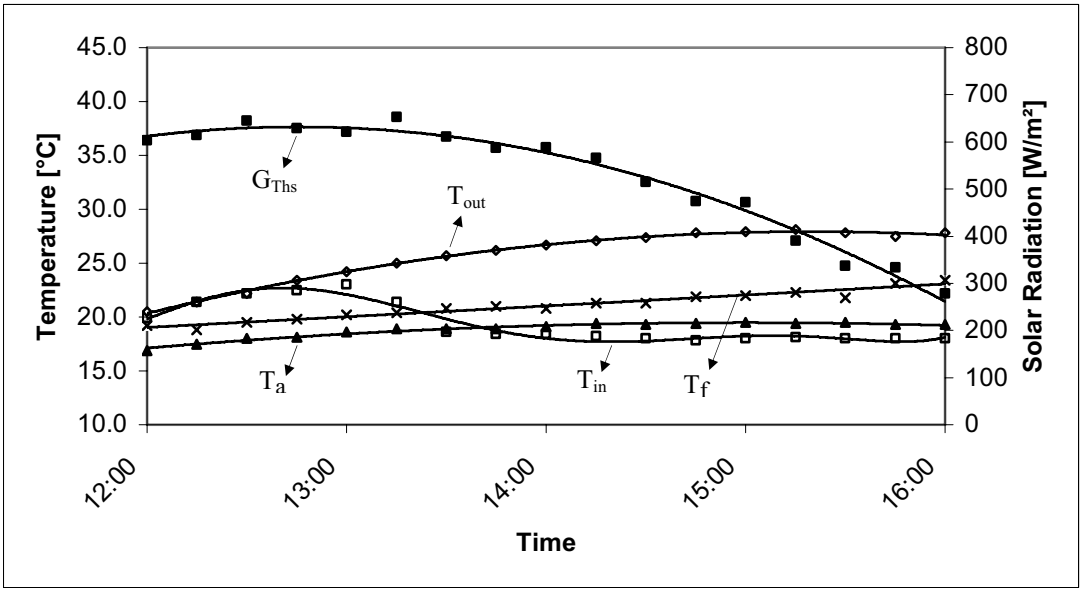

Figure 7.9 Change of Ambient Temperature, Mean Tank Temperature, Inlet Water Temperature, Outlet Water Temperature and Solar Radiation on 27 October 2005 ($\dot{m} = 0.0023 kg/s$)

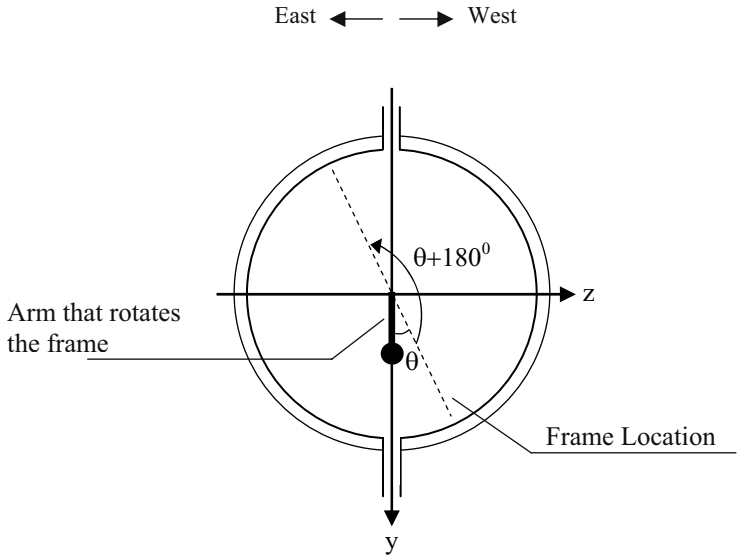

Figure 7.10 Locations of the Semicircular Frame within the Tank at θ and θ+180° Rotation Angles.

The figure above shows locations of the semicircular frame inside the collector. The frame is on the same plane at rotation angles of θ and $\theta + 180°$. Therefore, planer temperature distributions at θ and $\theta + 180°$ were shown on the same figure. In the experiments, water temperature distribution data were taken at θ values from 0^0 to 330^0 with 30^0 increments. Consequently, we can assume that water temperature distribution data were taken with a circular frame at θ values from 0^0 to 150^0 with 30^0 increments. Figures from 7.11 to 7.18 show water temperature distribution in the tank at various rotation angles. In these figures, black legends show the points where the temperature measurements are taken.

It is seen from these figures that there is stratification within the stored water, and the stratification increases near the hot absorber surface.

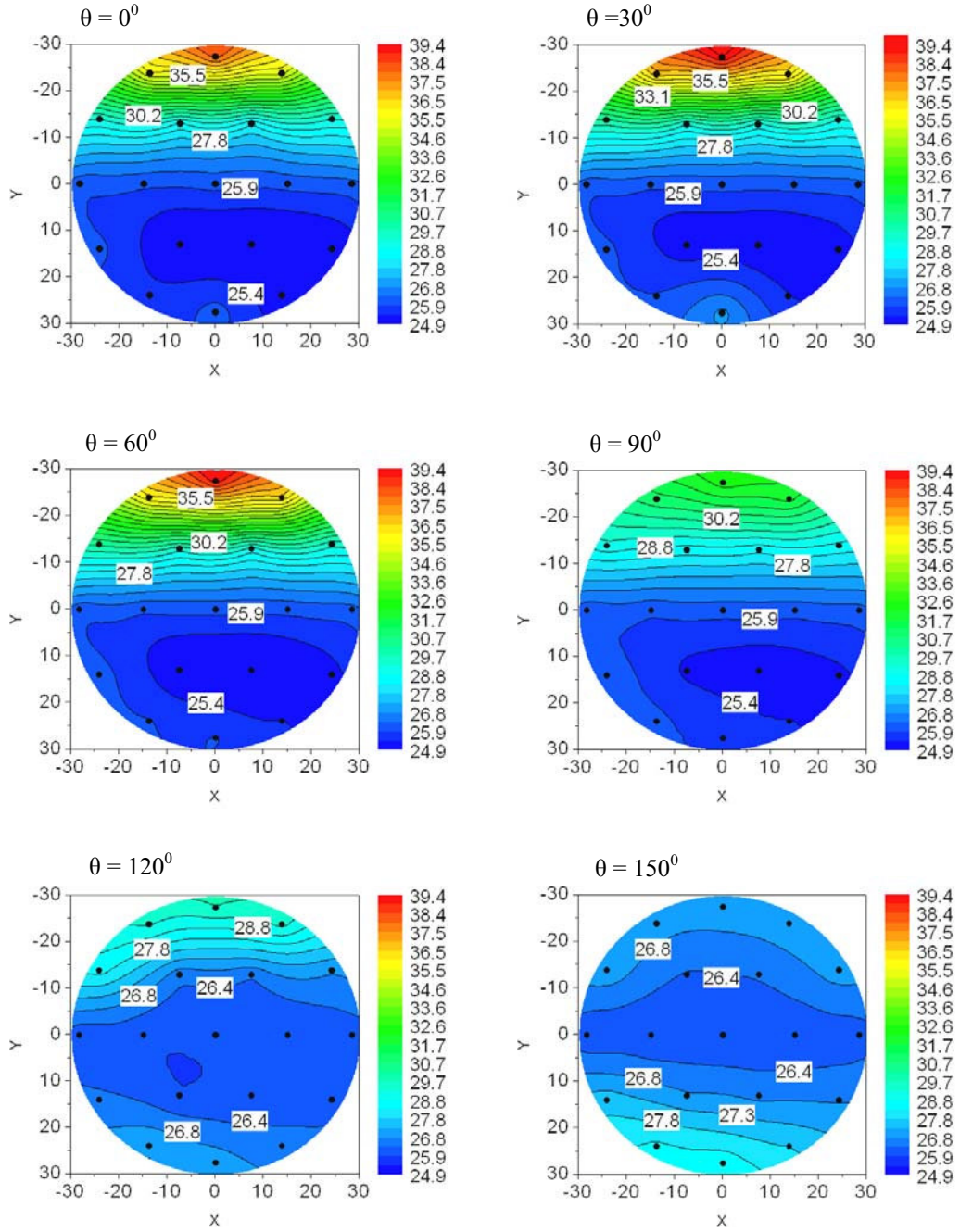

Figure 7.11 Water Temperature Distributions inside the Collector (13 September 2005, 13:15, No Flow)

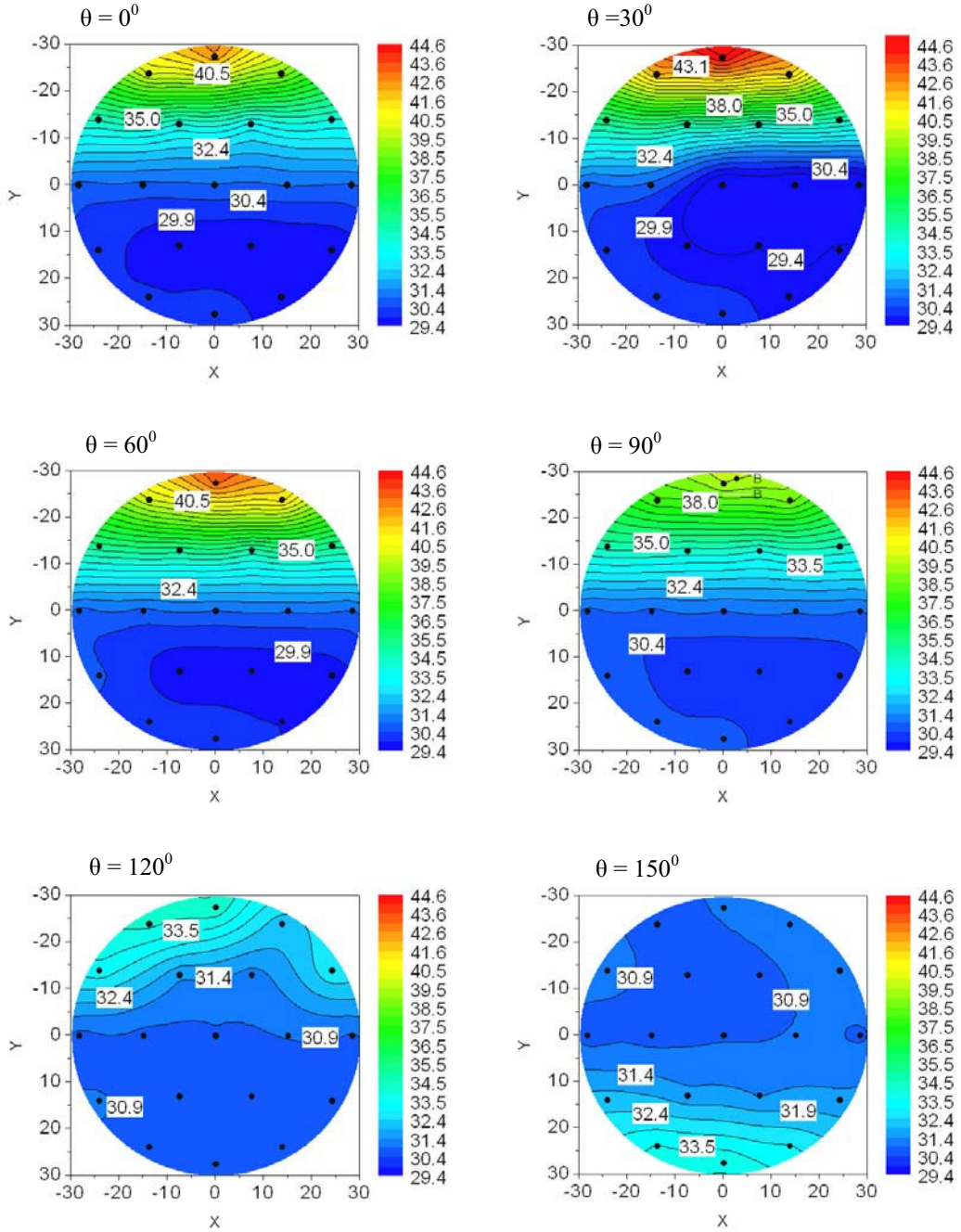

Figure 7.12 Water Temperature Distributions inside the Collector (13 September 2005, 15:15, No Flow)

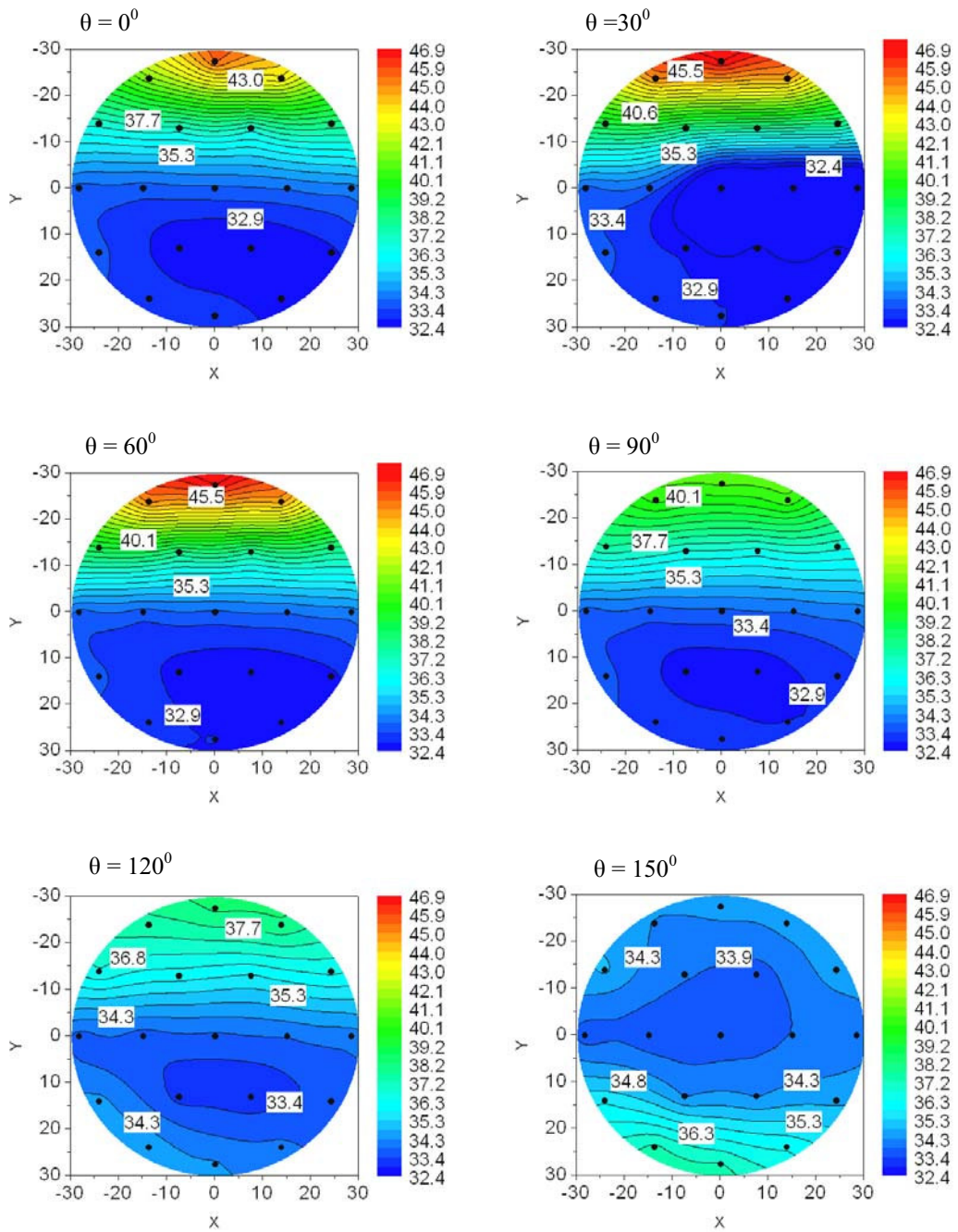

Figure 7.13 Water Temperature Distributions inside the Collector (13 September 2005, 17:15, No Flow)

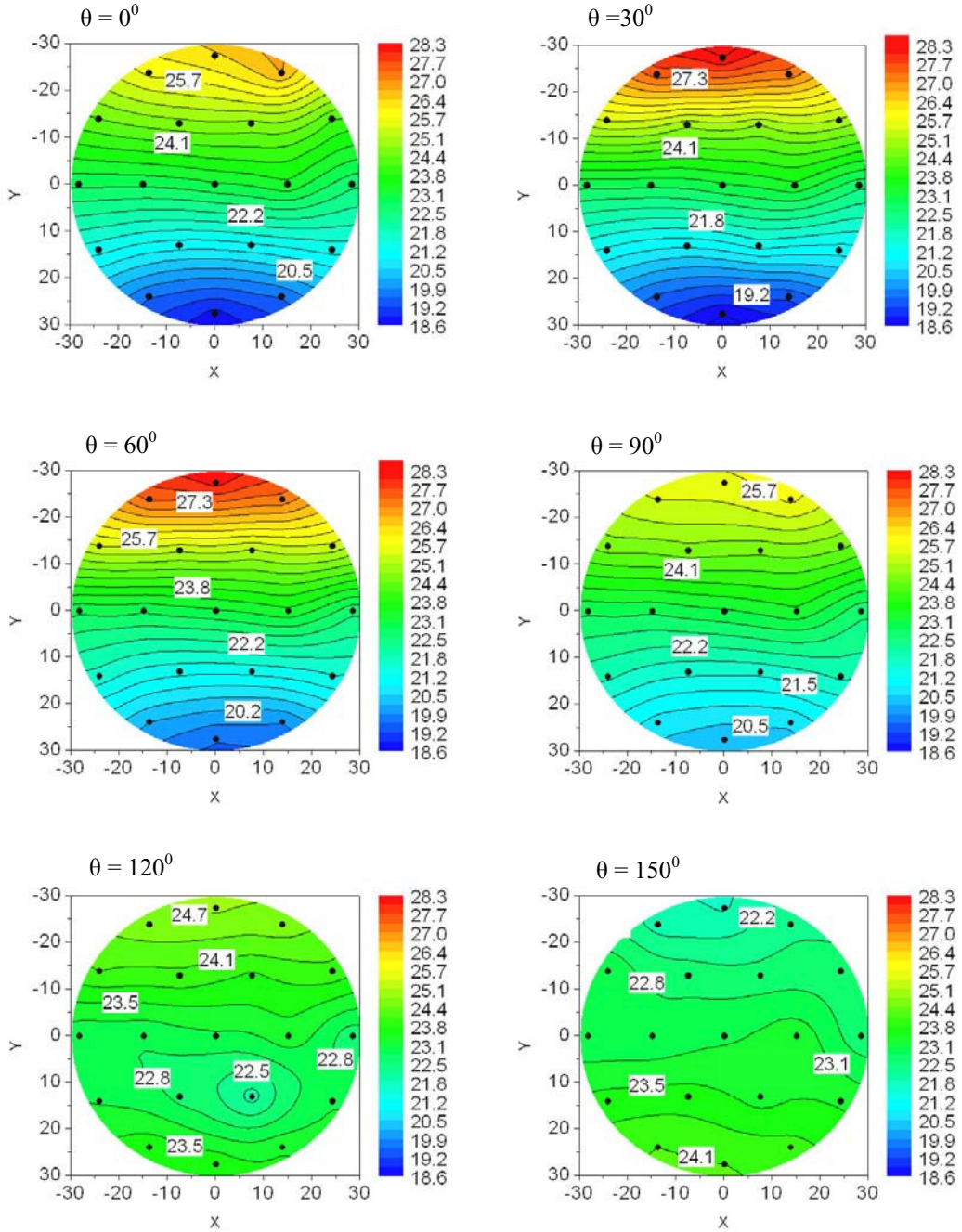

Figure 7.14 Water Temperature Distributions inside the Collector

(15 September 2005, 13:30, $\dot{m} = 0.0055 \text{kg/s}$)

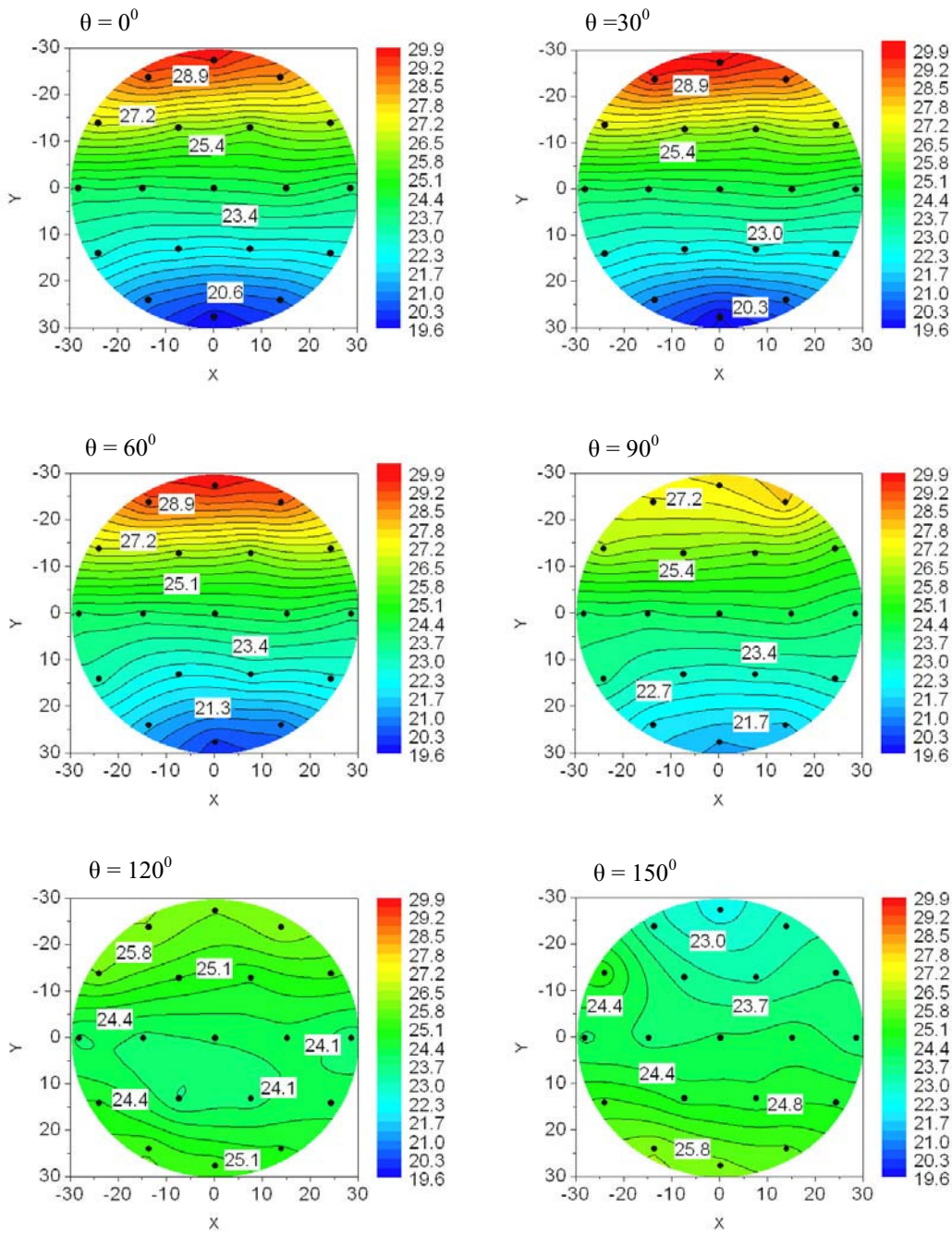

Figure 7.15 Water Temperature Distributions inside the Collector

(15 September 2005, 15:00, $\dot{m} = 0.0055 kg/s$)

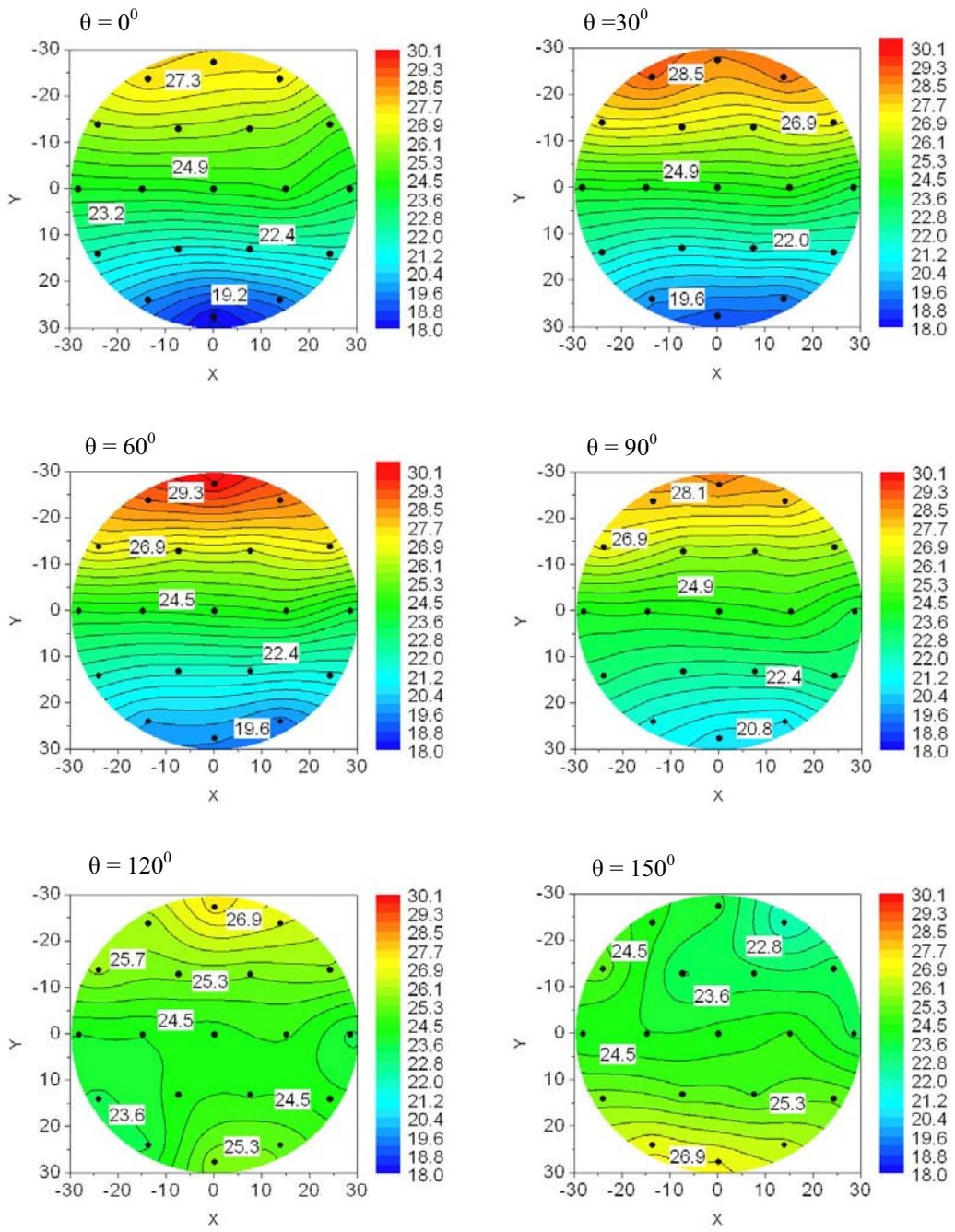

Figure 7.16 Water Temperature Distributions inside the Collector

(15 September 2005, 16:45, $\dot{m} = 0.0055 kg/s$)

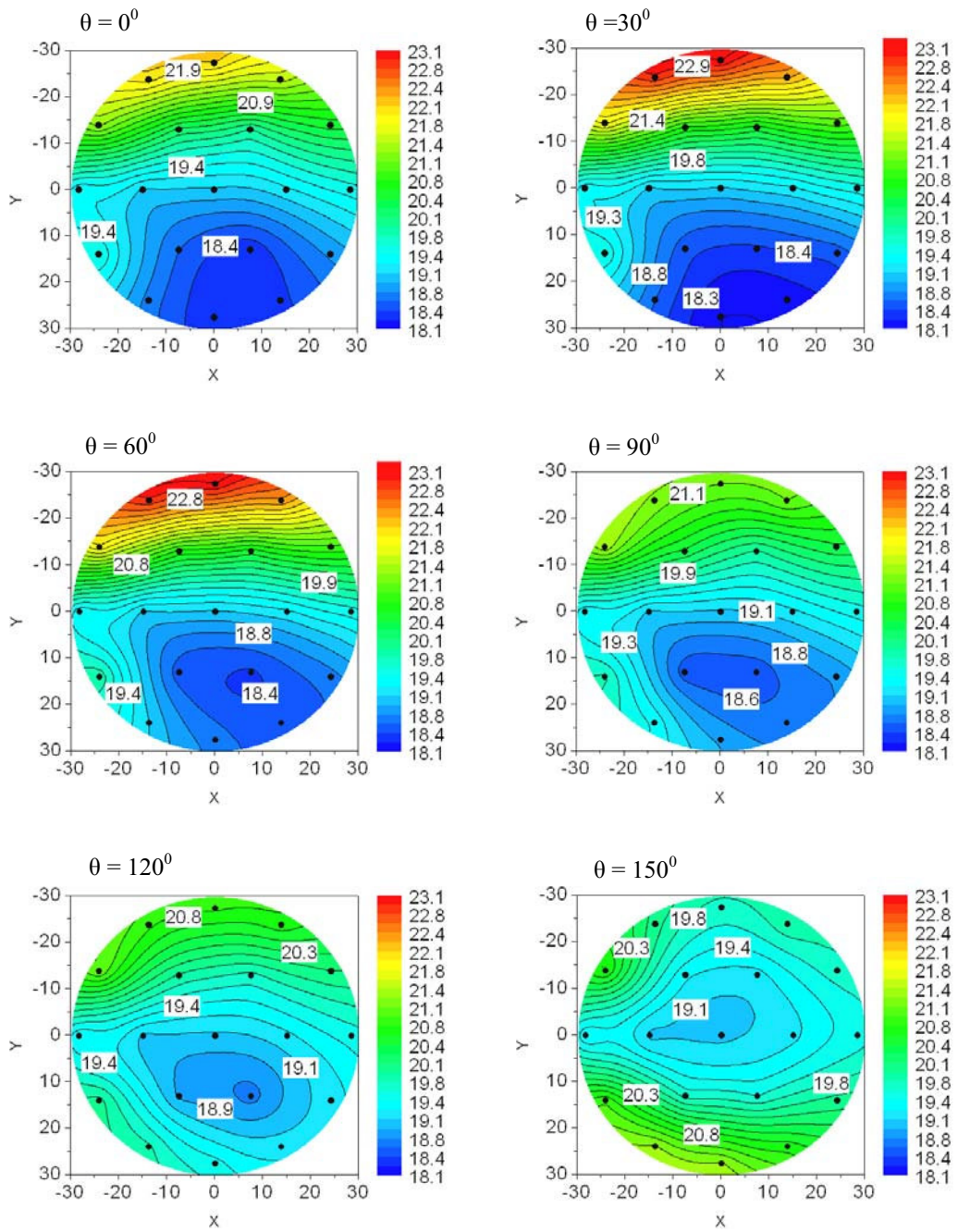

Figure 7.17 Water Temperature Distributions inside the Collector

(20 September 2005, 11:45, $\dot{m} = 0.011 kg/s$)

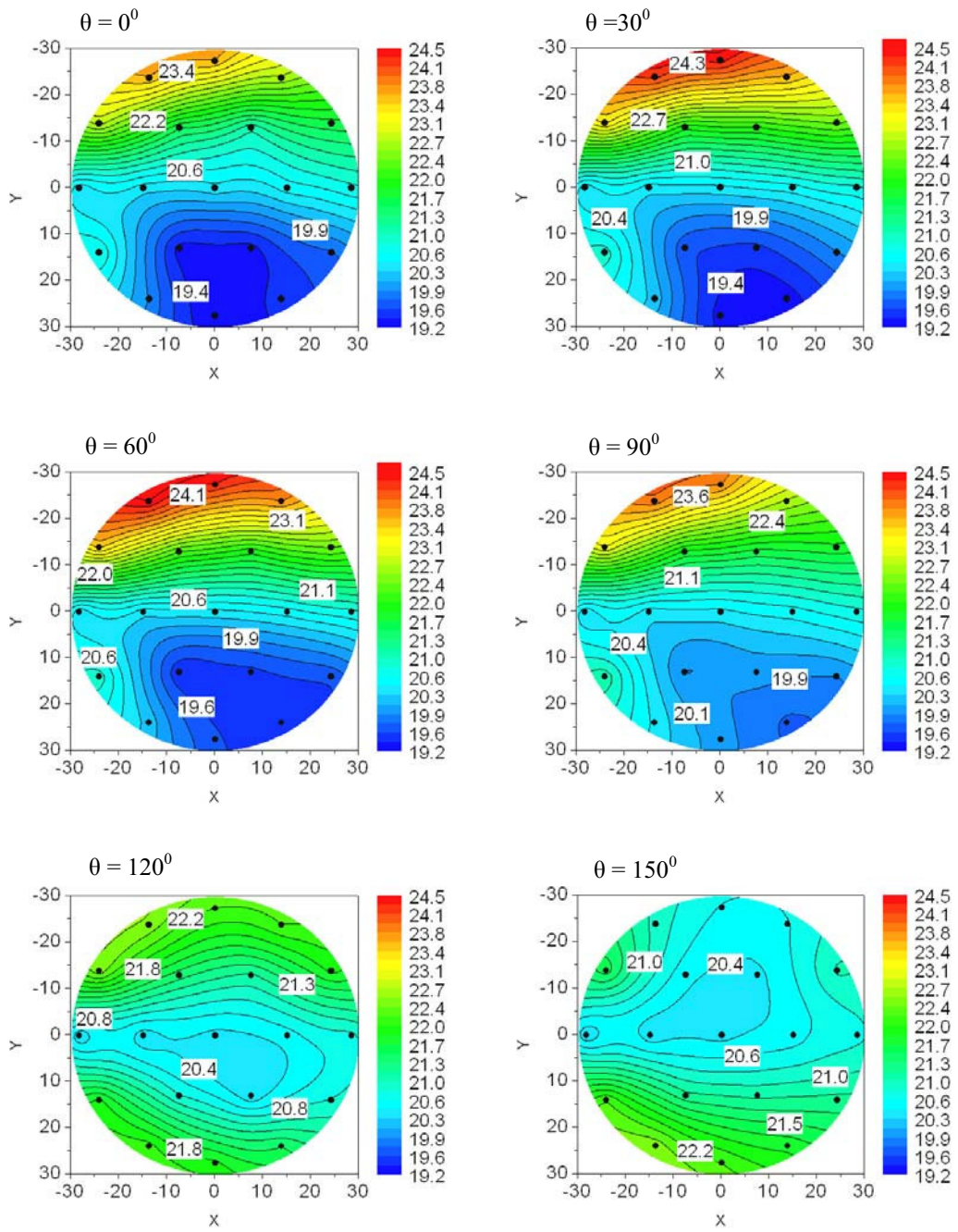

Figure 7.18 Water Temperature Distributions inside the Collector

(20 September 2005, 16:30, $\dot{m} = 0.011 kg/s$)

Total solar radiation incident on the cover and absorbed solar radiation were estimated by the small flat surfaces approximation described in Section 4.3 and Chapter 6. In the calculations, measured solar radiation on horizontal surface and methods in Chapter 3 were used. Firstly, diffuse and beam components of the solar radiation are calculated. Secondly, the spherical absorber and the spherical cover approximated to flat trapezoidal surfaces as described in Chapter 3. Thirdly, total solar radiation on each flat surface is calculated using the HDKR model [Section 3.3.2]. Then, total solar radiation incident on the cover and absorbed solar radiation were obtained. For the calculations, a computer program in Mathcad Software was written [Appendix F].

Results of the calculations are presented from Figure 7.19 to 7.27. These figures clearly show that, the variation of the total solar radiation incident on the cover and the variation of the absorbed solar radiation with time are small compared to the variation of total solar radiation on horizontal surface with time, during the day. It can be assumed that the total incident and absorbed radiation is constant for all practical considerations in the afternoon on a clear day.

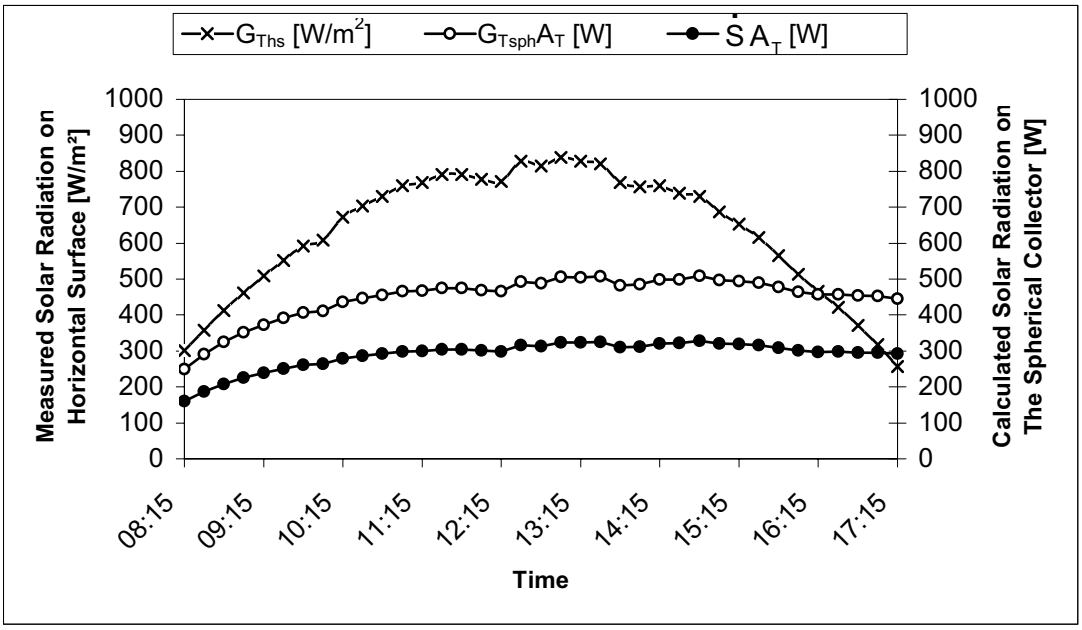

Figure 7.19 Measured and Calculated Solar Radiation Data on 13.09.2005

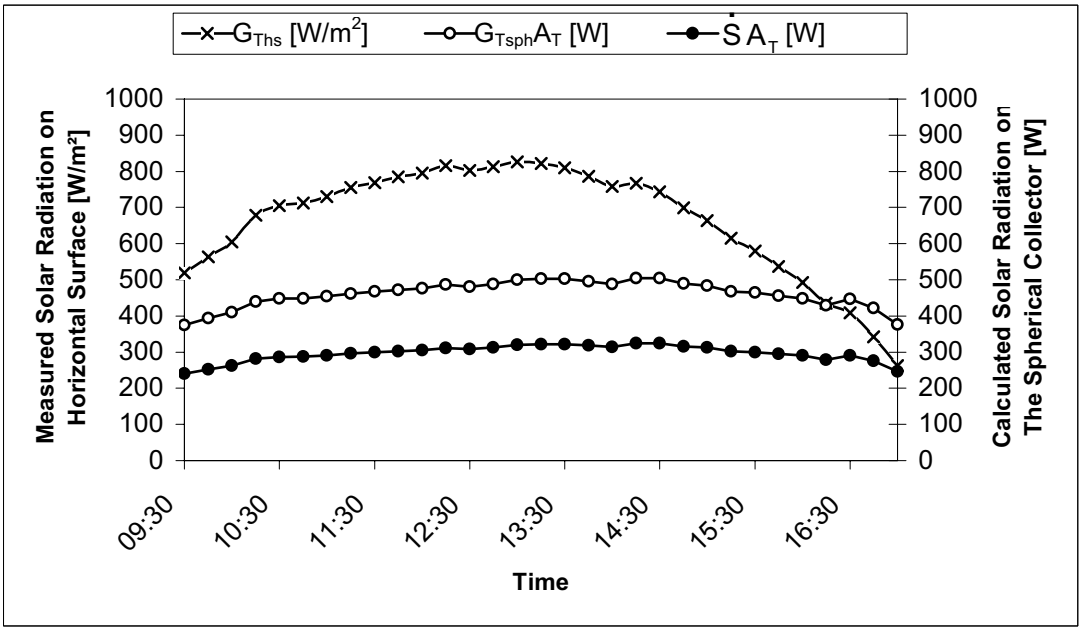

Figure 7.20 Measured and Calculated Solar Radiation Data on 14.09.2005

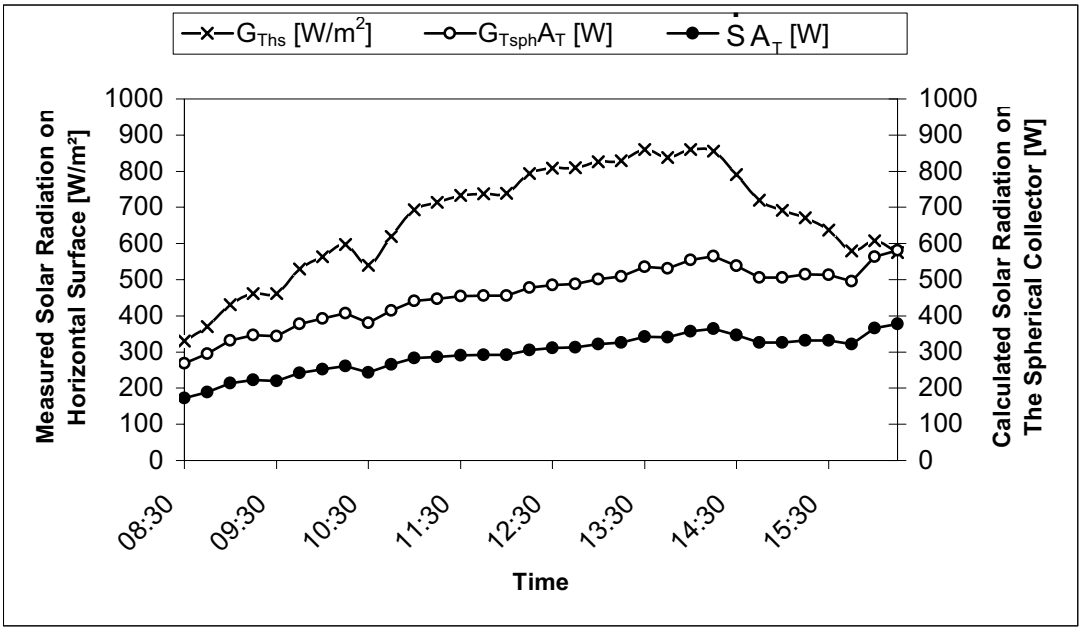

Figure 7.21 Measured and Calculated Solar Radiation Data on 15.09.2005

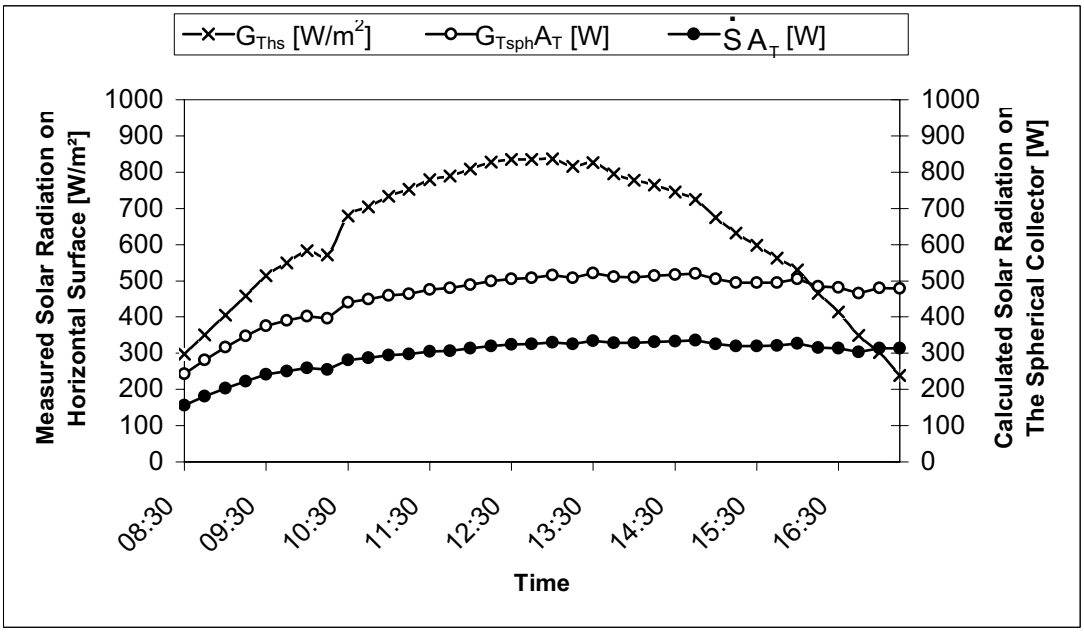

Figure 7.22 Measured and Calculated Solar Radiation Data on 19.09.2005

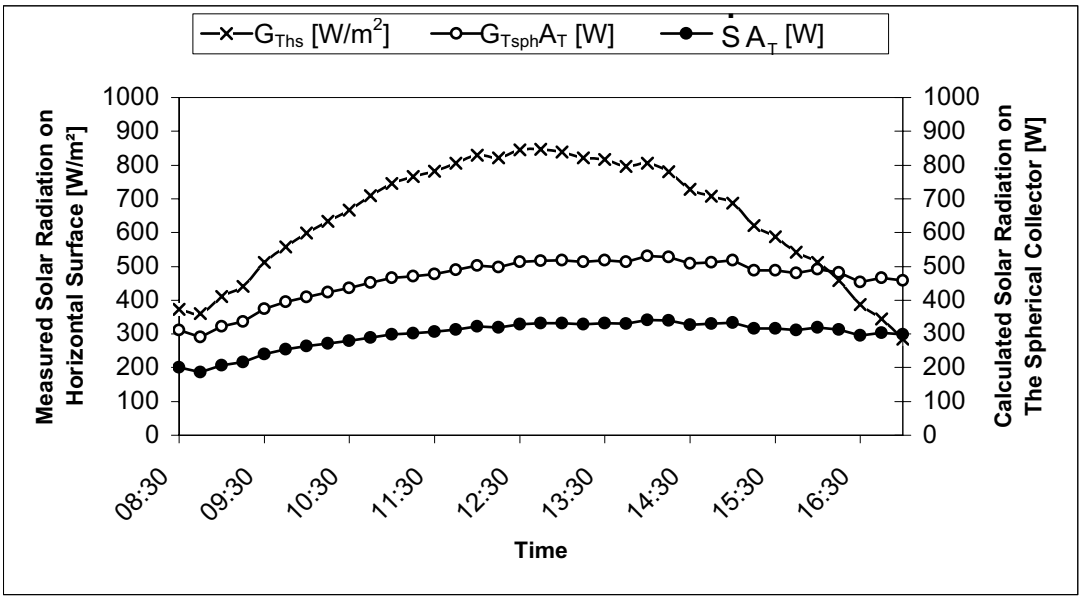

Figure 7.23 Measured and Calculated Solar Radiation Data on 20.09.2005

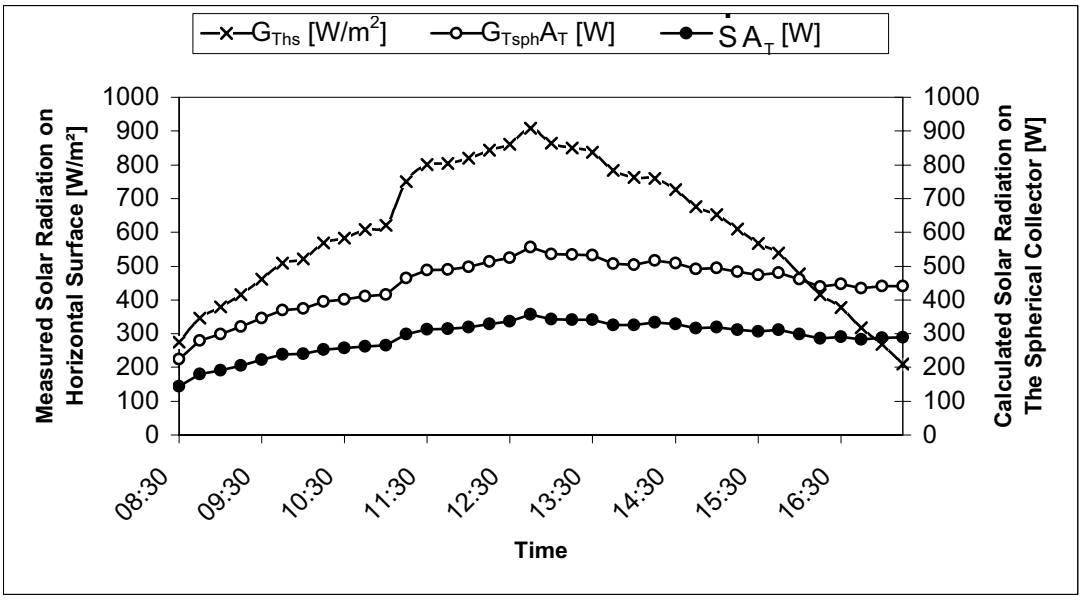

Figure 7.24 Measured and Calculated Solar Radiation Data on 21.09.2005

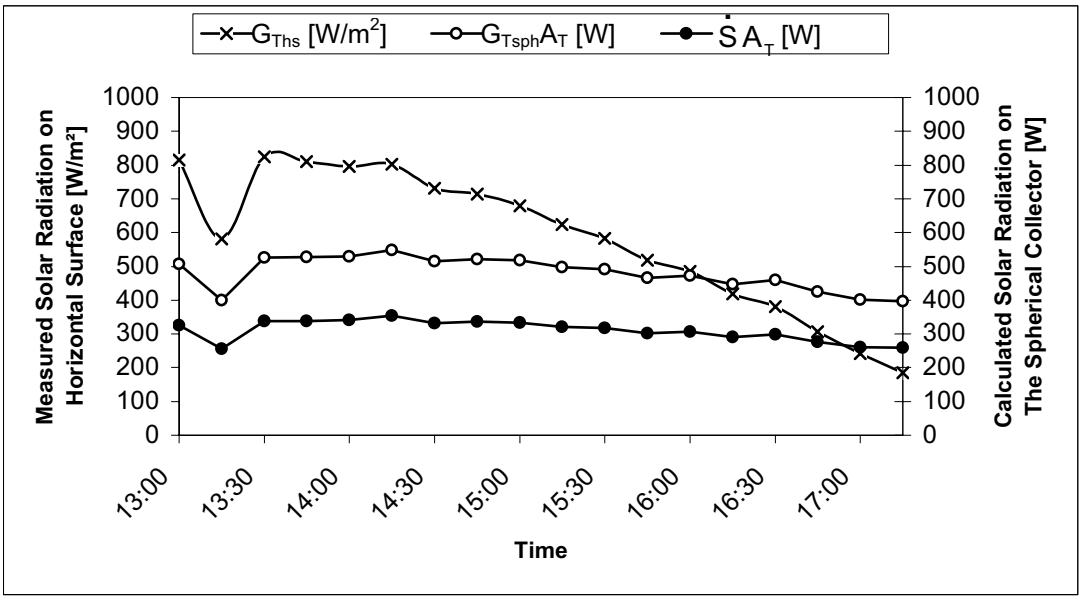

Figure 7.25 Measured and Calculated Solar Radiation Data on 22.09.2005

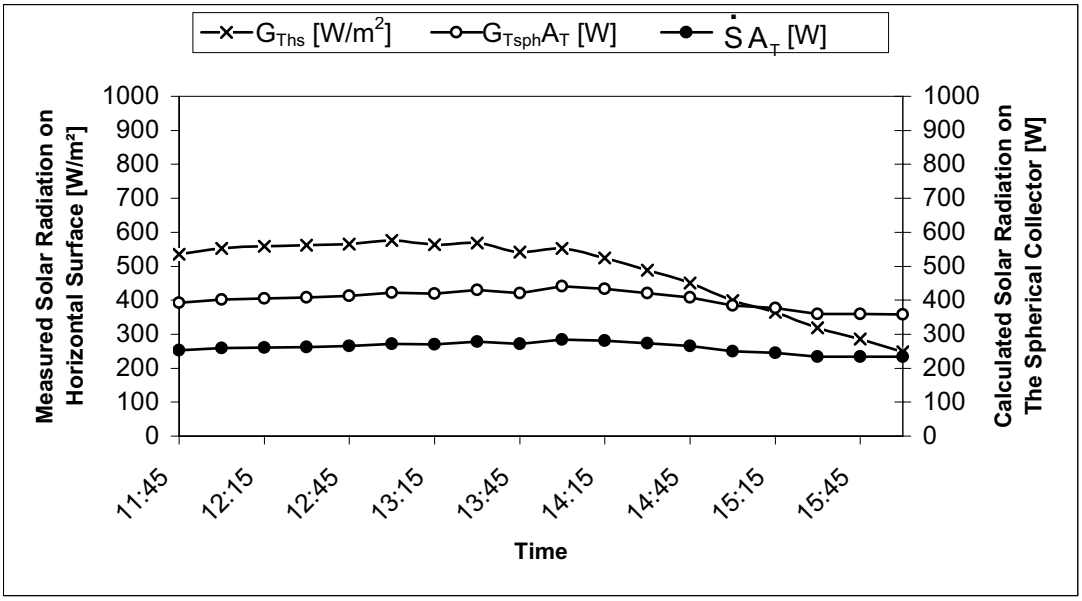

Figure 7.26 Measured and Calculated Solar Radiation Data on 26.10.2005

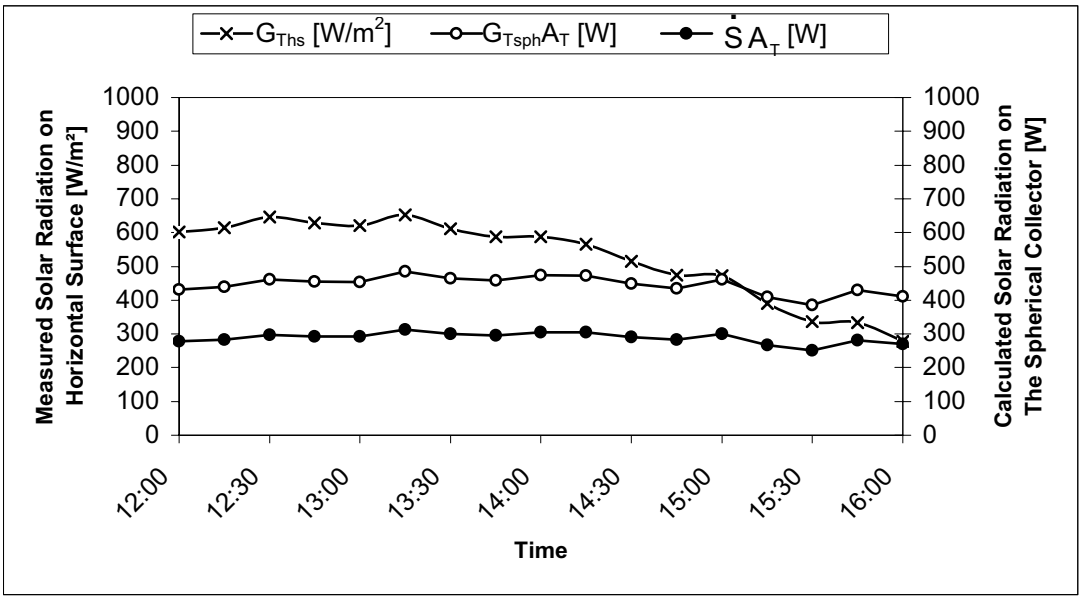

Figure 7.27 Measured and Calculated Solar Radiation Data on 27.10.2005

CHAPTER 8

DISCUSSION AND CONCLUSION

The equations of the efficiency curves of the spherical collector were obtained by a least-square fit to a straight line. The overall heat transfer loss coefficient was taken as a constant. On the mean fluid temperature based curves, η-intercept gives $F'(\tau\alpha)_{ave}$ and the slope gives $F'U_L$. Experimental performance parameters are summarized in Table 8.1. In this table, daily average transmittance-absorptance products for the absorber cover system were calculated by a program written in Mathcad Software [Appendix F].

Table 8.1 Experimental Performance Parameters for The Spherical Solar Collector

Mass Flow Rate [kg/s]	F'	UL [W/m²°C]	$(\tau\alpha)_{ave}$
No Flow	0.68	-0.49	0.64
0.0023	0.77	25.13	0.64
0.0055	0.83	19.29	0.64
0.0077	1.17	1.65	0.64
0.011	0.77	18.85	0.64

Performance curves for the collector are presented in the Figures from Figure 8.1 to 8.5.

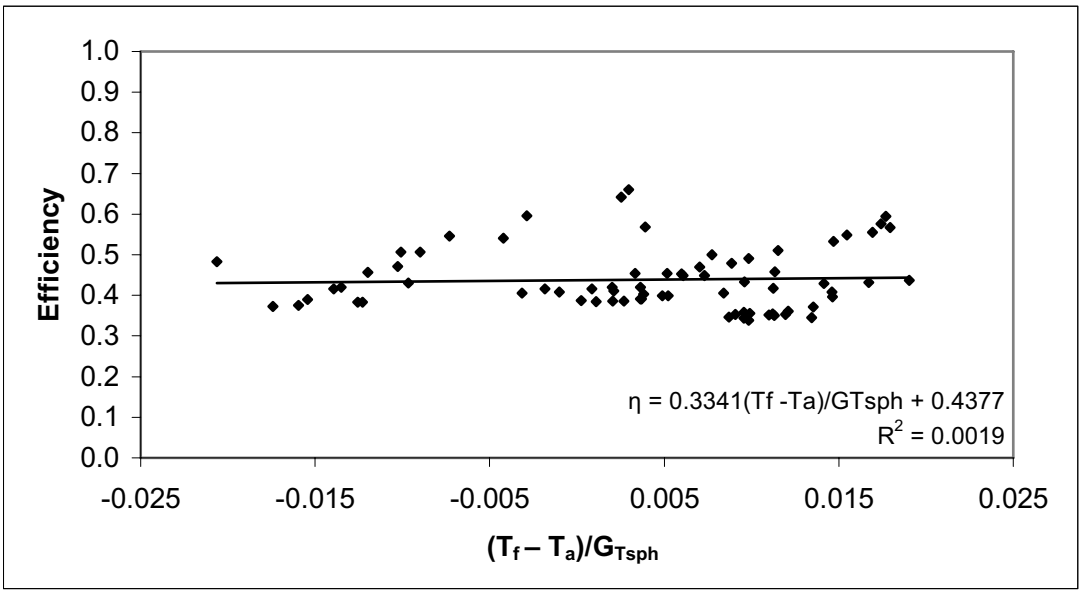

Figure 8.1 Performance Curve for the Spherical Solar Collector (No Flow)

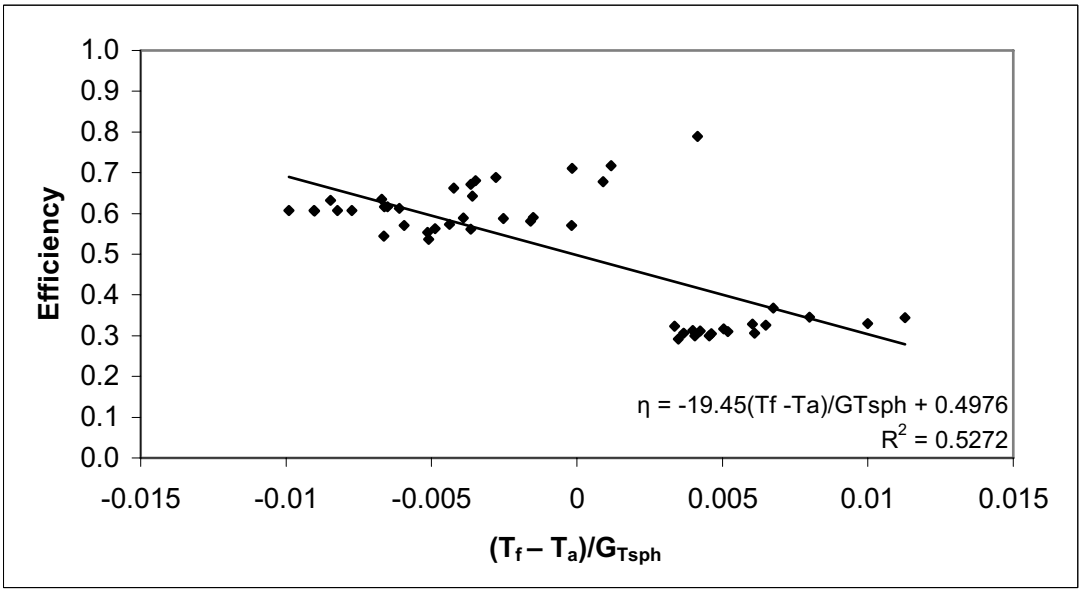

Figure 8.2 Performance Curve for the Spherical Solar Collector

$(\dot{m} = 0.0023 kg/s)$

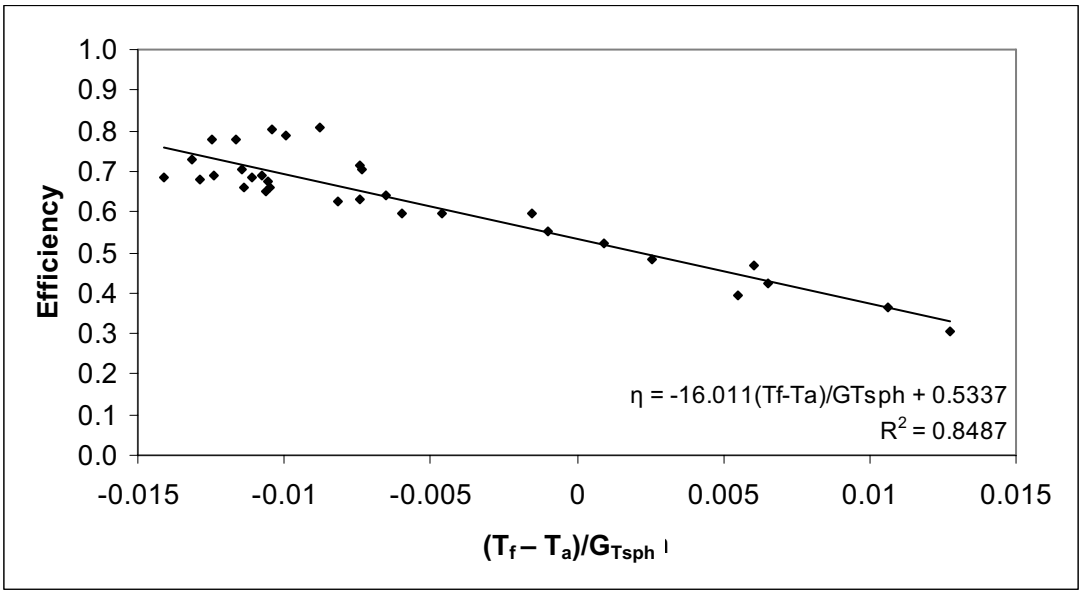

Figure 8.3 Performance Curve for the Spherical Solar Collector

$(\dot{m} = 0.0055 kg/s)$

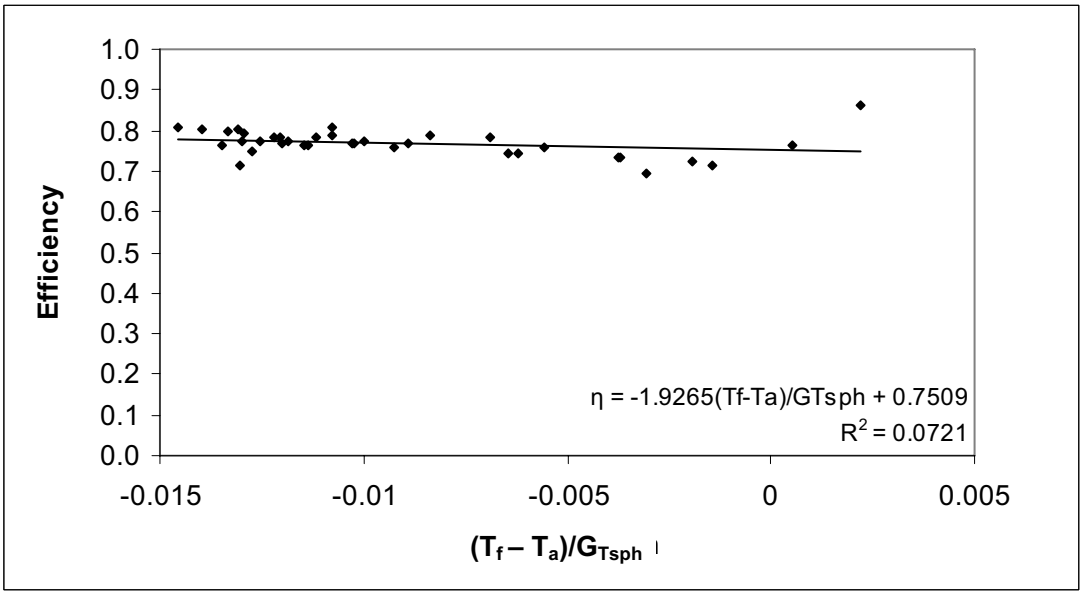

Figure 8.4 Performance Curve for the Spherical Solar Collector

$(\dot{m} = 0.0077 kg/s)$

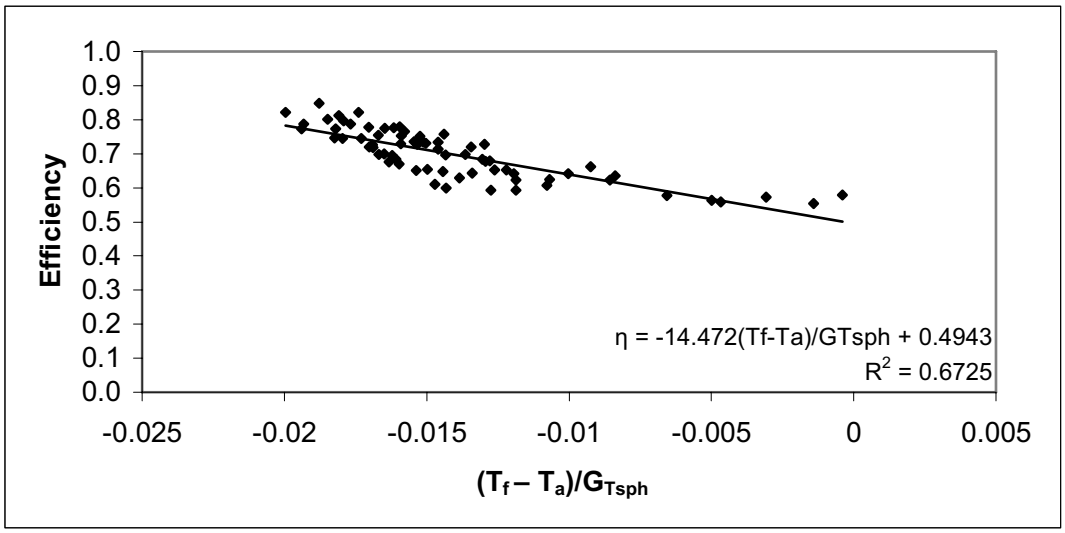

Figure 8.5 Performance Curve for the Spherical Solar Collector ($\dot{m} = 0.011 kg/s$)

8.1. Comparison of the Spherical Solar Collector with Flat Plate Solar Collectors

Flat plate solar collectors have been widely used in solar energy applications. These collectors are generally made of a set of parallel pipes that are embedded or soldered on a dark-colored metal plate. Glass or plastic covers (called glazing) are used on the top. The sides and bottom are usually insulated to minimize heat loss.

Flat plate solar collectors are mounted in a fixed position, facing south in northern hemisphere; or a sun tracking mechanism is used to minimize the angle of incidence of beam radiation.

Prior to compare performance of the spherical solar collector with a flat plate solar collector, analyzing the spherical collector with respect to incident beam radiation will provide some information for the comparison.

The spherical solar collector gains most of its energy from beam contribution of the solar energy incident on its hemispherical surface which faces the sun (Figure 8.6).

Beam contribution of the incoming solar radiation can be calculated as

$$\text{Incoming beam radiation} = \int_{A_1} G_{bhs}\ R_b dA \tag{8.1}$$

where dA is a differential surface area on the absorber and it is derived using Figure 8.7 as below :

$$dA = R_p^{\,2} \sin\theta\ d\phi\ d\theta \tag{8.2}$$

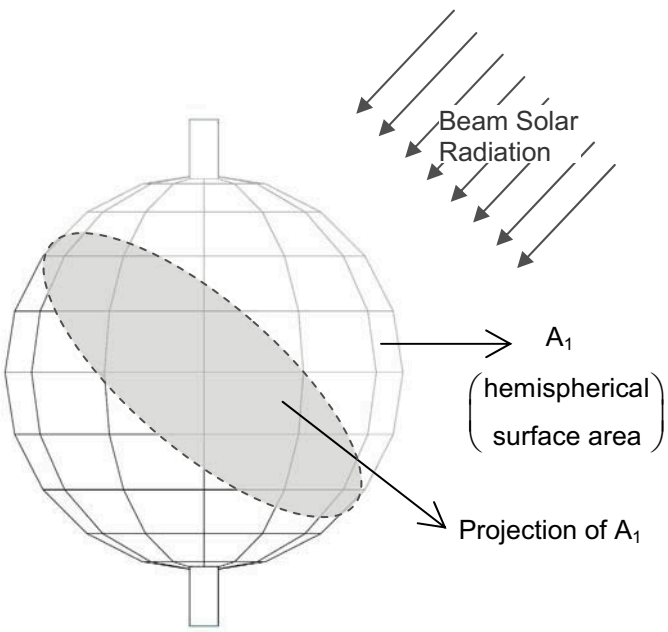

Figure 8.6 Beam Contribution of the Solar Radiation on the Spherical Solar Collector

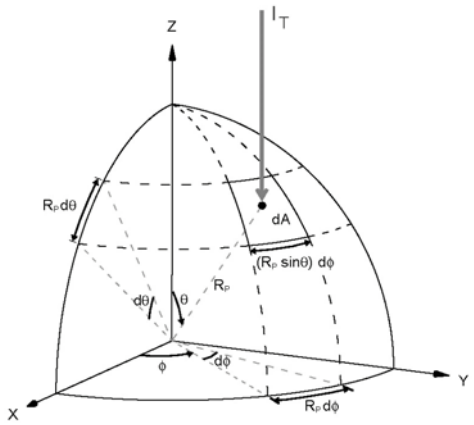

Figure 8.7 Differential Surface Element on the Irradiated Hemisphere A_1

After substituting Equation 8.2 for dA, Equation 3.20 for R_b, and solving the integral, Equation 8.1 takes the form below :

$$\text{Energy Gain} = G_{bhs} \quad \frac{1}{\cos\theta_z} \quad \pi R_p^{\,2} \tag{8.3}$$

From this equation it can be said that, the spherical collector acts as if a sun tracking flat plate solar collector of $\pi R_p^{\,2}$ in area, which is the projection of the hemispherical surface area, A_1.

To make a comparison between a flat plate solar collector and the spherical solar collector, under same weather conditions, a flat plate collector of 0.28 m^2 in area, equal to $\pi R_p^{\,2}$, was considered. In addition to this, another flat plate collector of 0.56 m^2 in area, equal to area of the hemispherical surface, was also considered in this analysis. Also, slope of the flat plate collectors are chosen as 40° from horizontal surface, which is close to the local latitude.

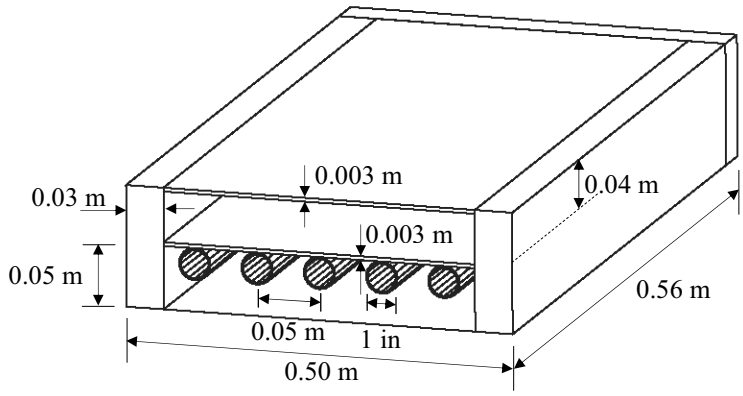

Figure 8.8 Dimensions of the Flat Plate Solar Collector of 0.28 m^2 in Area

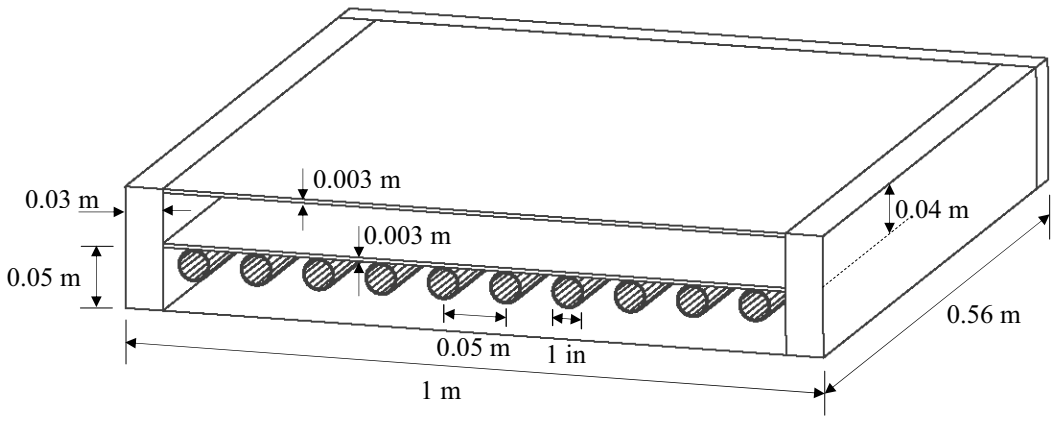

Figure 8.9 Dimensions of the Flat Plate Solar Collector of 0.56 m^2 in Area

Performance calculations of the flat plate collectors are made using appropriate equations taken from Reference [23] and a computer program in Mathcad software was written for these calculations [Appendix D]. The results are summarized in Appendix E, and hourly efficiencies of the flat plate collectors are compared with those of the spherical solar collector on the figures from Figure 8.10 to Figure 8.17.

It is seen on the figures that hourly efficiencies of the spherical solar collector are greater then those of the flat plate collectors under these experimental conditions ($T_f \leq 34.4$ °C). Also, increase in the hourly efficiency is greater for the spherical collector through out the day. Although there is decrease in the hourly efficiencies of the flat plate collectors in the afternoon, hourly efficiency of the spherical collector shows an increasing trend. Maximum hourly efficiency obtained for the flat plate collectors of 0.28 m^2 in area and 0.56 m^2 in area are 56% and 55%, respectively. Maximum hourly efficiency obtained for the spherical collector is 79%.

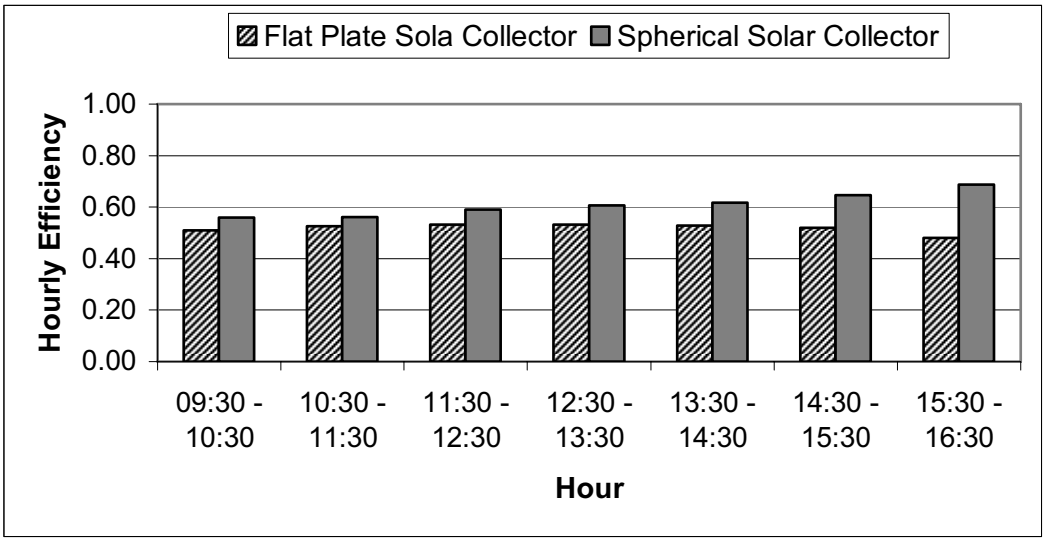

Figure 8.10 Comparison of the Spherical Solar Collector with Flat Plate Solar Collector of 0.28 m^2 ($\dot{m} = 0.0023 kg/s$)

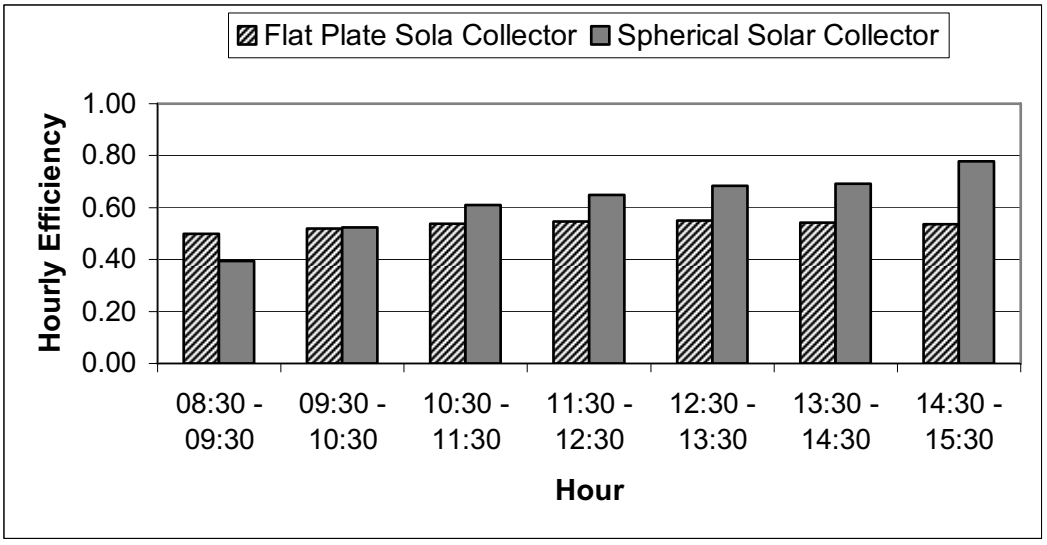

Figure 8.11 Comparison of the Spherical Solar Collector with Flat Plate Solar Collector of 0.28 m^2 ($\dot{m} = 0.0055 kg/s$)

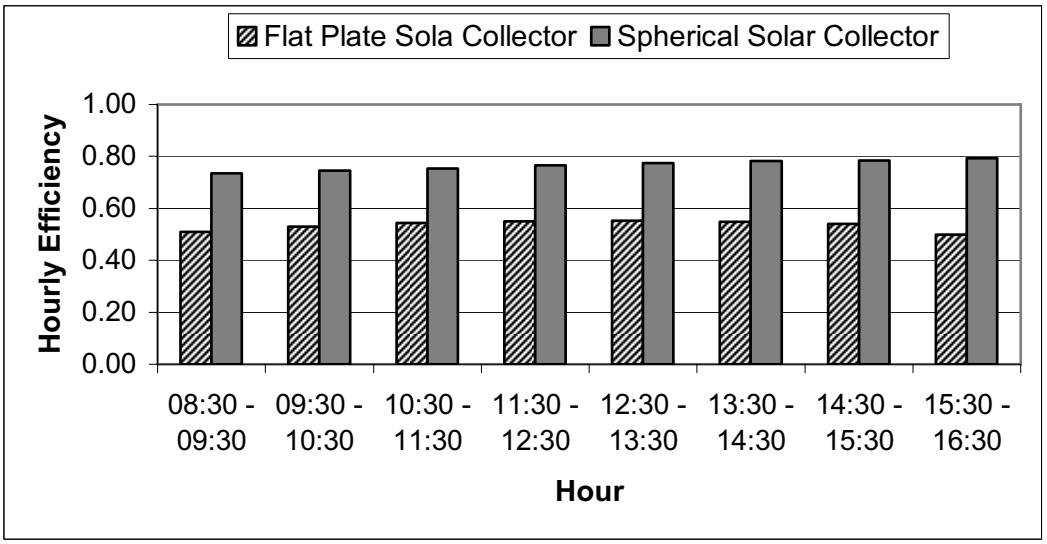

Figure 8.12 Comparison of the Spherical Solar Collector with Flat Plate Solar Collector of 0.28 m^2 ($\dot{m} = 0.0077 kg/s$)

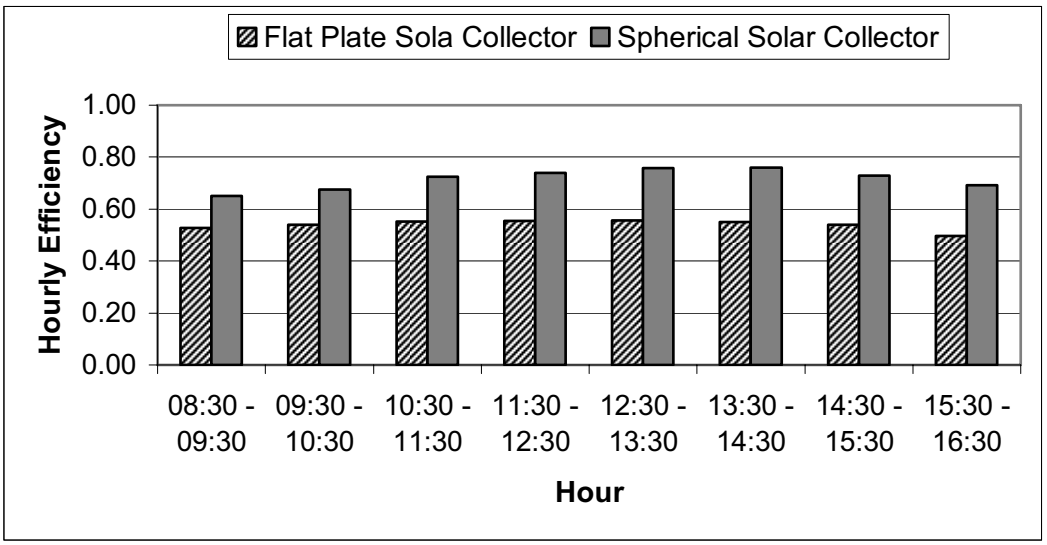

Figure 8.13 Comparison of the Spherical Solar Collector with Flat Plate Solar Collector of 0.28 m^2 ($\dot{m} = 0.011 kg/s$)

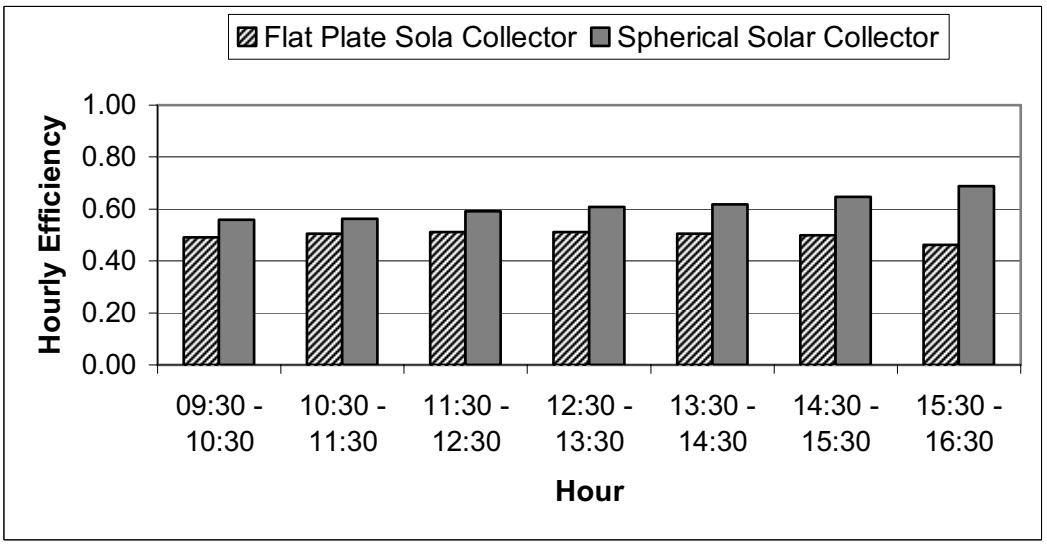

Figure 8.14 Comparison of the Spherical Solar Collector with Flat Plate Solar Collector of 0.56 m^2 ($\dot{m} = 0.0023 kg/s$)

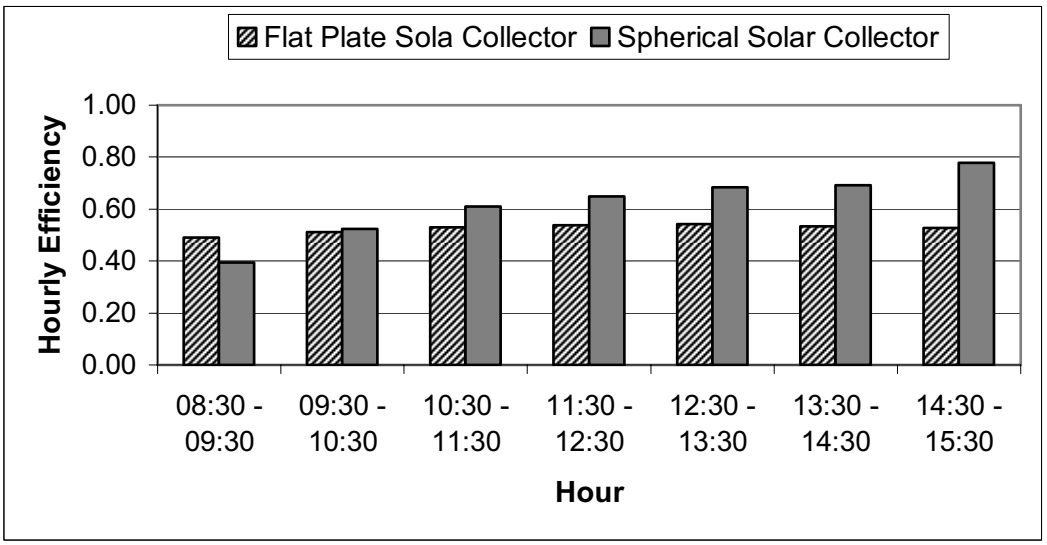

Figure 8.15 Comparison of the Spherical Solar Collector with Flat Plate Solar Collector of 0.56 m^2 ($\dot{m} = 0.0055 kg/s$)

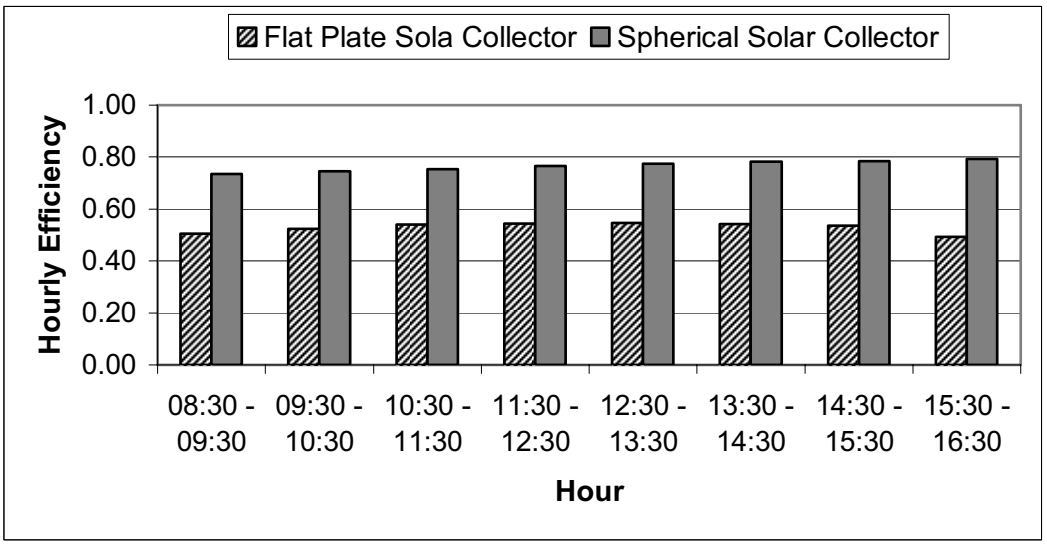

Figure 8.16 Comparison of the Spherical Solar Collector with Flat Plate Solar Collector of 0.56 m^2 ($\dot{m} = 0.0077 kg/s$)

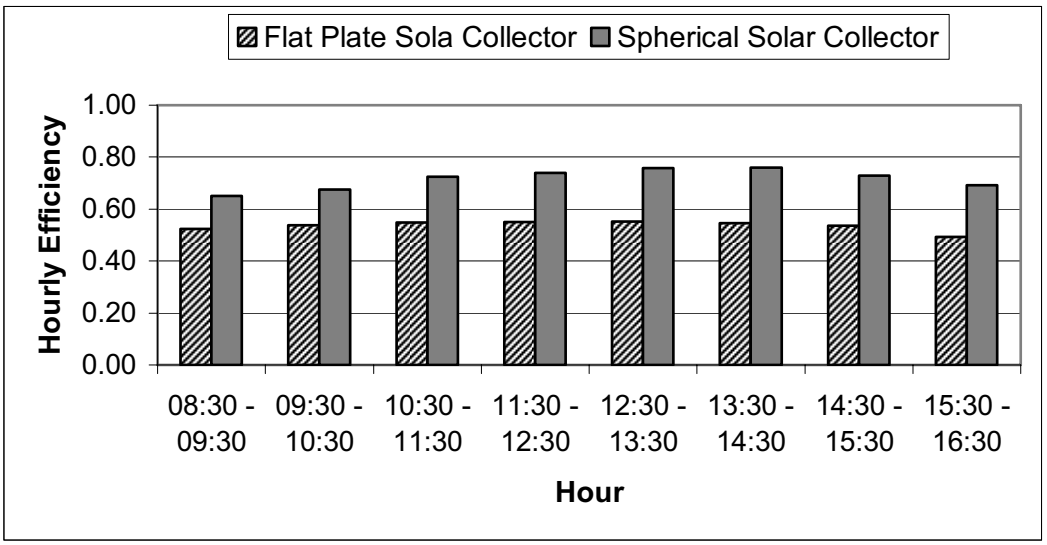

Figure 8.17 Comparison of the Spherical Solar Collector with Flat Plate Solar Collector of 0.56 m^2 ($\dot{m} = 0.011 kg/s$)

8.2. Cost Analysis for the Spherical Solar Collector

The collector components are relatively inexpensive and widely available. But construction requires a skilled work when compared to conventional solar water heaters. The cost analysis of the spherical solar collector including the cost of components and labor cost is as follows.

Steel Plate (2 m x 1 m) 3 mm thickness	:	100 YTL
Window Glass (2 m x 1 m) 3 mm thickness	:	90 YTL
1'' Copper Pipe (1 m)	:	10 YTL
Paint (Black Matt) 1 kg	:	9 YTL
Silicon (Transparent)	:	4 YTL
Valve (2 number)	:	20 YTL
Machine Shop Labor	:	+ 400 YTL
TOTAL		633 YTL

So, the collector costs 633 YTL. Total cost in terms of U.S. Dollars (1$=1.33 YTL) is 476 $.

8.3. Suggestions for Future Work

Following suggestions are made for the future work on the collector-storage system :

1. Because of the large storage volume of the system, inner compartment should be built to reach higher temperature and stratification in the water tank.

2. It was observed that most of the radiation is absorbed from the hemispherical surface which faces the sun. A hemispherical reflector system can be used to increase absorbed solar radiation from the shaded side of the collector.

3. An insulating baffle plate can be used inside the tank. As it was mentioned in the previous studies in the literature, a baffle plate protects the water from the cold sky during off-sunshine hours.

4. Two covers can be used instead of one to decrease heat losses.

5. The performance of the spherical solar collector should be compared to that of the flat plate solar collector with storage equal to the volume inside the spherical absorber, and a simulation should be done to study the variation of the efficiency with fluid temperature and time.

6. Spherical collector is only more efficient at low $(Tf-Ta)/G_T$. How its efficiency compares at high $(Tf-Ta)/G_T$ is not known (It may be more or less than flat plate). Performance of the spherical solar collector should be also studied at large values of $(Tf-Ta)/G_T$.

REFERENCES

1. J. C. V. Chinnappa and K. Granalingam, *Performance at Colombo Ceylon of a pressurized solar water heater of the combined collector and Storage type*. Solar Energy, Vol. 15, pp. 195-204 (1973).

2. H. P. Garg, *Year Round Performance Studies on a Built-in-Storage Type Solar Water Heater at Jodhpur, India*. Solar Energy, Vol. 17, pp. 167-172 (1975).

3. R. S. Chauham and V. Kadambi, *Performance of a Collector-cum-Storage Type of Solar Water Heater*. Solar Energy, Vol. 18, pp. 327-335 (1976).

4. M. S. Sodha, J. K. Nayak, S. C. Kanshik, S. P. Sabberwal, M. A. S. Malik, *Performance of a Collector/Storage Solar Water Heater*. Energy Conversion, Vol. 19, pp. 41 (1979).

5. M. S. Sodha, P. K. Bansal, S. C. Kaushik, *Performance of Collector/Storage Water Heaters: Arbitrary Demand Pattern*. Energy Conservation and Management, Vol. 21, pp. 229–238 (1981).

6. N. D. Kaushik, P. K. Bansal, S. C. Kaushik, *Transient Behaviour of Collector/Storage Solar Water Heaters for Generalised Demand Patterns*. Applied Energy, Vol. 12, pp. 259-267 (1982).
7. H. P. Garg, U. Rani, *Theoretical and Experimental Studies on Collector/Storage Type Solar Water Heater*. Solar Energy, Vol. 29, No. 6, pp. 467-478 (1982).

8. G. N. Tiwari, N. K. Dhiman, *Effect of the Baffle Plate on Transient Performance of Built-in-Storage Water Heater*. Energy Conversion and Management, Vol. 23, No. 3, pp. 151-155 (1983).

9. M. Sokolov, B. Vaxman, *Analysis of an Integral Compact Solar Water Heater*. Solar Energy, Vol. 30, pp. 237-246 (1983).

10. B. Vaxman, M. Sokolov, *Experiments with an Integral Compact Solar Water Heater*. Solar Energy, Vol. 34, No. 6, pp. 447-454 (1985).

11. A. A. Mohamad, *Integrated Solar Collector-Storage Tank System with Thermal Diode*, Solar Energy, Vol. 61, No. 3, pp. 211-218 (1997).

12. J. Prakash, H. P. Garg, G. Datta, *A solar water heater with a Built-in-latent Heat Storage*. Energy Conversion and Management, Vol. 25, pp. 51 (1985).

13. J. Prakash, H. P. Garg, D. S. Hrishikesan, *Effect of Tracking on the Performance of a Built-in-Storage Type Solar Water Heater*. Solar and Wind Technology, Vol. 5, No.4, pp. 433-440 (1988).

14. H. P. Garg, D. S. Hrishikesan, Ranjana Jha, *System Performance of Built-in-Storage Type Solar Water Heater with Transparent Insulation*. Solar and Wind Technology, Vol. 5, No. 5, pp. 533-538 (1988).

15. Tariq Muneer, *Effect of Design Parameters on Performance of Built-in-Storage Solar Water Heaters*. Energy Conversion and Management, Vol. 25, No. 3, pp. 227-281 (1985).

16. A. Ecevit, A. M. Al-Shariah, E. D. Apaydın, *Triangular Built-in-Storage Solar Water Heater*. Solar Energy, Vol. 42, No. 3, pp. 253-265 (1989).

17. S. C. Kaushik, R. Kumar, H. P. Garg, J. Prakash, *Transient Analysis of a Triangular Built-in-Storage Solar Water Heater under Winter Conditions*. Heat Recovery Systems and CHP, Vol. 14, No. 4, pp. 337-341 (1994).

18. J. Prakash, S. C. Kaushik, R. Kumar, H. P. Garg, *Performance Prediction for a Triangular Built-in-Storage Type Solar Water Heater with Transparent Insulation*. Energy, Vol. 19, No. 8, pp. 869-877 (1994).

19. İ. Necmi Kaptan, *The Thermal Analysis of a Novel Built-in-Storage Solar Water Heater*. PhD Thesis, İstanbul Technical University, Turkey (1994).

20. José M. S. Cruz, Geoffrey P. Hammond, Albino J. P. S. Reis, *Thermal Performance of a Trapezoidal-Shaped Solar Collector/Energy Store*. Applied Energy, Vol. 73, pp. 195-212 (2002).

21. K. A. Joudi, I. A. Hussein, A. A. Farhan, *Computational Model for a Prism Shaped Storage Solar Collector with a Right Triangular Cross Section*. Energy Conversion and Management, Vol. 45, pp. 391-409 (2004).

22. B. Samanta, Khamis Rajab Al Balushi, *Estimation of Incident Radiation on a Novel Spherical Solar Collector*. Renewable Energy, Vol. 14, No. 1-4, 241-247 (1998).

23. J. A. Duffie, W. A. Beckman, *Solar Engineering of Thermal Processes*, John Wiley & Sons Inc. (1991).

24. Frank P. Incropera, David P. DeWitt, *Introduction to Heat Transfer*, John Wiley & Sons Inc. (2000).

APPENDIX A

SPECIFICATIONS OF INSTRUMENTS

Table A.1 Specifications of Keithley Instruments Model 160 Digital Multimeter

Range	±1 microvolt per digit to ±1000 volts full scale in seven decade ranges 100% overranging on all except the 1000-volt range.
Accuracy	±0.1 % of reading on all ranges.
Input resistance	10 megohms on the 10-microvolt and higher ranges, 1 megohm on the 1-millivolt range.
Settling time	Less then 2 seconds to rated accuracy.

Table A.2 Specifications of Davis Instruments Wind Wizard Model 0281 Wind Speed Indicator

Range	Wind speeds from 0 to 60 mph
Reading	miles/hour, meters/second, and Beaufort
Power Supply	No batteries needed
Dimensions	92 x 73 x 25 mm with handle folded
Weight	71g

Table A.3 Specifications of Elimko Model E680 Data Logger

Accuracy Class	0.5
Display Resolution	1/9999
Display	9 Digit LED (14 mm)
A/D Conversion	16 bit
D/A Conversion	12 bit
Input Scan Time	0.2–9.9 Seconds / channel
Display Scan Time	1–99 Seconds / channel
Noise Suppression	120 dB at 50 Hz
Operating Temperature	-10 ÷ 55°C
Temperature Comp.	0-50°C
Set Adjustment	Between set point limits
Contact Forms	Low (LO) or High (HI)
Dead Band (Hysterisis)	0–9999 EU*
Power Supply	85–265 V AC 85–375 V DC 20–60 V AC 20–85 V DC
Power Consumption	Max. 10 VA
Relay Output Input Types Sensors	SPST-NO Contact 250 V AC 5A T/C, R/T, mA, mV, V Thermocouples Resistance Thermometer Others = Standard and non–standard transmitters and converters
Memory	EEPROM max. 10^5 writing

*(EU) °C or °F for the thermocouples and resistance thermometer inputs, for the linear inputs, same with the unit which is controlled.

APPENDIX B

EXPERIMENTAL DATA

Table B.1 Experimental Data on 13.09.2005 (No Flow)

Time	G_{Ths} [W/m²]	$G_{Tsph}A_T$ [W]	T_a [°C]	T_f [°C]	η
08:15	301	249.3	18.0	18.9	0.57
08:30	358	290.5	18.8	20.8	0.50
08:45	412	324.2	18.3	21.6	0.46
09:00	462	351.1	19.0	22.0	0.43
09:15	509	372.4	19.7	23.4	0.42
09:30	552	391.1	19.9	22.8	0.41
09:45	593	406.5	20.2	22.1	0.40
10:00	609	410.9	20.8	22.2	0.40
10:15	672	435.7	22.0	22.1	0.39
10:30	703	446.7	22.3	23.1	0.39
10:45	731	455.8	22.6	23.7	0.39
11:00	760	466.0	23.7	24.2	0.38
11:15	769	467.1	23.8	25.3	0.39
11:30	791	475.5	24.4	26.0	0.39
11:45	791	474.2	24.2	26.2	0.40
12:00	777	468.9	25.2	26.1	0.41
12:15	771	466.4	25.0	25.8	0.42
12:30	828	492.7	26.4	25.0	0.40
12:45	815	487.8	26.0	25.2	0.42
13:00	838	505.6	26.3	25.8	0.41
13:15	827	504.7	26.2	26.6	0.42
13:30	821	508.0	26.2	27.8	0.42
13:45	768	482.7	26.9	29.5	0.45
14:00	757	484.9	27.6	29.0	0.45
14:15	759	498.0	27.0	30.2	0.45
14:30	739	499.2	27.4	29.7	0.45
14:45	730	508.6	27.3	30.0	0.45
15:00	687	497.6	27.9	31.0	0.47
15:15	653	494.6	27.5	31.4	0.48

Table B.1 (Continued) Experimental Data on 13.09.2005 (No Flow)

15:30	615	489.7	27.7	32.0	0.49
15:45	566	477.5	27.8	32.7	0.51
16:00	513	463.7	27.5	33.5	0.53
16:15	466	457.0	27.3	33.6	0.55
16:30	422	457.3	27.2	34.1	0.56
16:45	371	453.9	27.0	34.2	0.57
17:00	317	452.2	27.2	34.2	0.58
17:15	256	444.4	27.4	34.4	0.59

Table B.2 Experimental Data on 14.09.2005 ($\dot{m} = 0.0023 kg/s$)

Time	G_{Ths} [W/m²]	$G_{Tsph}A_T$ [W]	T_a [°C]	T_{in} [°C]	T_{out} [°C]	T_f [°C]	η
09:30	519	375.4	20.1	16.0	18.3	18.5	0.56
09:45	563	393.3	20.2	16.5	20.5	18.7	0.57
10:00	604	409.8	21.6	16.5	21.5	19.4	0.57
10:15	679	438.9	21.7	16.7	22.1	19.7	0.54
10:30	705	448.0	22.4	16.6	23.0	19.8	0.54
10:45	712	448.9	23.0	16.9	24.0	21.0	0.55
11:00	731	454.8	23.5	17.0	25.0	22.0	0.56
11:15	756	462.3	23.7	17.0	26.0	23.6	0.57
11:30	769	466.9	24.5	17.1	27.1	23.8	0.58
11:45	784	472.3	25.1	17.2	28.0	24.0	0.59
12:00	795	476.9	25.4	17.3	28.7	24.8	0.59
12:15	816	486.1	26.1	17.4	29.5	24.4	0.59
12:30	803	481.4	25.9	17.3	30.2	22.6	0.61
12:45	813	488.0	26.4	17.3	30.8	22.8	0.61
13:00	825	499.7	27.0	17.2	31.6	22.6	0.61
13:15	821	502.6	26.4	17.4	32.1	22.4	0.61
13:30	809	502.5	27.1	17.8	32.7	23.1	0.61
13:45	786	495.6	27.2	17.9	33.0	24.3	0.62
14:00	758	487.6	27.0	17.8	33.4	23.3	0.63
14:15	767	505.1	27.4	17.9	33.8	24.7	0.61
14:30	743	504.3	27.3	17.8	34.0	24.4	0.62
14:45	699	489.5	27.7	17.8	34.2	24.8	0.64
15:00	664	483.7	27.5	17.8	34.4	26.0	0.64
15:15	615	468.2	28.1	17.7	34.4	26.3	0.66
15:30	580	464.1	27.7	17.5	34.5	26.2	0.67
15:45	537	455.7	27.7	17.5	34.5	26.3	0.68
16:00	492	447.9	27.9	17.5	34.5	26.8	0.69
16:15	435	429.7	27.4	17.4	34.3	27.3	0.71
16:30	408	446.9	27.5	17.4	34.2	27.9	0.68
16:45	342	422.5	27.5	17.2	34.2	27.9	0.72
17:00	263	376.7	27.0	17.0	33.6	28.4	0.79

Table B.3 Experimental Data on 15.09.2005 ($\dot{m} = 0.0055 kg/s$)

Time	G_{Ths} [W/m²]	$G_{Tsph}A_T$ [W]	T_a [°C]	T_{in} [°C]	T_{out} [°C]	T_f [°C]	η
08:30	330	268.7	18.3	16.5	20.2	21.3	0.31
08:45	371	294.6	18.7	16.0	20.6	21.5	0.36
09:00	431	332.2	19.6	16.0	21.5	21.2	0.39
09:15	461	346.1	19.9	15.9	21.9	21.9	0.42
09:30	462	343.8	19.9	15.9	22.4	21.7	0.47
09:45	530	377.7	20.9	16.0	23.3	21.8	0.48
10:00	564	392.5	21.6	16.0	24.1	21.9	0.52
10:15	597	406.4	22.4	16.0	24.8	22.0	0.55
10:30	540	381.2	22.5	16.0	24.8	22.0	0.60
10:45	620	414.7	23.7	16.0	25.5	22.0	0.59
11:00	694	441.6	24.0	16.1	26.2	21.7	0.60
11:15	714	447.3	24.7	16.1	26.8	21.8	0.63
11:30	733	453.8	25.3	16.1	26.8	22.0	0.63
11:45	738	455.9	25.2	16.2	27.1	22.6	0.64
12:00	739	456.2	26.3	16.3	27.4	22.1	0.66
12:15	793	477.5	26.4	16.4	27.8	21.9	0.65
12:30	808	484.9	26.8	16.5	28.2	21.9	0.66
12:45	810	487.7	27.7	16.5	28.7	22.3	0.69
13:00	826	501.9	28.7	16.5	28.9	22.4	0.69
13:15	829	509.2	27.6	16.6	29.2	22.7	0.69
13:30	859	535.2	29.1	16.6	29.6	23.0	0.68
13:45	838	530.5	28.5	16.6	29.8	23.1	0.70
14:00	860	555.0	28.7	16.7	29.9	23.5	0.68
14:15	856	565.5	29.1	16.7	30.3	23.5	0.69
14:30	791	539.0	29.5	16.8	30.4	23.2	0.73
14:45	720	506.4	29.2	16.8	30.4	23.6	0.78
15:00	691	506.3	29.4	16.7	30.1	24.2	0.78
15:15	671	514.8	29.0	16.7	30.5	24.5	0.79
15:30	637	513.6	29.0	16.6	30.5	24.3	0.80
15:45	579	496.0	28.4	16.5	29.7	24.5	0.81
16:00	608	563.0	28.3	16.3	29.4	24.6	0.71
16:15	575	581.6	28.3	16.1	29.5	24.5	0.71

Table B.4 Experimental Data on 19.09.2005 ($\dot{m} = 0.0077 kg/s$)

Time	G_{Ths} [W/m²]	$G_{Tsph}A_T$ [W]	T_a [°C]	T_{in} [°C]	T_{out} [°C]	T_f [°C]	η
08:30	298	243.4	18.8	15.8	19.4	19.3	0.86
08:45	351	282.0	19.3	15.9	19.7	19.4	0.76
09:00	405	317.1	20.3	15.9	20.2	19.8	0.72
09:15	457	346.9	20.8	15.9	20.6	19.9	0.69
09:30	514	375.3	20.7	15.9	21.5	20.2	0.71
09:45	549	389.6	21.4	15.9	22.1	20.1	0.73
10:00	584	402.8	22.0	15.9	22.6	19.8	0.74
10:15	572	396.5	22.4	16.0	23.1	20.0	0.78
10:30	679	439.9	22.2	16.0	23.5	20.7	0.73
10:45	704	448.5	23.4	16.0	23.9	20.8	0.74
11:00	733	459.0	23.6	16.0	24.4	21.3	0.76
11:15	752	464.3	24.1	16.0	24.7	20.4	0.77
11:30	779	475.0	24.6	16.1	25.0	20.7	0.76
11:45	789	479.5	25.3	16.1	25.3	20.2	0.77
12:00	808	488.6	25.6	16.1	25.6	21.2	0.77
12:15	827	499.8	26.1	16.2	25.9	21.0	0.76
12:30	834	505.0	26.9	16.2	26.1	20.9	0.76
12:45	835	508.5	26.9	16.1	26.4	21.5	0.78
13:00	837	515.2	27.3	16.1	26.5	21.6	0.77
13:15	816	508.0	26.5	16.2	26.5	22.0	0.77
13:30	826	521.9	28.0	16.2	26.8	23.2	0.77
13:45	796	511.6	27.7	16.3	27.0	23.9	0.79
14:00	777	509.5	28.0	16.3	27.0	23.1	0.79
14:15	764	514.0	28.7	16.4	27.2	23.2	0.78
14:30	746	517.7	28.7	16.4	27.2	23.3	0.78
14:45	724	520.4	28.7	16.4	27.1	23.5	0.76
15:00	674	504.6	28.6	16.4	27.1	23.6	0.78
15:15	632	495.3	29.5	16.3	27.2	23.1	0.81
15:30	598	494.4	29.2	16.4	27.2	23.4	0.80
15:45	562	495.0	29.3	16.2	27.2	23.2	0.80
16:00	530	504.9	29.3	16.3	27.1	23.5	0.77
16:15	466	484.3	29.2	16.2	27.0	23.6	0.80
16:30	414	481.5	29.2	16.1	26.8	23.7	0.80
16:45	349	465.3	28.3	16.0	26.5	23.9	0.81
17:00	302	480.1	28.6	16.0	26.0	23.2	0.75
17:15	238	478.4	28.4	16.0	25.6	22.9	0.72

Table B.5 Experimental Data on 20.09.2005 ($\dot{m} = 0.011 kg/s$)

Time	G_{Ths} [W/m²]	$G_{Tsph}A_T$ [W]	T_a [°C]	T_{in} [°C]	T_{out} [°C]	T_f [°C]	η
08:30	372	311.5	21.7	15.8	19.0	18.8	0.62
08:45	361	291.0	22.1	15.8	18.9	19.0	0.64
09:00	411	322.5	22.5	15.8	19.6	18.8	0.68
09:15	441	337.2	22.6	15.9	19.7	18.8	0.65
09:30	511	374.5	22.9	15.9	20.0	19.0	0.62
09:45	558	394.9	23.4	15.9	20.6	19.1	0.65
10:00	598	409.8	23.8	15.9	21.0	19.1	0.68
10:15	634	423.7	24.4	16.0	21.5	19.0	0.70
10:30	667	435.5	24.7	16.0	21.9	19.1	0.71
10:45	709	451.4	24.7	16.0	22.3	19.5	0.73
11:00	746	465.4	25.1	16.0	22.4	19.6	0.72
11:15	765	471.2	25.7	16.0	22.7	19.4	0.73
11:30	782	477.3	26.0	16.0	22.7	19.5	0.73
11:45	806	489.3	26.1	16.0	23.0	19.4	0.74
12:00	830	502.3	25.8	16.0	23.2	19.3	0.73
12:15	822	498.3	26.5	16.0	23.4	20.2	0.76
12:30	845	513.1	26.9	16.1	23.5	19.9	0.73
12:45	847	517.2	27.3	16.1	23.8	20.0	0.75
13:00	839	518.1	27.1	16.1	23.8	20.1	0.75
13:15	821	513.1	27.5	16.1	24.0	20.0	0.77
13:30	817	518.1	27.5	16.1	24.0	20.3	0.77
13:45	797	514.1	27.6	16.0	24.0	20.3	0.78
14:00	806	530.3	28.3	16.1	24.1	20.5	0.75
14:15	780	527.5	27.4	16.1	23.8	20.4	0.73
14:30	729	508.1	27.9	16.0	23.9	20.6	0.78
14:45	708	511.2	26.7	16.0	23.1	20.5	0.70
15:00	688	517.7	28.3	16.0	23.5	20.6	0.72
15:15	620	488.9	28.4	16.0	23.6	20.5	0.77
15:30	587	488.3	26.2	16.0	22.6	20.7	0.68
15:45	543	480.7	27.7	16.0	22.7	20.6	0.70
16:00	512	491.5	27.8	16.0	22.7	20.7	0.68
16:15	458	481.5	27.6	16.0	22.7	20.7	0.69
16:30	387	454.1	27.5	16.0	22.6	20.7	0.72
16:45	345	466.3	27.4	16.0	22.4	20.8	0.68
17:00	284	458.5	27.0	16.0	22.0	20.9	0.65

Table B.6 Experimental Data on 21.09.2005 ($\dot{m} = 0.011 kg/s$)

Time	G_{Ths} [W/m²]	$G_{Tsph}A_T$ [W]	T_a [°C]	T_{in} [°C]	T_{out} [°C]	T_f [°C]	η
08:30	275	223.7	18.3	15.7	17.9	18.2	0.58
08:45	346	280.0	18.6	15.7	18.5	18.3	0.55
09:00	379	299.2	19.3	15.7	18.8	18.5	0.57
09:15	415	320.4	19.8	15.6	18.9	18.5	0.56
09:30	462	346.5	20.3	15.6	19.2	18.8	0.56
09:45	509	370.3	21.1	15.6	19.6	19.0	0.58
10:00	522	374.0	21.6	15.7	20.1	18.8	0.62
10:15	568	395.4	21.9	15.8	20.6	19.0	0.64
10:30	584	401.0	22.9	15.8	20.9	19.6	0.66
10:45	608	410.8	23.0	15.8	20.9	19.4	0.64
11:00	620	415.6	23.3	15.9	20.7	19.3	0.61
11:15	750	465.1	23.9	15.9	21.2	19.0	0.59
11:30	801	488.7	24.7	15.9	21.5	19.2	0.59
11:45	805	490.3	25.4	16.0	22.0	19.4	0.63
12:00	820	498.1	25.4	16.0	22.3	19.0	0.65
12:15	844	513.6	26.3	16.0	22.6	19.3	0.65
12:30	860	524.0	25.7	16.0	22.6	19.5	0.64
12:45	908	555.8	26.3	16.0	22.5	19.3	0.60
13:00	864	535.3	26.8	16.0	23.1	19.2	0.67
13:15	850	533.3	27.4	16.0	23.4	19.6	0.70
13:30	837	532.4	26.8	16.0	22.3	19.9	0.61
13:45	783	507.5	27.2	16.0	23.3	19.6	0.73
14:00	764	504.7	27.6	16.0	23.4	19.9	0.75
14:15	760	516.6	28.1	16.0	23.6	19.8	0.75
14:30	727	509.3	27.9	16.0	23.5	19.8	0.74
14:45	677	491.0	28.2	16.0	23.6	19.8	0.79
15:00	653	493.8	28.6	16.0	23.5	20.1	0.77
15:15	610	483.2	28.1	16.0	23.6	20.2	0.80
15:30	567	474.1	27.3	16.0	23.3	19.9	0.79
15:45	538	480.7	28.0	16.0	23.5	20.4	0.80
16:00	477	460.6	28.4	16.0	23.4	20.3	0.82
16:15	415	438.7	27.7	16.0	23.3	20.4	0.85
16:30	377	447.6	27.8	16.0	23.1	20.6	0.81
16:45	318	434.4	27.5	16.0	22.9	20.8	0.82
17:00	269	441.1	27.5	16.0	22.6	20.9	0.78
17:15	209	440.2	27.0	15.9	22.0	20.8	0.73

Table B.7 Experimental Data on 22.09.2005 (No Flow)

Time	G_{Ths} [W/m²]	$G_{Tsph}A_T$ [W]	T_a [°C]	T_f [°C]	η
13:00	815	506.9	26.1	18.3	0.37
13:15	582	400.2	26.0	18.7	0.48
13:30	825	526.4	26.4	19.0	0.38
13:45	810	526.9	25.0	19.3	0.38
14:00	796	528.9	26.7	19.5	0.39
14:15	803	548.6	26.0	19.9	0.38
14:30	731	514.9	26.7	20.4	0.42
14:45	714	520.8	27.1	20.9	0.42
15:00	679	517.5	26.5	22.1	0.43
15:15	624	497.8	27.4	22.1	0.46
15:30	583	491.4	27.1	22.6	0.47
15:45	517	465.3	26.8	22.6	0.51
16:00	485	473.1	26.4	22.6	0.51
16:15	419	447.5	26.8	23.9	0.55
16:30	381	459.3	26.1	24.4	0.54
16:45	306	424.3	26.0	24.9	0.60
17:00	241	400.7	24.4	25.3	0.64
17:15	185	395.9	24.5	25.5	0.66

Table B.8 Experimental Data on 26.10.2005 (No Flow)

Time	G_{Ths} [W/m²]	$G_{Tsph}A_T$ [W]	T_a [°C]	T_f [°C]	η
11:45	535	391.9	16.2	20.4	0.36
12:00	552	401.5	16.6	20.1	0.36
12:15	560	405.3	17.6	21.6	0.35
12:30	562	408.4	17.2	21.5	0.35
12:45	566	412.7	17.7	21.7	0.35
13:00	577	422.2	17.6	22.6	0.35
13:15	563	419.0	18.0	22.2	0.35
13:30	568	430.1	18.4	22.0	0.34
13:45	542	420.1	18.9	22.3	0.35
14:00	552	441.0	18.8	22.6	0.34
14:15	525	433.7	19.4	22.7	0.35
14:30	488	421.0	19.2	22.8	0.36
14:45	450	408.5	19.2	24.1	0.37
15:00	399	385.0	19.2	24.2	0.40
15:15	363	376.6	19.2	24.1	0.41
15:30	319	359.8	19.4	23.9	0.43
15:45	286	359.3	19.0	24.3	0.43
16:00	248	357.2	19.5	25.5	0.44

Table B.9 Experimental Data on 27.10.2005 ($\dot{m} = 0.0023 kg/s$)

Time	G_{Ths} [W/m²]	$G_{Tsph}A_T$ [W]	T_a [°C]	T_{in} [°C]	T_{out} [°C]	T_f [°C]	η
12:00	603	431.0	16.9	19.9	20.5	19.2	0.33
12:15	614	438.7	17.5	21.4	21.4	18.8	0.32
12:30	645	461.8	18.0	22.2	22.2	19.5	0.31
12:45	629	454.4	18.1	22.5	23.4	19.8	0.31
13:00	621	453.9	18.6	23.0	24.2	20.2	0.31
13:15	653	485.5	18.9	21.4	25.0	20.4	0.29
13:30	611	464.8	18.9	18.6	25.7	20.8	0.30
13:45	587	457.6	18.9	18.4	26.2	21.0	0.31
14:00	588	473.2	19.1	18.4	26.7	20.8	0.30
14:15	566	471.9	19.4	18.2	27.1	21.3	0.30
14:30	515	448.2	19.3	18.0	27.4	21.3	0.32
14:45	474	434.6	19.4	17.8	27.8	21.9	0.33
15:00	472	461.9	19.5	18.0	27.9	22.0	0.31
15:15	390	409.7	19.4	18.1	28.1	22.3	0.35
15:30	337	385.6	19.5	18.0	27.8	21.8	0.37
15:45	334	429.9	19.3	18.0	27.5	23.1	0.33
16:00	278	411.1	19.3	18.0	27.8	23.4	0.34

APPENDIX C

COMPUTER PROGRAM FOR THE NUMERICAL SIMULATION

Number of Longitudes : $K := 12$

Number of Latitudes : $L := 10$

$\Delta\xi := \frac{\pi}{L+1}$ $\Delta\phi := \frac{2\cdot\pi}{K}$

Time Increment (s) : $\Delta t := 1$

Stefan - Boltzmann Constant (W/m^2K^4) : $\sigma := 5.67\cdot 10^{-8}$

Radius of the Tank (m) : $R_p := 0.3$

Cover-Plate Spacing (m) : $\delta_{pc} := 0.04$

Thickness of the Absorber (m) : $\delta_p := 0.003$

Thickness of the Cover (m) : $\delta_c := 0.003$

Density of the Absorber Material (kg/m^3) : $\rho_a := 8055$

Specific Heat of the Absorber Material ($J/kg.^0C$) : $c_a := 480$

Thermal Conductivity of the Absorber Material ($W/m.^0C$) : $kond := 15.1$

Emissivity of the Absorber : $\varepsilon_p := 0.30$

Density of the Cover, glass (kg/m^3) : $\rho_c := 2800$

Specific Heat of the Cover, glass ($J/kg.^0C$) : $c_c := 750$

Emissivity of the Cover : $\varepsilon_c := 0.88$

Absorptivity of the Absorber at Normal Incidence : $\alpha_n := 0.9$

Ground Reflectance : $\rho_g := 0.4$

$$
\text{Dimensions} := \left|
\begin{array}{l}
y \leftarrow \sqrt{2}\cdot R_p\cdot\sqrt{1-\cos(\Delta\xi)} \\
\text{for } \; j \in 1..L+1 \\
\quad \left|
\begin{array}{l}
\xi \leftarrow \pi - j\cdot\Delta\xi \\
x_0 \leftarrow \sqrt{2}\cdot R_p\cdot\sin(\xi+\Delta\xi)\cdot\sqrt{1-\cos(\Delta\phi)} \\
x_1 \leftarrow \sqrt{2}\cdot R_p\cdot\sin(\xi)\cdot\sqrt{1-\cos(\Delta\phi)} \\
a \leftarrow R_p\cdot(\cos(\xi)-\cos(\xi+\Delta\xi)) \\
h \leftarrow \sqrt{y^2-\left(\dfrac{x_0-x_1}{2}\right)^2} \\
A \leftarrow \dfrac{x_0+x_1}{2}\cdot h \\
\beta \leftarrow \operatorname{asin}\left(\dfrac{a}{h}\right) \;\; \text{if} \;\; \xi \le \left(\dfrac{\pi}{2}\right) \\
\beta \leftarrow \pi - \operatorname{asin}\left(\dfrac{a}{h}\right) \;\; \text{otherwise} \\
Va \leftarrow \left[\dfrac{1}{2}\cdot\left(R_p\cdot\sin(\xi)\right)^2\cdot\sin(\Delta\phi)\right]\cdot a \;\; \text{if} \;\; \cos(\xi)\ge 0 \\
Va \leftarrow \left[\dfrac{1}{2}\cdot\left(R_p\cdot\sin(\xi+\Delta\xi)\right)^2\cdot\sin(\Delta\phi)\right]\cdot a \;\; \text{otherwise} \\
Vb \leftarrow \dfrac{a\cdot\sqrt{h^2-a^2}}{2}\cdot x_1 \;\; \text{if} \;\; \cos(\xi)\ge 0 \\
Vb \leftarrow \dfrac{a\cdot\sqrt{h^2-a^2}}{2}\cdot x_0 \;\; \text{otherwise} \\
Vcd \leftarrow \dfrac{\left[\dfrac{1}{2}\cdot\left[R_p\cdot(\sin(\xi+\Delta\xi)-\sin(\xi))\right]^2\cdot\sin(\Delta\phi)\right]\cdot a}{3} \\
V \leftarrow K\cdot(Va+Vb+Vcd) \\
\text{Dimensions}_{j-1,0} \leftarrow x_0 \\
\text{Dimensions}_{j-1,1} \leftarrow x_1 \\
\text{Dimensions}_{j-1,2} \leftarrow a \\
\text{Dimensions}_{j-1,3} \leftarrow h \\
\text{Dimensions}_{j-1,4} \leftarrow A \\
\text{Dimensions}_{j-1,5} \leftarrow \beta \\
\text{Dimensions}_{j-1,6} \leftarrow V
\end{array}
\right.
\end{array}
\right.
$$

Input := ...\14.09.2005.xls

$$MN := \left| \begin{array}{l} r \leftarrow 0 \\ nom \leftarrow Input_{5,0} \\ \text{while } nom \neq 0 \\ \quad \left| \begin{array}{l} nom \leftarrow Input_{5+r,0} \\ r \leftarrow r + 1 \end{array} \right. \\ Number\_of\_measurements \leftarrow r - 1 \\ Number\_of\_measurements \end{array} \right.$$

Date : $Input_{0,2} =$

Day of the year : $n := Input_{1,2}$

Declination : $\delta := \frac{\pi}{180} \cdot 23.45 \cdot \sin\left(360 \cdot \frac{284 + n}{365} \cdot \frac{\pi}{180}\right)$

Latitude : $\phi := 39.95 \cdot \frac{\pi}{180}$

Mass Flow Rate (kg/s) : $md := Input_{2,2}$ $md =$

Number of measurement times : $MN =$

Ambient Temperature at Initial Conditions (^{0}C) : $T_a := Input_{5,3}$ $T_a =$

Water Inlet Temperature at Initial Conditions (^{0}C): $T_{in} := Input_{5,4}$ $T_{in} =$

Mean Water Temperature at Initial Conditions : $T_w :=$ for $j \in 0..L+2$

$$T_{w_j} \leftarrow \left| \begin{array}{ll} Input_{5,4} & \text{if } Input_{2,2} = 0 \\ Input_{5,6} & \text{otherwise} \end{array} \right.$$

Absorber Temperature at Initial Conditions : $T_p :=$ for $j \in 0..L+2$

for $i \in 1..K$

$T_{p_{i,j}} \leftarrow T_{w_j}$

Cover Temperature at Initial Conditions : $T_c :=$ for $j \in 0..L+2$

for $i \in 1..K$

$T_{c_{i,j}} \leftarrow T_a$

$$\text{Inputs} := \left| \begin{array}{l}
\delta \leftarrow \frac{\pi}{180} \cdot 23.45 \cdot \sin\left(360 \cdot \frac{284 + n}{365} \cdot \frac{\pi}{180}\right) \\
\phi \leftarrow 39.95 \cdot \frac{\pi}{180} \\
p \leftarrow 0 \\
\text{while} \quad p \le \frac{(MN - 1) \cdot 15 \cdot 60}{\Delta t} \\
\quad \left| \begin{array}{l}
Gx \leftarrow \begin{pmatrix} \text{trunc}\left(\frac{p \cdot \Delta t}{15 \cdot 60}\right) \\ \text{trunc}\left(\frac{p \cdot \Delta t}{15 \cdot 60}\right) + 1 \end{pmatrix} \\
Gy \leftarrow \begin{pmatrix} \text{Input}_{5+\text{trunc}\left(\frac{p \cdot \Delta t}{15 \cdot 60}\right), 1} \\ \text{Input}_{5+\text{trunc}\left(\frac{p \cdot \Delta t}{15 \cdot 60}\right)+1, 1} \end{pmatrix} \\
G \leftarrow \text{linterp}\left(Gx, Gy, \frac{p \cdot \Delta t}{15 \cdot 60}\right) \\
\omega x \leftarrow Gx \\
\omega y \leftarrow \begin{pmatrix} \left| \begin{array}{ll} \frac{\pi}{180} \cdot \text{Input}_{5+\text{trunc}\left(\frac{p \cdot \Delta t}{15 \cdot 60}\right), 6} & \text{if} \quad \text{Input}_{2,2} = 0 \\ \frac{\pi}{180} \cdot \text{Input}_{5+\text{trunc}\left(\frac{p \cdot \Delta t}{15 \cdot 60}\right), 8} & \text{otherwise} \end{array} \right. \\ \left| \begin{array}{ll} \frac{\pi}{180} \cdot \text{Input}_{5+\text{trunc}\left(\frac{p \cdot \Delta t}{15 \cdot 60}\right)+1, 6} & \text{if} \quad \text{Input}_{2,2} = 0 \\ \frac{\pi}{180} \cdot \text{Input}_{5+\text{trunc}\left(\frac{p \cdot \Delta t}{15 \cdot 60}\right)+1, 8} & \text{otherwise} \end{array} \right. \end{pmatrix} \\
\omega \leftarrow \text{linterp}\left(\omega x, \omega y, \frac{p \cdot \Delta t}{15 \cdot 60}\right) \\
Tx_a \leftarrow Gx \\
Ty_a \leftarrow \begin{pmatrix} \text{Input}_{5+\text{trunc}\left(\frac{p \cdot \Delta t}{15 \cdot 60}\right), 3} \\ \text{Input}_{5+\text{trunc}\left(\frac{p \cdot \Delta t}{15 \cdot 60}\right)+1, 3} \end{pmatrix} \\
T_a \leftarrow \text{linterp}\left(Tx_a, Ty_a, \frac{p \cdot \Delta t}{15 \cdot 60}\right)
\end{array} \right.
\end{array} \right.$$

$$Tx_{in} \leftarrow Gx$$

$$Ty_{in} \leftarrow \begin{pmatrix} Input_{5+trunc\left(\frac{p\cdot\Delta t}{15\cdot 60}\right),4} \\ Input_{5+trunc\left(\frac{p\cdot\Delta t}{15\cdot 60}\right)+1,4} \end{pmatrix}$$

$$T_{in} \leftarrow \begin{cases} 0 & \text{if } Input_{2,2} = 0 \\ linterp\left(Tx_{in}, Ty_{in}, \frac{p\cdot\Delta t}{15\cdot 60}\right) & \text{otherwise} \end{cases}$$

$$G_0 \leftarrow 1367\cdot\left(1 + 0.033\cdot\cos\left(\frac{360\cdot n}{365}\cdot\frac{\pi}{180}\right)\right)\cdot\left(\begin{matrix}\cos(\phi)\cdot\cos(\delta)\cdot\cos(\omega) \ ... \\ + \sin(\phi)\cdot\sin(\delta)\end{matrix}\right)$$

$$\cos\theta_z \leftarrow \cos(\phi)\cdot\cos(\delta)\cdot\cos(\omega) + \sin(\phi)\cdot\sin(\delta)$$

$$Tx_{m\_actual} \leftarrow Gx$$

$$Ty_{m\_actual} \leftarrow \begin{pmatrix} \begin{cases} Input_{5+trunc\left(\frac{p\cdot\Delta t}{15\cdot 60}\right),4} & \text{if } Input_{2,2} = 0 \\ Input_{5+trunc\left(\frac{p\cdot\Delta t}{15\cdot 60}\right),6} & \text{otherwise} \end{cases} \\ \begin{cases} Input_{5+trunc\left(\frac{p\cdot\Delta t}{15\cdot 60}\right)+1,4} & \text{if } Input_{2,2} = 0 \\ Input_{5+trunc\left(\frac{p\cdot\Delta t}{15\cdot 60}\right)+1,6} & \text{otherwise} \end{cases} \end{pmatrix}$$

$$T_{m\_actual} \leftarrow linterp\left(Tx_{m\_actual}, Ty_{m\_actual}, \frac{p\cdot\Delta t}{15\cdot 60}\right)$$

$$Tx_{out\_actual} \leftarrow Gx$$

$$Ty_{out\_actual} \leftarrow \begin{pmatrix} Input_{5+trunc\left(\frac{p\cdot\Delta t}{15\cdot 60}\right),5} \\ Input_{5+trunc\left(\frac{p\cdot\Delta t}{15\cdot 60}\right)+1,5} \end{pmatrix}$$

$$T_{out\_actual} \leftarrow \begin{cases} 0 & \text{if } Input_{2,2} = 0 \\ linterp\left(Tx_{out\_actual}, Ty_{out\_actual}, \frac{p\cdot\Delta t}{15\cdot 60}\right) & \text{otherwise} \end{cases}$$

$$Inputs_{p,0} \leftarrow G$$

$$Inputs_{p,1} \leftarrow \omega$$

$$Inputs_{p,2} \leftarrow T_a$$

$$Inputs_{p,3} \leftarrow T_{in}$$

$$\text{Inputs}_{p,4} \leftarrow G_0$$

$$\text{Inputs}_{p,5} \leftarrow \cos\theta_z$$

$$\text{Inputs}_{p,6} \leftarrow T_{m\_actual}$$

$$\text{Inputs}_{p,7} \leftarrow T_{out\_actual}$$

$$p \leftarrow p + 1$$

Inputs

$$T := \left| \begin{array}{l}
y \leftarrow \sqrt{2} \cdot R_p \cdot \sqrt{1 - \cos(\Delta\xi)} \\
\delta \leftarrow \frac{\pi}{180} \cdot 23.45 \cdot \sin\left(360 \cdot \frac{284 + n}{365} \cdot \frac{\pi}{180}\right) \\
\phi \leftarrow 39.95 \cdot \frac{\pi}{180} \\
\text{for } j \in 0..L+2 \\
\quad T_{w_j} \leftarrow \text{Inputs}_{0,6} \\
\text{for } j \in 0..L+2 \\
\quad \text{for } i \in 1..K \\
\quad\quad \left| \begin{array}{l} T_{p_{i,j}} \leftarrow T_{w_j} \\ T_{c_{i,j}} \leftarrow T_a \end{array} \right. \\
T_{wnew_{L+2}} \leftarrow 0 \\
T_{pnew_{K,L+2}} \leftarrow 0 \\
T_{cnew_{K,L+2}} \leftarrow 0 \\
T_{m_{\frac{(MN-1)\cdot 15\cdot 60}{\Delta t},2}} \leftarrow 0 \\
p \leftarrow 0 \\
\text{while } p \le \frac{(MN-1)\cdot 15\cdot 60}{\Delta t} \\
\quad \left| \begin{array}{l} G \leftarrow \text{Inputs}_{p,0} \\ \omega \leftarrow \text{Inputs}_{p,1} \\ T_a \leftarrow \text{Inputs}_{p,2} \\ T_{in} \leftarrow \text{Inputs}_{p,3} \end{array} \right.
\end{array} \right.$$

$G_0 \leftarrow Inputs_{p,4}$

$\cos\theta_z \leftarrow Inputs_{p,5}$

$T_s \leftarrow T_a - 6$

$T_{w_0} \leftarrow T_{in}$

for $j \in 1..L+1$

$\xi \leftarrow \pi - j\cdot\Delta\xi$

$x_0 \leftarrow Dimensions_{j-1,0}$

$x_1 \leftarrow Dimensions_{j-1,1}$

$a \leftarrow Dimensions_{j-1,2}$

$s \leftarrow Dimensions_{j-1,3}$

$A \leftarrow Dimensions_{j-1,4}$

$\beta \leftarrow Dimensions_{j-1,5}$

$Vj \leftarrow Dimensions_{j-1,6}$

$$c_{w_j} \leftarrow 3.178\cdot10^{-6}\cdot\left(T_{w_j}\right)^4 - 7.791\cdot10^{-4}\cdot\left(T_{w_j}\right)^3 + 0.076\cdot\left(T_{w_j}\right)^2 \ldots + -2.963\cdot T_{w_j} + 4.217\cdot10^3$$

$$\rho_{w_j} \leftarrow -1.768\cdot10^{-7}\cdot\left(T_{w_j}\right)^4 + 5.061\cdot10^{-5}\cdot\left(T_{w_j}\right)^3 \ldots + -8.13\cdot10^{-3}\cdot\left(T_{w_j}\right)^2 + 0.065\cdot T_{w_j} + 999.784$$

for $i \in 1..K$

$h_{w_{i,j}} \leftarrow 300$

$$T_{wnew_j} \leftarrow T_{w_j} + \frac{\Delta t}{Vj\cdot\rho_{w_j}\cdot c_{w_j}}\cdot\left[md\cdot c_{w_j}\cdot\left(T_{w_{j-1}} - T_{w_j}\right) \ldots + A\cdot\left[\sum_{i=1}^{K}\left[h_{w_{i,j}}\cdot\left(T_{p_{i,j}} - T_{w_j}\right)\right]\right]\right]$$

for $i \in 1..K$

$\gamma \leftarrow -[(i-1)\cdot\Delta\phi]$

$$\cos\theta \leftarrow \sin(\delta)\cdot\sin(\phi)\cdot\cos(\beta) - \sin(\delta)\cdot\cos(\phi)\cdot\sin(\beta)\cdot\cos(\gamma) \ldots + \cos(\delta)\cdot\cos(\phi)\cdot\cos(\beta)\cdot\cos(\omega) \ldots + \cos(\delta)\cdot\sin(\phi)\cdot\sin(\beta)\cdot\cos(\gamma)\cdot\cos(\omega) \ldots + \cos(\delta)\cdot\sin(\beta)\cdot\sin(\gamma)\cdot\sin(\omega)$$

$$R_b \leftarrow \frac{\cos\theta}{\cos\theta_z}$$

$$k_T \leftarrow \frac{G}{G_0}$$

$$\text{ratio} \leftarrow 1.0 - 0.09 \cdot k_T \quad \text{if} \quad k_T \le 0.22$$

$$\text{ratio} \leftarrow 0.9511 - 0.1604 \cdot k_T + 4.388 \cdot k_T^{\,2} \ldots \quad \text{if} \quad 0.22 < k_T \le 0.80$$
$$+ -16.638 \cdot k_T^{\,3} + 12.336 \cdot k_T^{\,4}$$

$$\text{ratio} \leftarrow 0.165 \quad \text{if} \quad k_T > 0.80$$

$$G_d \leftarrow \text{ratio} \cdot G$$

$$G_b \leftarrow 0 \quad \text{if} \quad \cos\theta \le 0$$

$$G_b \leftarrow G - G_d \quad \text{otherwise}$$

$$A_i \leftarrow \frac{G_b}{G_0}$$

$$f \leftarrow \sqrt{\frac{G_b}{G}}$$

$$G_{T_{i,j}} \leftarrow \left(G_b + G_d \cdot A_i\right) \cdot R_b \ldots$$
$$+ G_d \cdot \left(1 - A_i\right) \cdot \left(\frac{1 + \cos\left(\beta \cdot \frac{\pi}{180}\right)}{2}\right) \cdot \left(1 + f \cdot \sin\left(\frac{\beta}{2} \cdot \frac{\pi}{180}\right)^3\right) \ldots$$
$$+ G \cdot \rho_g \cdot \left(\frac{1 - \cos\left(\beta \cdot \frac{\pi}{180}\right)}{2}\right)$$

$$\tau\alpha_b \leftarrow \left|\begin{array}{l}
\theta \leftarrow \operatorname{acos}(\cos\theta) \\
\theta_2 \leftarrow \operatorname{asin}\left(\frac{1}{1.526} \cdot \sin(\theta)\right) \\
\tau_a \leftarrow \exp\left(\frac{-30 \cdot \delta_c}{\cos\left(\theta_2\right)}\right) \\
r_{dik} \leftarrow \frac{\sin\left(\theta_2 - \theta\right)^2}{\sin\left(\theta_2 + \theta\right)^2} \\
r_{yatay} \leftarrow \frac{\tan\left(\theta_2 - \theta\right)^2}{\tan\left(\theta_2 + \theta\right)^2} \\
\tau \leftarrow \frac{\tau_a}{2} \cdot \left[\frac{1 - r_{dik}}{1 + r_{dik}} \cdot \frac{1 - r_{dik}^{\,2}}{1 - \left(r_{dik} \cdot \tau_a\right)^2} + \frac{1 - r_{yatay}}{1 + r_{yatay}} \cdot \frac{1 - r_{yatay}^{\,2}}{1 - \left(r_{yatay} \cdot \tau_a\right)^2}\right.
\end{array}\right.$$

$$\alpha \leftarrow \alpha_n \cdot \left[1 + 2.0345 \cdot 10^{-3} \cdot \left(\theta \cdot \frac{180}{\pi} \right) \ldots + -1.990 \cdot 10^{-4} \cdot \left(\theta \cdot \frac{180}{\pi} \right)^2 \ldots + 5.324 \cdot 10^{-6} \cdot \left(\theta \cdot \frac{180}{\pi} \right)^3 - 4.799 \cdot 10^{-8} \cdot \left(\theta \cdot \frac{180}{\pi} \right)^4 \right]$$

$$\tau\alpha \leftarrow 1.01 \cdot \tau \cdot \alpha$$

$$\tau\alpha$$

$$\tau\alpha_d \leftarrow \theta \leftarrow \frac{\pi}{180} \cdot \left[59.7 - 0.1388 \cdot \left(\beta \cdot \frac{180}{\pi} \right) + 0.001497 \cdot \left(\beta \cdot \frac{180}{\pi} \right)^2 \right]$$

$$\theta_2 \leftarrow \operatorname{asin}\left(\frac{1}{1.526} \cdot \sin(\theta) \right)$$

$$\tau_a \leftarrow \exp\left(\frac{-30 \cdot \delta_c}{\cos(\theta_2)} \right)$$

$$r_{dik} \leftarrow \frac{\sin(\theta_2 - \theta)^2}{\sin(\theta_2 + \theta)^2}$$

$$r_{yatay} \leftarrow \frac{\tan(\theta_2 - \theta)^2}{\tan(\theta_2 + \theta)^2}$$

$$\tau \leftarrow \frac{\tau_a}{2} \cdot \left[\frac{1 - r_{dik}}{1 + r_{dik}} \cdot \frac{1 - r_{dik}^2}{1 - (r_{dik} \cdot \tau_a)^2} + \frac{1 - r_{yatay}}{1 + r_{yatay}} \cdot \frac{1 - r_{yatay}^2}{1 - (r_{yatay} \cdot \tau_a)^2} \right.$$

$$\alpha \leftarrow \alpha_n \cdot \left[1 + 2.0345 \cdot 10^{-3} \cdot \left(\theta \cdot \frac{180}{\pi} \right) \ldots + -1.990 \cdot 10^{-4} \cdot \left(\theta \cdot \frac{180}{\pi} \right)^2 \ldots + 5.324 \cdot 10^{-6} \cdot \left(\theta \cdot \frac{180}{\pi} \right)^3 - 4.799 \cdot 10^{-8} \cdot \left(\theta \cdot \frac{180}{\pi} \right)^4 \right]$$

$$\tau\alpha \leftarrow 1.01 \cdot \tau \cdot \alpha$$

$$\tau\alpha$$

$$\tau\alpha_g \leftarrow \theta \leftarrow \frac{\pi}{180} \cdot \left[90 - 0.5788 \cdot \left(\beta \cdot \frac{180}{\pi} \right) + 0.002693 \cdot \left(\beta \cdot \frac{180}{\pi} \right)^2 \right]$$

$$\theta_2 \leftarrow \operatorname{asin}\left(\frac{1}{1.526} \cdot \sin(\theta) \right)$$

$$\tau_a \leftarrow \exp\left(\frac{-30 \cdot \delta_c}{\cos(\theta_2)} \right)$$

$$r_{dik} \leftarrow \frac{\sin\left(\theta_2 - \theta\right)^2}{\sin\left(\theta_2 + \theta\right)^2}$$

$$r_{yatay} \leftarrow \frac{\tan\left(\theta_2 - \theta\right)^2}{\tan\left(\theta_2 + \theta\right)^2}$$

$$\tau \leftarrow \frac{\tau_a}{2} \cdot \left[\frac{1 - r_{dik}}{1 + r_{dik}} \cdot \frac{1 - r_{dik}^{\ 2}}{1 - \left(r_{dik} \cdot \tau_a\right)^2} + \frac{1 - r_{yatay}}{1 + r_{yatay}} \cdot \frac{1 - r_{yatay}^{\ 2}}{1 - \left(r_{yatay} \cdot \tau_a\right)^2} \right.$$

$$\alpha \leftarrow \alpha_n \cdot \left[\begin{array}{l} 1 + 2.0345 \cdot 10^{-3} \cdot \left(\theta \cdot \frac{180}{\pi}\right) \ldots \\ + -1.990 \cdot 10^{-4} \cdot \left(\theta \cdot \frac{180}{\pi}\right)^2 \ldots \\ + 5.324 \cdot 10^{-6} \cdot \left(\theta \cdot \frac{180}{\pi}\right)^3 - 4.799 \cdot 10^{-8} \cdot \left(\theta \cdot \frac{180}{\pi}\right)^4 \end{array} \right]$$

$$\tau\alpha \leftarrow 1.01 \cdot \tau \cdot \alpha$$

$$\tau\alpha$$

$$S_{T_{i,j}} \leftarrow \left(G_b + G_d \cdot A_i\right) \cdot R_b \cdot \tau\alpha_b \ldots$$
$$+ G_d \cdot \left(1 - A_i\right) \cdot \tau\alpha_d \cdot \left(\frac{1 + \cos(\beta)}{2}\right) \cdot \left(1 + f \cdot \sin\left(\frac{\beta}{2}\right)^3\right) \ldots$$
$$+ G \cdot \rho_g \cdot \tau\alpha_g \cdot \left(\frac{1 - \cos(\beta)}{2}\right)$$

$$\alpha c_{i,j} \leftarrow 0.06 \cdot \left[\begin{array}{l} 1 + 2.0345 \cdot 10^{-3} \cdot \left(\theta \cdot \frac{180}{\pi}\right) - 1.990 \cdot 10^{-4} \cdot \left(\theta \cdot \frac{180}{\pi}\right)^2 \ldots \\ + 5.324 \cdot 10^{-6} \cdot \left(\theta \cdot \frac{180}{\pi}\right)^3 - 4.799 \cdot 10^{-8} \cdot \left(\theta \cdot \frac{180}{\pi}\right)^4 \end{array} \right]$$

$$T_{p_{i+1,j}} \leftarrow T_{p_{1,j}} \quad \text{if} \quad i = K$$

$$T_{p_{i-1,j}} \leftarrow T_{p_{K,j}} \quad \text{if} \quad i = 1$$

$$V \leftarrow A \cdot \delta_p$$

$$h_{pc_{i,j}} \leftarrow 7$$

$$h_{ca_{i,j}} \leftarrow 5$$

$$h_{rpc_{i,j}} \leftarrow \frac{\sigma \cdot \left[\begin{array}{l}\left(T_{p_{i,j}} + 273\right) \ldots \\ + \left(T_{c_{i,j}} + 273\right)\end{array}\right] \cdot \left[\begin{array}{l}\left(T_{p_{i,j}} + 273\right)^2 \ldots \\ + \left(T_{c_{i,j}} + 273\right)^2\end{array}\right]}{\frac{1}{\varepsilon_p} + \frac{1}{\varepsilon_c} - 1}$$

$$h_{rca_{i,j}} \leftarrow 0 \quad \text{if} \quad T_{c_{i,j}} = T_a$$

$$h_{rca_{i,j}} \leftarrow \frac{\sigma \cdot \varepsilon_c \cdot \left[\begin{array}{l}\left(\begin{array}{l}T_{c_{i,j}} \ldots \\ + 273\end{array}\right) \ldots \\ + \left(\begin{array}{l}T_s \ldots \\ + 273\end{array}\right)\end{array}\right] \cdot \left[\begin{array}{l}\left(\begin{array}{l}T_{c_{i,j}} \ldots \\ + 273\end{array}\right)^2 \ldots \\ + \left(\begin{array}{l}T_s \ldots \\ + 273\end{array}\right)^2\end{array}\right] \cdot \left(\begin{array}{l}T_{c_{i,j}} \ldots \\ + -T_s\end{array}\right)}{T_{c_{i,j}} - T_a} \quad \text{otherwise}$$

$$T_{pnew_{i,j}} \leftarrow T_{p_{i,j}} + \frac{\Delta t}{V \cdot \rho_a \cdot c_a} \cdot \left[\begin{array}{l}A \cdot S_{T_{i,j}} \ldots \\ + -\left(h_{pc_{i,j}} + h_{rpc_{i,j}}\right) \cdot A \cdot \left(T_{p_{i,j}} - T_{c_{i,j}}\right) \ldots \\ + \left(-h_w\right)_{i,j} \cdot A \cdot \left(T_{p_{i,j}} - T_{w_j}\right) \ldots \\ + -kond \cdot \left(x_1 \cdot \delta_p\right) \cdot \frac{T_{p_{i,j}} - T_{p_{i,j+1}}}{y} \ldots \\ + -kond \cdot \left(x_0 \cdot \delta_p\right) \cdot \frac{T_{p_{i,j}} - T_{p_{i,j-1}}}{y} \ldots \\ + -kond \cdot \left(y \cdot \delta_p\right) \cdot \frac{T_{p_{i,j}} - T_{p_{i+1,j}}}{\frac{x_0 + x_1}{2}} \ldots \\ + -kond \cdot \left(y \cdot \delta_p\right) \cdot \frac{T_{p_{i,j}} - T_{p_{i-1,j}}}{\frac{x_0 + x_1}{2}}\end{array}\right]$$

$$T_{cnew_{i,j}} \leftarrow T_{c_{i,j}} + \frac{\Delta t}{V \cdot \rho_c \cdot c_c} \cdot \left[\begin{array}{l}A \cdot G_{T_{i,j}} \cdot \alpha c_{i,j} \ldots \\ + -\left(h_{ca_{i,j}} + h_{rca_{i,j}}\right) \cdot A \cdot \left(T_{c_{i,j}} - T_a\right) \ldots \\ + \left(h_{pc_{i,j}} + h_{rpc_{i,j}}\right) \cdot A \cdot \left(T_{p_{i,j}} - T_{c_{i,j}}\right)\end{array}\right]$$

$$T_{wnew_{L+2}} \leftarrow T_{wnew_{L+1}}$$

for $i \in 1 .. K$

$$T_{pnew_{i,L+2}} \leftarrow T_{pnew_{i,L+1}}$$

$$T_{pnew_{i,0}} \leftarrow T_{pnew_{i,1}}$$

$$
\begin{array}{l}
\text{for } j \in 0..L+2 \\
\quad \text{for } i \in 1..K \\
\quad\quad T_{p_{i,j}} \leftarrow T_{pnew_{i,j}} \\
\quad\quad T_{c_{i,j}} \leftarrow T_{cnew_{i,j}} \\
\text{for } j \in 1..L+2 \\
\quad T_{w_j} \leftarrow T_{wnew_j} \\
T_{m_{p,1}} \leftarrow \dfrac{\displaystyle\sum_{j=1}^{L+1} \left(T_{w_j} \cdot \rho_{w_j} \cdot Dimensions_{j-1,6}\right)}{\displaystyle\sum_{j=1}^{L+1} \left(\rho_{w_j} \cdot Dimensions_{j-1,6}\right)} \\
T_{m\_actual} \leftarrow Inputs_{p,6} \\
T_{m_{p,2}} \leftarrow T_{m\_actual} \\
T_{out\_actual} \leftarrow Inputs_{p,7} \\
T_{m_{p,3}} \leftarrow T_{out\_actual} \\
T_{m_{p,4}} \leftarrow T_{w_0} \\
T_{m_{p,5}} \leftarrow T_{w_{L+2}} \\
p \leftarrow p+1 \\
T_m
\end{array}
$$

APPENDIX D

COMPUTER PROGRAM FOR THE COMPERATIVE STUDY BETWEEN A FLAT PLATE COLLECTOR AND THE SPHERICAL SOLARCOLLECTOR

Number of tubes : $N := 5$

Stefan-Boltzmann constant : $\sigma := 5.67 \cdot 10^{-8} \cdot \frac{watt}{m^2 \cdot K^4}$

Slope : $\beta := 40deg$

Wind heat transfer coefficient : $h_w := 5 \cdot \frac{watt}{m^2 \cdot K}$

Plate emittance : $\varepsilon_p := 0.30$

Glass emittance : $\varepsilon_c := 0.88$

Insulation thermal conductivity : $k_{ins} := 0.025 \cdot \frac{watt}{m \cdot K}$

Back insulation thickness : $L := 0.05 \cdot m$

Edge insulation thickness : $t_{edge} := 0.030 \cdot m$

Collector length : $L_{len} := 0.56 \cdot m$

Collector width : $L_{wid} := 0.50 \cdot m$

Collector thickness : $L_{thic} := 0.04 \cdot m$

Plate thickness : $\delta := 0.003 \cdot m$

Plate thermal conductivity : $k := 15.1 \cdot \frac{watt}{m K}$

Tube inside diameter : $D_i := 0.0224 \cdot m$

Tube outside diameter : $D := 0.0254 \cdot m$

Tube spacing : $W := 0.0474 \cdot m$

Bond Conductance : $C_b := 30 \cdot \frac{watt}{m \cdot K}$

Heat transfer coeficient inside tubes : $h_{fi} := 300 \cdot \frac{watt}{m^2 K}$

Cover thickness : $\delta_c := 0.003 \cdot m$

Fluid specific heat : $c_w := 4190 \cdot \frac{joule}{kg \cdot K}$

Fluid density : $\rho_w := 998 \frac{kg}{m^3}$

Absorptivity of the Absorber at Normal Incidence : $\alpha_n := 0.9$

Ground Reflectance : $\rho_g := 0.4$

Input := ...\19.09.2005.xls

```
MN := | r ← 0
      | nom ← Input[5,0]
      | while nom ≠ 0
      |   | nom ← Input[5+r,0]
      |   | r ← r + 1
      | Number_of_measurements ← r − 1
      | Number_of_measurements
```

Date : $Input_{0,2} = \text{"09/14/2005"}$

Day of the year : $n := Input_{1,2}$

Number of measurement times : $MN = 35$

Ambient Temperature at Initial Conditions : $T_a := \left(Input_{5,3} + 273\right)K$

Water Inlet Temperature at Initial Conditions : $T_{in} := \left(Input_{5,4} + 273\right)K$

Mass Flow Rate : $md := Input_{2,2} \cdot \frac{kg}{sec}$ $md = 0.0023 \frac{kg}{s}$

c_values :=

$$\delta \leftarrow 23.45\text{deg}\cdot\sin\left(360\text{deg}\cdot\frac{284+n}{365}\right)$$

$$\phi \leftarrow 39.95\cdot\text{deg}$$

$$p \leftarrow 0$$

while $p \le \text{trunc}\left(\frac{MN-5}{4}\right)$

$$T_a \leftarrow \frac{1}{4}\cdot\left(\frac{\text{Input}_{5+4p,3}+\text{Input}_{5+4p+4,3}}{2}+\sum_{i=1}^{3}\text{Input}_{5+4p+i,3}\right)\cdot K$$

$$I \leftarrow 15\cdot\text{min}\cdot 60\cdot\frac{\text{sec}}{\text{min}}\cdot\left(\frac{\text{Input}_{5+4p,1}+\text{Input}_{5+4p+4,1}}{2}+\sum_{i=1}^{3}\text{Input}_{5+4p+i,1}\right)\cdot\frac{\text{watt}}{m^2}$$

$$\omega_1 \leftarrow \begin{cases}\left(\text{Input}_{5+4p,6}\right)\cdot\text{deg} & \text{if } \text{Input}_{2,2}=0\\ \left(\text{Input}_{5+4p,8}\right)\cdot\text{deg} & \text{otherwise}\end{cases}$$

$$\omega_2 \leftarrow \begin{cases}\left(\text{Input}_{5+4p+4,6}\right)\cdot\text{deg} & \text{if } \text{Input}_{2,2}=0\\ \left(\text{Input}_{5+4p+4,8}\right)\cdot\text{deg} & \text{otherwise}\end{cases}$$

$$I_0 \leftarrow \frac{12\cdot 3600\text{sec}\cdot\left(1367\cdot\frac{\text{watt}}{m^2}\right)}{\pi}\cdot\left(1+0.033\cdot\cos\left(\frac{360\cdot n}{365}\cdot\frac{\pi}{180}\right)\right)\cdot\left[\cos(\phi)\cdot\cos(\delta)\cdot\left(\sin(\omega_2)-\sin(\omega_1)\right)+(\omega_2-\omega_1)\cdot\sin(\phi)\cdot\sin(\delta)\right]$$

$$\cos\theta_z \leftarrow \cos(\phi)\cdot\cos(\delta)\cdot\cos\left(\frac{\omega_1+\omega_2}{2}\right)+\sin(\phi)\cdot\sin(\delta)$$

$$\gamma \leftarrow 0$$

$$\begin{aligned}\cos\theta \leftarrow\ & \sin(\delta)\cdot\sin(\phi)\cdot\cos(\beta)-\sin(\delta)\cdot\cos(\phi)\cdot\sin(\beta)\cdot\cos(\gamma)\ \ldots\\ & +\cos(\delta)\cdot\cos(\phi)\cdot\cos(\beta)\cdot\cos\left(\frac{\omega_1+\omega_2}{2}\right)\ \ldots\\ & +\cos(\delta)\cdot\sin(\phi)\cdot\sin(\beta)\cdot\cos(\gamma)\cdot\cos\left(\frac{\omega_1+\omega_2}{2}\right)\ \ldots\\ & +\cos(\delta)\cdot\sin(\beta)\cdot\sin(\gamma)\cdot\sin\left(\frac{\omega_1+\omega_2}{2}\right)\end{aligned}$$

$$R_b \leftarrow \frac{\cos\theta}{\cos\theta_z}$$

$$k_T \leftarrow \frac{I}{I_0}$$

$$\text{ratio} \leftarrow 1.0-0.09\cdot k_T \quad \text{if } k_T \le 0.22$$

$$\text{ratio} \leftarrow 0.9511-0.1604\cdot k_T+4.388\cdot k_T^{\,2}\ \ldots \quad \text{if } 0.22 < k_T \le 0.80$$

$$+ -16.638 \cdot k_T^{\,3} + 12.336 \cdot k_T^{\,4}$$

$$\text{ratio} \leftarrow 0.165 \quad \text{if} \quad k_T > 0.80$$

$$I_d \leftarrow \text{ratio} \cdot I$$

$$I_b \leftarrow 0 \quad \text{if} \quad \cos\theta \le 0$$

$$I_b \leftarrow I - I_d \quad \text{otherwise}$$

$$A_i \leftarrow \frac{I_b}{I_0}$$

$$f \leftarrow \sqrt{\frac{I_b}{I}}$$

$$I_T \leftarrow \left(I_b + I_d \cdot A_i\right) \cdot R_b + I_d \cdot \left(1 - A_i\right) \cdot \left(\frac{1 + \cos(\beta)}{2}\right) \cdot \left(1 + f \cdot \sin\left(\frac{\beta}{2}\right)^3\right) \ldots$$
$$+ I \cdot \rho_g \cdot \left(\frac{1 - \cos(\beta)}{2}\right)$$

$$\tau\alpha_b \leftarrow \left| \begin{array}{l}
\theta \leftarrow \operatorname{acos}(\cos\theta) \\
\theta_2 \leftarrow \operatorname{asin}\left(\frac{1}{1.526} \cdot \sin(\theta)\right) \\
\tau_a \leftarrow \exp\left(\frac{-0.3 \cdot cm^{-1} \cdot \delta_c}{\cos(\theta_2)}\right) \\
r_{dik} \leftarrow \frac{\sin(\theta_2 - \theta)^2}{\sin(\theta_2 + \theta)^2} \\
r_{yatay} \leftarrow \frac{\tan(\theta_2 - \theta)^2}{\tan(\theta_2 + \theta)^2} \\
\tau \leftarrow \frac{\tau_a}{2} \cdot \left[\frac{1 - r_{dik}}{1 + r_{dik}} \cdot \frac{1 - r_{dik}^{\,2}}{1 - \left(r_{dik} \cdot \tau_a\right)^2} + \frac{1 - r_{yatay}}{1 + r_{yatay}} \cdot \frac{1 - r_{yatay}^{\,2}}{1 - \left(r_{yatay} \cdot \tau_a\right)^2}\right] \\
\alpha \leftarrow \alpha_n \cdot \left[1 + 2.0345 \cdot 10^{-3} \cdot \left(\theta \cdot \frac{180}{\pi}\right) - 1.990 \cdot 10^{-4} \cdot \left(\theta \cdot \frac{180}{\pi}\right)^2 \ldots \right. \\
\left. + 5.324 \cdot 10^{-6} \cdot \left(\theta \cdot \frac{180}{\pi}\right)^3 - 4.799 \cdot 10^{-8} \cdot \left(\theta \cdot \frac{180}{\pi}\right)^4\right] \\
\tau\alpha \leftarrow 1.01 \cdot \tau \cdot \alpha \\
\tau\alpha
\end{array} \right.$$

$$\tau\alpha_d \leftarrow \left| \theta \leftarrow \frac{\pi}{180} \cdot \left[59.7 - 0.1388 \cdot \left(\beta \cdot \frac{180}{\pi}\right) + 0.001497 \cdot \left(\beta \cdot \frac{180}{\pi}\right)^2\right] \right.$$

$$\theta_2 \leftarrow \operatorname{asin}\left(\frac{1}{1.526}\cdot\sin(\theta)\right)$$

$$\tau_a \leftarrow \exp\left(\frac{-0.3\cdot cm^{-1}\cdot\delta_c}{\cos(\theta_2)}\right)$$

$$r_{dik} \leftarrow \frac{\sin(\theta_2-\theta)^2}{\sin(\theta_2+\theta)^2}$$

$$r_{yatay} \leftarrow \frac{\tan(\theta_2-\theta)^2}{\tan(\theta_2+\theta)^2}$$

$$\tau \leftarrow \frac{\tau_a}{2}\cdot\left[\frac{1-r_{dik}}{1+r_{dik}}\cdot\frac{1-r_{dik}^2}{1-(r_{dik}\cdot\tau_a)^2}+\frac{1-r_{yatay}}{1+r_{yatay}}\cdot\frac{1-r_{yatay}^2}{1-(r_{yatay}\cdot\tau_a)^2}\right]$$

$$\alpha \leftarrow \alpha_n\cdot\left[1+2.0345\cdot10^{-3}\cdot\left(\theta\cdot\frac{180}{\pi}\right)-1.990\cdot10^{-4}\cdot\left(\theta\cdot\frac{180}{\pi}\right)^2 \ldots +5.324\cdot10^{-6}\cdot\left(\theta\cdot\frac{180}{\pi}\right)^3-4.799\cdot10^{-8}\cdot\left(\theta\cdot\frac{180}{\pi}\right)^4\right]$$

$$\tau\alpha \leftarrow 1.01\cdot\tau\cdot\alpha$$

$$\tau\alpha$$

$$\tau\alpha_g \leftarrow \theta \leftarrow \frac{\pi}{180}\cdot\left[90-0.5788\cdot\left(\beta\cdot\frac{180}{\pi}\right)+0.002693\cdot\left(\beta\cdot\frac{180}{\pi}\right)^2\right]$$

$$\theta_2 \leftarrow \operatorname{asin}\left(\frac{1}{1.526}\cdot\sin(\theta)\right)$$

$$\tau_a \leftarrow \exp\left(\frac{-0.3\cdot cm^{-1}\cdot\delta_c}{\cos(\theta_2)}\right)$$

$$r_{dik} \leftarrow \frac{\sin(\theta_2-\theta)^2}{\sin(\theta_2+\theta)^2}$$

$$r_{yatay} \leftarrow \frac{\tan(\theta_2-\theta)^2}{\tan(\theta_2+\theta)^2}$$

$$\tau \leftarrow \frac{\tau_a}{2}\cdot\left[\frac{1-r_{dik}}{1+r_{dik}}\cdot\frac{1-r_{dik}^2}{1-(r_{dik}\cdot\tau_a)^2}+\frac{1-r_{yatay}}{1+r_{yatay}}\cdot\frac{1-r_{yatay}^2}{1-(r_{yatay}\cdot\tau_a)^2}\right]$$

$$\alpha \leftarrow \alpha_n \cdot \left[1 + 2.0345 \cdot 10^{-3} \cdot \left(\theta \cdot \frac{180}{\pi} \right) - 1.990 \cdot 10^{-4} \cdot \left(\theta \cdot \frac{180}{\pi} \right)^2 \ldots + 5.324 \cdot 10^{-6} \cdot \left(\theta \cdot \frac{180}{\pi} \right)^3 - 4.799 \cdot 10^{-8} \cdot \left(\theta \cdot \frac{180}{\pi} \right)^4 \right]$$

$$\tau\alpha \leftarrow 1.01 \cdot \tau \cdot \alpha$$

$$\tau\alpha$$

$$S \leftarrow \left(I_b + I_d \cdot A_i \right) \cdot R_b \cdot \tau\alpha_b \ldots + I_d \cdot \left(1 - A_i \right) \cdot \tau\alpha_d \cdot \left(\frac{1 + \cos(\beta)}{2} \right) \cdot \left(1 + f \cdot \sin\left(\frac{\beta}{2} \right)^3 \right) \ldots + I \cdot \rho_g \cdot \tau\alpha_g \cdot \left(\frac{1 - \cos(\beta)}{2} \right)$$

$$p \leftarrow p + 1$$

$$c\_inputs_{0,0} \leftarrow \text{"Ta,ave (C)"}$$

$$c\_inputs_{0,1} \leftarrow \text{"I (J/m2)"}$$

$$c\_inputs_{0,2} \leftarrow \text{"Ib (J/m2)"}$$

$$c\_inputs_{0,3} \leftarrow \text{"Id (J/m2)"}$$

$$c\_inputs_{0,4} \leftarrow \text{"I0 (J/m2)"}$$

$$c\_inputs_{0,5} \leftarrow \text{"IT (J/m2)"}$$

$$c\_inputs_{0,6} \leftarrow \text{"S (J/m2)"}$$

$$c\_inputs_{0,7} \leftarrow \text{"kT"}$$

$$c\_inputs_{0,8} \leftarrow \text{"t÷a÷b"}$$

$$c\_inputs_{0,9} \leftarrow \text{"t÷a÷d"}$$

$$c\_inputs_{0,10} \leftarrow \text{"t÷a÷g"}$$

$$c\_inputs_{p,0} \leftarrow \frac{T_a}{K}$$

$$c\_inputs_{p,1} \leftarrow \frac{I}{1m^{-2}\,joule}$$

$$c\_inputs_{p,2} \leftarrow \frac{I_b}{1m^{-2}\,joule}$$

$$c\_inputs_{p,3} \leftarrow \frac{I_d}{1m^{-2}\,joule}$$

$$c\_inputs_{p,4} \leftarrow \frac{I_0}{1m^{-2}\,joule}$$

$$c\_inputs_{p,5} \leftarrow \frac{I_T}{1m^{-2}\,joule}$$

$$c\_inputs_{p,6} \leftarrow \frac{S}{1m^{-2}\,joule}$$

$$c\_inputs_{p,7} \leftarrow k_T$$

$$c\_inputs_{p,8} \leftarrow \tau\alpha_b$$

$$c\_inputs_{p,9} \leftarrow \tau\alpha_d$$

$$c\_inputs_{p,10} \leftarrow \tau\alpha_g$$

$$c\_inputs$$

$$c2_value := \left|\begin{array}{l}
\Delta err \leftarrow 0.1K \\
p \leftarrow 1 \\
T_p \leftarrow T_{in} \\
T_c \leftarrow T_a \\
\text{while } p \le trunc\left(\frac{MN-5}{4}\right)+1 \\
\quad difference2 \leftarrow \Delta err + 1\cdot K \\
\quad T_a \leftarrow \left(c_values_{p,0}+273\right)K \\
\quad T_s \leftarrow T_a - 6K \\
\quad \text{while } difference2 > \Delta err \\
\quad\quad difference \leftarrow \Delta err + 1\cdot K \\
\quad\quad \text{while } difference > \Delta err \\
\quad\quad\quad h_{rca} \leftarrow \left|\begin{array}{ll} 0 & \text{if } T_c = T_a \\ \varepsilon_c\cdot\dfrac{\sigma\cdot\left(T_c+T_s\right)\cdot\left(T_c^{\,2}+T_s^{\,2}\right)\cdot\left(T_c-T_s\right)}{T_c-T_a} & \text{otherwise}\end{array}\right. \\
\quad\quad\quad h_{rpc} \leftarrow \dfrac{\sigma\cdot\left(T_p^{\,2}+T_c^{\,2}\right)\cdot\left(T_p+T_c\right)}{\dfrac{1}{\varepsilon_p}+\dfrac{1}{\varepsilon_c}-1} \\
\quad\quad\quad h_w \leftarrow 5\cdot\dfrac{watt}{m^2\cdot K} \\
\quad\quad\quad T_m \leftarrow \dfrac{T_p+T_c}{2}
\end{array}\right.$$

$$\beta p \leftarrow \frac{1}{T_m}$$

$$\nu \leftarrow \begin{bmatrix} 8.1954113764E\text{-}11\left(\frac{T_m}{1K}\right)^3 - 7.9725182481E\text{-}08\cdot\left(\frac{T_m}{1K}\right)^2 \ldots \\ + 2.5891077606E\text{-}05\cdot\frac{T_m}{1K} - 2.7905447066E\text{-}03 \end{bmatrix}\cdot\frac{m^2}{sec}$$

$$k \leftarrow \begin{bmatrix} -9.3503060597E\text{-}10\left(\frac{T_m}{1K}\right)^3 + 8.6711630805E\text{-}07\cdot\left(\frac{T_m}{1K}\right)^2 \ldots \\ + -1.9382938843E\text{-}04\cdot\frac{T_m}{1K} + 3.1411778780E\text{-}02 \end{bmatrix}\cdot\frac{watt}{m\cdot K}$$

$$Pr \leftarrow -3.2841172502E\text{-}07\cdot\left(\frac{T_m}{1K}\right)^3 + 3.2070827481E\text{-}04\cdot\left(\frac{T_m}{1K}\right)^2 \ldots$$
$$+ -1.0434484229E\text{-}01\cdot\frac{T_m}{1K} + 1.2022130144E+01$$

$$g \leftarrow 9.81\cdot\frac{m}{sec^2}$$

$$Ra \leftarrow \frac{g\cdot\beta p\cdot\left(T_p - T_c\right)\cdot L_{thic}^{\ 3}}{\nu^2}\cdot Pr$$

$$Nu \leftarrow 1 + 1.44\cdot if\left(1 - \frac{1708}{Ra\cdot\cos(\beta)} > 0, 1 - \frac{1708}{Ra\cdot\cos(\beta)}, 0\right) \ldots$$
$$\cdot\left(1 - \frac{\sin(1.8\cdot\beta)^{1.6}\cdot 1708}{Ra\cdot\cos(\beta)}\right) \ldots$$
$$+ if\left(\sqrt[3]{\frac{Ra\cdot\cos(\beta)}{5830}} - 1 > 0, \sqrt[3]{\frac{Ra\cdot\cos(\beta)}{5830}} - 1 > 0, 0\right)$$

$$h_{pc} \leftarrow Nu\cdot\frac{k}{L_{thic}}$$

$$U_t \leftarrow \left(\frac{1}{h_{pc} + h_{rpc}} + \frac{1}{h_w + h_{rca}}\right)^{-1}$$

$$T_{cnew} \leftarrow T_p - \frac{U_t\cdot\left(T_p - T_a\right)}{h_{pc} + h_{rpc}}$$

$$difference \leftarrow \left|T_{cnew} - T_c\right|$$

$$T_c \leftarrow T_{cnew}$$

$$I_T \leftarrow c\_values_{p,5}\cdot\frac{joule}{m^2}$$

$$S \leftarrow c\_values_{p,6} \cdot \frac{joule}{m^2}$$

$$U_b \leftarrow \frac{k_{ins}}{L}$$

$$perim \leftarrow 2 \cdot \left(L_{len} + L_{wid}\right)$$

$$A_c \leftarrow L_{len} \cdot L_{wid}$$

$$U_e \leftarrow \frac{\frac{k_{ins}}{t_{edge}} \cdot perim \cdot L_{thic}}{L_{len} \cdot L_{wid}}$$

$$U_L \leftarrow U_t + U_b + U_e$$

$$MM \leftarrow \sqrt{\frac{U_L}{k \cdot \delta}}$$

$$F \leftarrow \frac{\tanh\left(MM \cdot \frac{W - D}{2}\right)}{MM \cdot \frac{W - D}{2}}$$

$$h_{fi} \leftarrow 300 \cdot \frac{watt}{m^2 K}$$

$$\Delta err3 \leftarrow 1 \cdot \frac{watt}{m^2 K}$$

$$difference3 \leftarrow \Delta err3 + 1 \cdot \frac{watt}{m^2 K}$$

while $difference3 > \Delta err3$

$$Fp \leftarrow \frac{\frac{1}{U_L}}{W \cdot \left[\frac{1}{U_L \cdot [D + (W - D) \cdot F]} + \frac{1}{\pi \cdot D_i \cdot h_{fi}} + \frac{1}{C_b}\right]}$$

$$Fpp \leftarrow \frac{md \cdot c_w}{A_c \cdot U_L \cdot Fp} \cdot \left(1 - \exp\left(\frac{-1}{\frac{md \cdot c_w}{A_c \cdot U_L \cdot Fp}}\right)\right)$$

$$F_R \leftarrow Fp \cdot Fpp$$

$$q_u \leftarrow F_R \cdot \left[S - U_L \cdot \left(T_{in} - T_a\right) \cdot 3600 \cdot sec\right]$$

$$T_{fm} \leftarrow T_{in} + \frac{\frac{q_u}{3600 \cdot sec}}{F_R \cdot U_L} \cdot (1 - Fpp)$$

$$mdt \leftarrow \frac{md}{N}$$

$$\mu_f \leftarrow \begin{bmatrix} -1.7575444851E\text{-}09\cdot\left(\frac{T_{fm}-273\cdot K}{1K}\right)^3 \ldots \\ +4.3029264337E\text{-}07\cdot\left(\frac{T_{fm}-273\cdot K}{1K}\right)^2 \ldots \\ +-3.9139980745E\text{-}05\cdot\left(\frac{T_{fm}-273\cdot K}{1K}\right)+1.6393044376E\text{-}03 \end{bmatrix}\cdot\frac{kg}{m\cdot s}$$

$$Re \leftarrow \frac{4\cdot mdt}{\pi\cdot D_i\cdot\mu_f}$$

$$Pr \leftarrow -1.5027050693E\text{-}05\cdot\left(\frac{T_{fm}-273\cdot K}{1K}\right)^3 \ldots$$
$$+3.6151850214E\text{-}03\cdot\left(\frac{T_{fm}-273\cdot K}{1K}\right)^2 \ldots$$
$$+-3.1579725606E\text{-}01\cdot\left(\frac{T_{fm}-273\cdot K}{1K}\right)+1.2107564499E+01$$

$$ac \leftarrow \left| \begin{array}{ll} a \leftarrow \text{linterp}\left[\begin{pmatrix}0.7\\5\end{pmatrix},\begin{pmatrix}0.0791\\0.0534\end{pmatrix},Pr\right] & \text{if } Pr \le 5 \\ a \leftarrow \dfrac{Pr}{\dfrac{Pr}{0.0461}-14.827} & \text{otherwise} \end{array}\right.$$

$$bc \leftarrow \left| \begin{array}{ll} b \leftarrow \text{linterp}\left[\begin{pmatrix}0.7\\5\end{pmatrix},\begin{pmatrix}0.0331\\0.0335\end{pmatrix},Pr\right] & \text{if } Pr \le 5 \\ b \leftarrow \dfrac{Pr}{\dfrac{Pr}{0.0316}-8.974} & \text{otherwise} \end{array}\right.$$

$$nc \leftarrow \left| \begin{array}{ll} n \leftarrow 0.82 & \text{if } Pr \le 5 \\ n \leftarrow \dfrac{Pr}{\dfrac{Pr}{0.084}+1.452} & \text{otherwise} \end{array}\right.$$

$$mc \leftarrow 1.15$$

$$Nu_{inf} \leftarrow 3.7$$

$$Nu \leftarrow Nu_{inf} + \frac{ac\cdot\left(\frac{Re\cdot Pr\cdot D_i}{L_{len}}\right)^{mc}}{1+bc\cdot\left(\frac{Re\cdot Pr\cdot D_i}{L_{len}}\right)^{nc}}$$

$$k_f \leftarrow \begin{bmatrix} 4.878506426522070E\text{-}09\cdot\left(\frac{T_{fm}-273\cdot K}{1K}\right)^3 \ldots \\ +-1.067374318147480E\text{-}05\cdot\left(\frac{T_{fm}-273\cdot K}{1K}\right)^2 \ldots \\ +2.221874204225790E\text{-}03\cdot\left(\frac{T_{fm}-273\cdot K}{1K}\right) \ldots \\ +5.582538699690650E\text{-}01 \end{bmatrix}\cdot\frac{watt}{m\cdot K}$$

$$h_{finew} \leftarrow Nu\cdot\frac{k_f}{D_i}$$

$$difference3 \leftarrow \left|h_{finew}-h_{fi}\right|$$

$$h_{fi} \leftarrow h_{finew}$$

$$T_{out} \leftarrow T_{in}+\frac{\frac{q_u\cdot A_c}{3600\cdot sec}}{md\cdot c_w}$$

$$T_{pnew} \leftarrow T_{in}+\frac{\frac{q_u}{3600\cdot sec}}{F_R\cdot U_L}\cdot\left(1-F_R\right)$$

$$difference2 \leftarrow \left|T_{pnew}-T_p\right|$$

$$deneme \leftarrow \left(\frac{T_p-273K}{1K}\ \ \frac{T_{pnew}-273K}{1K}\ \ \frac{difference2}{1K}\ \ \frac{U_t}{1m^{-2}K^{-1}watt}\right)$$

APPENDPRN("duz_kollektor.txt" , deneme)

$$T_p \leftarrow T_{pnew}$$

$c2\_value_{0,0} \leftarrow$ "Tp for each hour interval (C)"

$c2\_value_{0,1} \leftarrow$ "Tc for each hour interval (C)"

$c2\_value_{0,2} \leftarrow$ "Tout for each hour interval (C)"

$c2\_value_{0,3} \leftarrow$ "IT (J/m2)"

$c2\_value_{0,4} \leftarrow$ "qu (J/m2)"

$c2\_value_{0,5} \leftarrow$ "Hourly Efficieny"

$c2\_value_{0,6} \leftarrow$ "Tin for each hour interval (C)"

$c2\_value_{0,7} \leftarrow$ "hfi for each hour interval (W/m2K)"

$c2\_value_{0,8} \leftarrow$ "Re for each hour interval (W/m2K)"

$$c2\_value_{p,0} \leftarrow \frac{T_p-273\cdot K}{1\cdot K}$$

$$c2\_value_{p,1} \leftarrow \frac{T_c - 273\cdot K}{1\cdot K}$$

$$c2\_value_{p,2} \leftarrow \frac{T_{out} - 273\cdot K}{1\cdot K}$$

$$c2\_value_{p,3} \leftarrow \frac{I_T}{1\cdot m^{-2}\cdot joule}$$

$$c2\_value_{p,4} \leftarrow \frac{q_u}{1\cdot m^{-2}\cdot joule}$$

$$c2\_value_{p,5} \leftarrow \frac{q_u}{I_T}$$

$$c2\_value_{p,6} \leftarrow \frac{T_{in} - 273\cdot K}{1\cdot K}$$

$$c2\_value_{p,7} \leftarrow \frac{h_{fi}}{1\cdot \frac{watt}{m^2 K}}$$

$$c2\_value_{p,8} \leftarrow Re$$

$$p \leftarrow p + 1$$

$$c2\_value$$

$$values2 = \begin{pmatrix} \text{"Tin (C)"} & \text{"Tout (C)"} & \text{"IT (MJ/m2)"} & \text{"qu (MJ/m2)"} & \text{"Hourly Efficieny"} \\ 15.8 & 17.9 & 1.71 & 0.87 & 0.51 \\ 15.8 & 19.12 & 2.6 & 1.38 & 0.53 \\ 15.8 & 20.3 & 3.42 & 1.87 & 0.55 \\ 15.8 & 20.88 & 3.83 & 2.11 & 0.55 \\ 15.8 & 21.06 & 3.94 & 2.18 & 0.55 \\ 15.8 & 20.7 & 3.71 & 2.03 & 0.55 \\ 15.8 & 19.98 & 3.21 & 1.74 & 0.54 \\ 15.8 & 18.75 & 2.45 & 1.22 & 0.5 \end{pmatrix}$$

$$Daily\_efficiency := \frac{\sum_{i=0}^{trunc\left(\frac{MN-5}{4}\right)} values2_{i+1,3}}{\sum_{j=0}^{trunc\left(\frac{MN-5}{4}\right)} values2_{j+1,2}} \qquad Daily\_efficiency = 0.539$$

APPENDIX E

RESULTS OF THE MATHCAD PROGRAM FOR FLAT PLATE SOLAR COLLECTOR CALCULATIONS

Table E.1 Results for the Flat Plate Collector of 0.56 m^2 Surface Area (14.09.2005).

Mass Flow Rate : 0.0023 kg/s					
Daily Efficiency : 0.501					
Time Interval	Tin [°C]	Tout [°C]	IT [MJ/m²]	qu [MJ/m²]	η (Hourly)
09:30 - 10:30	16.0	37.7	2.74	1.34	0.49
10:30 - 11:30	16.0	43.2	3.34	1.69	0.51
11:30 - 12:30	16.0	46.2	3.66	1.87	0.51
12:30 - 13:30	16.0	47.2	3.77	1.93	0.51
13:30 - 14:30	16.0	45.0	3.55	1.80	0.51
14:30 - 15:30	16.0	40.3	3.02	1.51	0.50
15:30 - 16:30	16.0	32.4	2.20	1.01	0.46

Table E.2 Results for the Flat Plate Collector of 0.56 m^2 Surface Area (15.09.2005).

Mass Flow Rate : 0.0055 kg/s					
Daily Efficiency : 0.529					
Time Interval	Tin [°C]	Tout [°C]	IT [MJ/m²]	qu [MJ/m²]	η (Hourly)
08:30 - 09:30	16.5	22.2	1.71	0.84	0.49
09:30 - 10:30	16.5	24.6	2.36	1.21	0.51
10:30 - 11:30	16.5	27.1	2.97	1.58	0.53
11:30 - 12:30	16.5	29.2	3.49	1.88	0.54
12:30 - 13:30	16.5	30.5	3.83	2.07	0.54
13:30 - 14:30	16.5	30.6	3.93	2.10	0.53
14:30 - 15:30	16.5	28.0	3.22	1.70	0.53

Table E.3 Results for the Flat Plate Collector of 0.56 m^2 Surface Area (19.09.2005).

Mass Flow Rate : 0.0077 kg/s					
Daily Efficiency : 0.533					
Time Interval	Tin [°C]	Tout [°C]	IT [MJ/m²]	qu [MJ/m²]	η (Hourly)
08:30 - 09:30	15.8	20.0	1.71	0.86	0.51
09:30 - 10:30	15.8	22.4	2.60	1.36	0.52
10:30 - 11:30	15.8	24.7	3.43	1.85	0.54
11:30 - 12:30	15.8	25.9	3.83	2.09	0.55
12:30 - 13:30	15.8	26.2	3.94	2.16	0.55
13:30 - 14:30	15.8	25.5	3.71	2.01	0.54
14:30 - 15:30	15.8	24.1	3.21	1.72	0.54
15:30 - 16:30	15.8	21.6	2.45	1.21	0.49

Table E.4 Results for the Flat Plate Collector of 0.56 m^2 Surface Area (20.09.2005).

Mass Flow Rate : 0.011 kg/s					
Daily Efficiency : 0.539					
Time Interval	Tin [°C]	Tout [°C]	IT [MJ/m²]	qu [MJ/m²]	η (Hourly)
08:30 - 09:30	15.8	18.9	1.78	0.93	0.52
09:30 - 10:30	15.8	20.8	2.74	1.47	0.54
10:30 - 11:30	15.8	22.3	3.49	1.91	0.55
11:30 - 12:30	15.8	23.1	3.90	2.15	0.55
12:30 - 13:30	15.8	23.2	3.99	2.21	0.55
13:30 - 14:30	15.8	22.8	3.78	2.06	0.55
14:30 - 15:30	15.8	21.6	3.20	1.72	0.54
15:30 - 16:30	15.8	19.8	2.40	1.18	0.49

Table E.5 Results for the Flat Plate Collector of 0.28 m^2 Surface Area (14.09.2005).

Mass Flow Rate : 0.0023 kg/s					
Daily Efficiency : 0.521					
Time Interval	Tin [°C]	Tout [°C]	IT [MJ/m²]	qu [MJ/m²]	η (Hourly)
09:30 - 10:30	16.0	27.3	2.74	1.40	0.51
10:30 - 11:30	16.0	30.2	3.34	1.76	0.53
11:30 - 12:30	16.0	31.7	3.66	1.95	0.53
12:30 - 13:30	16.0	32.2	3.77	2.01	0.53
13:30 - 14:30	16.0	31.1	3.55	1.87	0.53
14:30 - 15:30	16.0	28.6	3.02	1.57	0.52
15:30 - 16:30	16.0	24.5	2.20	1.05	0.48

Table E.6 Results for the Flat Plate Collector of 0.28 m^2 Surface Area (15.09.2005).

Mass Flow Rate : 0.0055 kg/s					
Daily Efficiency : 0.537					
Time Interval	Tin [°C]	Tout [°C]	IT [MJ/m²]	qu [MJ/m²]	η (Hourly)
08:30 - 09:30	16.5	19.4	1.71	0.85	0.50
09:30 - 10:30	16.5	20.6	2.36	1.22	0.52
10:30 - 11:30	16.5	21.9	2.97	1.60	0.54
11:30 - 12:30	16.5	22.9	3.49	1.91	0.55
12:30 - 13:30	16.5	23.6	3.83	2.11	0.55
13:30 - 14:30	16.5	23.7	3.93	2.13	0.54
14:30 - 15:30	16.5	22.3	3.22	1.73	0.54

Table E.7 Results for the Flat Plate Collector of 0.28 m^2 Surface Area (19.09.2005).

Mass Flow Rate : 0.0077 kg/s					
Daily Efficiency : 0.539					
Time Interval	Tin [°C]	Tout [°C]	IT [MJ/m²]	qu [MJ/m²]	η (Hourly)
08:30 - 09:30	15.8	17.9	1.71	0.87	0.51
09:30 - 10:30	15.8	19.1	2.60	1.38	0.53
10:30 - 11:30	15.8	20.3	3.43	1.87	0.55
11:30 - 12:30	15.8	20.9	3.83	2.11	0.55
12:30 - 13:30	15.8	21.1	3.94	2.18	0.55
13:30 - 14:30	15.8	20.7	3.71	2.03	0.55
14:30 - 15:30	15.8	20.0	3.21	1.74	0.54
15:30 - 16:30	15.8	18.7	2.45	1.22	0.50

Table E.8 Results for the Flat Plate Collector of 0.28 m^2 Surface Area (20.09.2005).

Mass Flow Rate : 0.011 kg/s					
Daily Efficiency : 0.543					
Time Interval	Tin [°C]	Tout [°C]	IT [MJ/m²]	qu [MJ/m²]	η (Hourly)
08:30 - 09:30	15.8	17.4	1.78	0.94	0.53
09:30 - 10:30	15.8	18.3	2.74	1.48	0.54
10:30 - 11:30	15.8	19.1	3.49	1.93	0.55
11:30 - 12:30	15.8	19.5	3.90	2.17	0.56
12:30 - 13:30	15.8	19.5	3.99	2.22	0.56
13:30 - 14:30	15.8	19.3	3.78	2.08	0.55
14:30 - 15:30	15.8	18.7	3.20	1.73	0.54
15:30 - 16:30	15.8	17.8	2.40	1.19	0.50

APPENDIX F

COMPUTER PROGRAM FOR CALCULATION OF THE TOTAL SOLAR RADIATION ON THE SPHERICAL SOLAR COLLECTOR

Number of Longitudes : $K := 12$

Number of Latitudes : $L := 10$

$\Delta\xi := \frac{\pi}{L + 1}$ $\Delta\phi := \frac{2 \cdot \pi}{K}$

Radius of the Tank (m) : $R_p := 0.3$

Cover thickness : $\delta_c := 0.003 \cdot m$

Absorptivity of the Absorber at Normal Incidence : $\alpha_n := 0.9$

Ground Reflectance : $\rho_g := 0.4$

$$
\text{Dimensions} := \left|
\begin{array}{l}
y \leftarrow \sqrt{2}\cdot R_p\cdot\sqrt{1-\cos(\Delta\xi)} \\
\text{for } j \in 1..L+1 \\
\quad \left|
\begin{array}{l}
\xi \leftarrow \pi - j\cdot\Delta\xi \\
x_0 \leftarrow \sqrt{2}\cdot R_p\cdot\sin(\xi+\Delta\xi)\cdot\sqrt{1-\cos(\Delta\phi)} \\
x_1 \leftarrow \sqrt{2}\cdot R_p\cdot\sin(\xi)\cdot\sqrt{1-\cos(\Delta\phi)} \\
a \leftarrow R_p\cdot(\cos(\xi)-\cos(\xi+\Delta\xi)) \\
h \leftarrow \sqrt{y^2-\left(\dfrac{x_0-x_1}{2}\right)^2} \\
A \leftarrow \dfrac{x_0+x_1}{2}\cdot h \\
\beta \leftarrow \operatorname{asin}\left(\dfrac{a}{h}\right) \ \text{ if } \ \xi \le \left(\dfrac{\pi}{2}\right) \\
\beta \leftarrow \pi - \operatorname{asin}\left(\dfrac{a}{h}\right) \ \text{ otherwise} \\
Va \leftarrow \left[\dfrac{1}{2}\cdot\left(R_p\cdot\sin(\xi)\right)^2\cdot\sin(\Delta\phi)\right]\cdot a \ \text{ if } \ \cos(\xi) \ge 0 \\
Va \leftarrow \left[\dfrac{1}{2}\cdot\left(R_p\cdot\sin(\xi+\Delta\xi)\right)^2\cdot\sin(\Delta\phi)\right]\cdot a \ \text{ otherwise} \\
Vb \leftarrow \dfrac{a\cdot\sqrt{h^2-a^2}}{2}\cdot x_1 \ \text{ if } \ \cos(\xi) \ge 0 \\
Vb \leftarrow \dfrac{a\cdot\sqrt{h^2-a^2}}{2}\cdot x_0 \ \text{ otherwise} \\
Vcd \leftarrow \dfrac{\left[\dfrac{1}{2}\cdot\left[R_p\cdot(\sin(\xi+\Delta\xi)-\sin(\xi))\right]^2\cdot\sin(\Delta\phi)\right]\cdot a}{3} \\
V \leftarrow K\cdot(Va+Vb+Vcd) \\
\text{Dimensions}_{j-1,0} \leftarrow x_0 \\
\text{Dimensions}_{j-1,1} \leftarrow x_1 \\
\text{Dimensions}_{j-1,2} \leftarrow a \\
\text{Dimensions}_{j-1,3} \leftarrow h \\
\text{Dimensions}_{j-1,4} \leftarrow A \\
\text{Dimensions}_{j-1,5} \leftarrow \beta \\
\text{Dimensions}_{j-1,6} \leftarrow V
\end{array}
\right.
\end{array}
\right.
$$

Input := ...\19.09.2005.xls

$$MN := \left| \begin{array}{l} r \leftarrow 0 \\ nom \leftarrow Input_{5,0} \\ \text{while } nom \neq 0 \\ \quad \left| \begin{array}{l} nom \leftarrow Input_{5+r,0} \\ r \leftarrow r + 1 \end{array} \right. \\ Number\_of\_measurements \leftarrow r - 1 \\ Number\_of\_measurements \end{array} \right.$$

Date : $Input_{0,2} = \text{"09/14/2005"}$

Day of the year : $n := Input_{1,2}$

Declination : $\delta := \frac{\pi}{180} \cdot 23.45 \cdot \sin\left(360 \cdot \frac{284 + n}{365} \cdot \frac{\pi}{180}\right)$

Latitude : $\phi := 39.95 \cdot \frac{\pi}{180}$

Number of measurement times : $MN = 31$

$$
\begin{aligned}
SRad := \;& TIS_{MN-1,4} \leftarrow 0 \\
& p \leftarrow 0 \\
& \text{while } p \le MN - 1 \\
& \quad G \leftarrow Input_{5+p,1} \\
& \quad TIS_{p+1,0} \leftarrow Input_{5+p,0} \\
& \quad TIS_{p+1,1} \leftarrow G \\
& \quad \omega \leftarrow \begin{cases} \frac{\pi}{180}\cdot Input_{5+p,6} & \text{if } Input_{2,2} = 0 \\ \frac{\pi}{180}\cdot Input_{5+p,8} & \text{otherwise} \end{cases} \\
& \quad G_0 \leftarrow 1367\cdot\left(1 + 0.033\cdot\cos\left(\frac{360\cdot n}{365}\cdot\frac{\pi}{180}\right)\right)\cdot\left(\cos(\phi)\cdot\cos(\delta)\cdot\cos(\omega) + \sin(\phi)\cdot\sin(\delta)\right) \\
& \quad \cos\theta_z \leftarrow \cos(\phi)\cdot\cos(\delta)\cdot\cos(\omega) + \sin(\phi)\cdot\sin(\delta) \\
& \quad \text{for } j \in 1..L+1 \\
& \quad\quad A \leftarrow Dimensions_{j-1,4} \\
& \quad\quad \beta \leftarrow Dimensions_{j-1,5} \\
& \quad\quad \text{for } i \in 1..K \\
& \quad\quad\quad \gamma \leftarrow -\left[(i-1)\cdot\Delta\phi\right] \\
& \quad\quad\quad \cos\theta \leftarrow \sin(\delta)\cdot\sin(\phi)\cdot\cos(\beta) - \sin(\delta)\cdot\cos(\phi)\cdot\sin(\beta)\cdot\cos(\gamma) \ldots \\
& \quad\quad\quad\quad + \cos(\delta)\cdot\cos(\phi)\cdot\cos(\beta)\cdot\cos(\omega) \ldots \\
& \quad\quad\quad\quad + \cos(\delta)\cdot\sin(\phi)\cdot\sin(\beta)\cdot\cos(\gamma)\cdot\cos(\omega) + \cos(\delta)\cdot\sin(\beta)\cdot\sin(\gamma)\cdot\sin(\omega) \\
& \quad\quad\quad R_b \leftarrow \frac{\cos\theta}{\cos\theta_z} \\
& \quad\quad\quad k_T \leftarrow \frac{G}{G_0} \\
& \quad\quad\quad ratio \leftarrow 1.0 - 0.09\cdot k_T \;\; \text{if } k_T \le 0.22 \\
& \quad\quad\quad ratio \leftarrow 0.9511 - 0.1604\cdot k_T + 4.388\cdot k_T^{\,2} - 16.638\cdot k_T^{\,3} \ldots \;\; \text{if } 0.22 < k_T \le 0.80 \\
& \quad\quad\quad\quad + 12.336\cdot k_T^{\,4} \\
& \quad\quad\quad ratio \leftarrow 0.165 \;\; \text{if } k_T > 0.80 \\
& \quad\quad\quad G_d \leftarrow ratio\cdot G \\
& \quad\quad\quad G_b \leftarrow 0 \;\; \text{if } \cos\theta \le 0 \\
& \quad\quad\quad G_b \leftarrow G - G_d \;\; \text{otherwise} \\
& \quad\quad\quad A_i \leftarrow \frac{G_b}{G_0}
\end{aligned}
$$

$$f \leftarrow \sqrt{\frac{G_b}{G}}$$

$$G_{T_{i,j}} \leftarrow \left(G_b + G_d \cdot A_i\right) \cdot R_b \ldots + G_d \cdot \left(1 - A_i\right) \cdot \left(\frac{1 + \cos(\beta)}{2}\right) \cdot \left(1 + f \cdot \sin\left(\frac{\beta}{2}\right)^3\right) \ldots + G \cdot \rho_g \cdot \left(\frac{1 - \cos(\beta)}{2}\right)$$

$$TIS_{p+1,2} \leftarrow TIS_{p+1,2} + \left(A \cdot G_{T_{i,j}}\right)$$

$$\tau\alpha_b \leftarrow \left| \begin{array}{l}
\theta \leftarrow \operatorname{acos}(\cos\theta) \\
\theta_2 \leftarrow \operatorname{asin}\left(\frac{1}{1.526} \cdot \sin(\theta)\right) \\
\tau_a \leftarrow \exp\left(\frac{-0.3 \cdot cm^{-1} \cdot \delta_c}{\cos(\theta_2)}\right) \\
r_{dik} \leftarrow \frac{\sin(\theta_2 - \theta)^2}{\sin(\theta_2 + \theta)^2} \\
r_{yatay} \leftarrow \frac{\tan(\theta_2 - \theta)^2}{\tan(\theta_2 + \theta)^2} \\
\tau \leftarrow \frac{\tau_a}{2} \cdot \left[\frac{1 - r_{dik}}{1 + r_{dik}} \cdot \frac{1 - r_{dik}^2}{1 - \left(r_{dik} \cdot \tau_a\right)^2} + \frac{1 - r_{yatay}}{1 + r_{yatay}} \cdot \frac{1 - r_{yatay}^2}{1 - \left(r_{yatay} \cdot \tau_a\right)^2}\right] \\
\alpha \leftarrow \alpha_n \cdot \left[1 + 2.0345 \cdot 10^{-3} \cdot \left(\theta \cdot \frac{180}{\pi}\right) - 1.990 \cdot 10^{-4} \cdot \left(\theta \cdot \frac{180}{\pi}\right)^2 \ldots + 5.324 \cdot 10^{-6} \cdot \left(\theta \cdot \frac{180}{\pi}\right)^3 - 4.799 \cdot 10^{-8} \cdot \left(\theta \cdot \frac{180}{\pi}\right)^4\right] \\
\tau\alpha \leftarrow 1.01 \cdot \tau \cdot \alpha \\
\tau\alpha
\end{array} \right.$$

$$\tau\alpha_d \leftarrow \left| \begin{array}{l}
\theta \leftarrow \frac{\pi}{180} \cdot \left[59.7 - 0.1388 \cdot \left(\beta \cdot \frac{180}{\pi}\right) + 0.001497 \cdot \left(\beta \cdot \frac{180}{\pi}\right)^2\right] \\
\theta_2 \leftarrow \operatorname{asin}\left(\frac{1}{1.526} \cdot \sin(\theta)\right) \\
\tau_a \leftarrow \exp\left(\frac{-0.3 \cdot cm^{-1} \cdot \delta_c}{\cos(\theta_2)}\right)
\end{array} \right.$$

$$r_{dik} \leftarrow \frac{\sin\left(\theta_2 - \theta\right)^2}{\sin\left(\theta_2 + \theta\right)^2}$$

$$r_{yatay} \leftarrow \frac{\tan\left(\theta_2 - \theta\right)^2}{\tan\left(\theta_2 + \theta\right)^2}$$

$$\tau \leftarrow \frac{\tau_a}{2}\cdot\left[\frac{1 - r_{dik}}{1 + r_{dik}}\cdot\frac{1 - r_{dik}^{\ 2}}{1 - \left(r_{dik}\cdot\tau_a\right)^2} + \frac{1 - r_{yatay}}{1 + r_{yatay}}\cdot\frac{1 - r_{yatay}^{\ 2}}{1 - \left(r_{yatay}\cdot\tau_a\right)^2}\right]$$

$$\alpha \leftarrow \alpha_n\cdot\left[1 + 2.0345\cdot 10^{-3}\cdot\left(\theta\cdot\frac{180}{\pi}\right) - 1.990\cdot 10^{-4}\cdot\left(\theta\cdot\frac{180}{\pi}\right)^2 \ldots + 5.324\cdot 10^{-6}\cdot\left(\theta\cdot\frac{180}{\pi}\right)^3 - 4.799\cdot 10^{-8}\cdot\left(\theta\cdot\frac{180}{\pi}\right)^4\right]$$

$$\tau\alpha \leftarrow 1.01\cdot\tau\cdot\alpha$$

$$\tau\alpha$$

$$\tau\alpha_g \leftarrow \theta \leftarrow \frac{\pi}{180}\cdot\left[90 - 0.5788\cdot\left(\beta\cdot\frac{180}{\pi}\right) + 0.002693\cdot\left(\beta\cdot\frac{180}{\pi}\right)^2\right]$$

$$\theta_2 \leftarrow \operatorname{asin}\left(\frac{1}{1.526}\cdot\sin(\theta)\right)$$

$$\tau_a \leftarrow \exp\left(\frac{-0.3\cdot cm^{-1}\cdot\delta_c}{\cos\left(\theta_2\right)}\right)$$

$$r_{dik} \leftarrow \frac{\sin\left(\theta_2 - \theta\right)^2}{\sin\left(\theta_2 + \theta\right)^2}$$

$$r_{yatay} \leftarrow \frac{\tan\left(\theta_2 - \theta\right)^2}{\tan\left(\theta_2 + \theta\right)^2}$$

$$\tau \leftarrow \frac{\tau_a}{2}\cdot\left[\frac{1 - r_{dik}}{1 + r_{dik}}\cdot\frac{1 - r_{dik}^{\ 2}}{1 - \left(r_{dik}\cdot\tau_a\right)^2} + \frac{1 - r_{yatay}}{1 + r_{yatay}}\cdot\frac{1 - r_{yatay}^{\ 2}}{1 - \left(r_{yatay}\cdot\tau_a\right)^2}\right]$$

$$\alpha \leftarrow \alpha_n\cdot\left[1 + 2.0345\cdot 10^{-3}\cdot\left(\theta\cdot\frac{180}{\pi}\right) - 1.990\cdot 10^{-4}\cdot\left(\theta\cdot\frac{180}{\pi}\right)^2 \ldots + 5.324\cdot 10^{-6}\cdot\left(\theta\cdot\frac{180}{\pi}\right)^3 - 4.799\cdot 10^{-8}\cdot\left(\theta\cdot\frac{180}{\pi}\right)^4\right]$$

$$\tau\alpha \leftarrow 1.01\cdot\tau\cdot\alpha$$

$$\tau\alpha$$

$$S_{T_{i,j}} \leftarrow \left(G_b + G_d \cdot A_i\right) \cdot R_b \cdot \tau\alpha_b \ldots$$
$$+ G_d \cdot \left(1 - A_i\right) \cdot \tau\alpha_d \cdot \left(\frac{1 + \cos(\beta)}{2}\right) \cdot \left(1 + f \cdot \sin\left(\frac{\beta}{2}\right)^3\right) \ldots$$
$$+ G \cdot \rho_g \cdot \tau\alpha_g \cdot \left(\frac{1 - \cos(\beta)}{2}\right)$$
$$TIS_{p+1,3} \leftarrow TIS_{p+1,3} + \left(A \cdot S_{T_{i,j}}\right)$$
$$\tau\alpha_{ave} \leftarrow \frac{TIS_{p+1,3}}{TIS_{p+1,2}}$$
$$TIS_{p+1,4} \leftarrow \tau\alpha_{ave}$$
$$p \leftarrow p + 1$$
$$TIS_{0,0} \leftarrow \text{"Time"}$$
$$TIS_{0,1} \leftarrow \text{"GHorizontal"}$$
$$TIS_{0,2} \leftarrow \text{"GTotal"}$$
$$TIS_{0,3} \leftarrow \text{"STotal"}$$
$$TIS_{0,4} \leftarrow \text{"Ave. Trans.-Abs. Prod."}$$
$$TIS$$

SRad =

	0	1	2	3	4
0	"Time"	"GHorizontal"	"GTotal"	"STotal"	ans.-Abs. Prod."
1	"08:30:00"	298.12	243.403	156.04	0.641
2	"08:45:00"	350.94	281.962	180.817	0.641
3	"09:00:00"	404.655	317.079	203.468	0.642
4	"09:15:00"	457.475	346.915	222.801	0.642
5	"09:30:00"	513.876	375.331	241.008	0.642
6	"09:45:00"	548.791	389.622	250.453	0.643
7	"10:00:00"	583.706	402.788	258.663	0.642
8	"10:15:00"	572.068	396.529	254.087	0.641
9	"10:30:00"	678.603	439.911	281.787	0.641
10	"10:45:00"	703.671	448.455	287.095	0.64
11	"11:00:00"	733.214	458.987	293.874	0.64
12	"11:15:00"	752.014	464.324	297.741	0.641
13	"11:30:00"	778.872	475.008	304.528	0.641
14	"11:45:00"	788.72	479.49	307.014	0.64
15	"12:00:00"	808.415	488.641	313.028	0.641
16	"12:15:00"	827.216	499.786	320.039	0.64
17	"12:30:00"	834.378	505.007	323.806	0.641
18	"12:45:00"	835.273	508.538	326.187	0.641
19	"13:00:00"	837.064	515.242	329.978	0.64
20	"13:15:00"	815.577	507.971	325.319	0.64
21	"13:30:00"	826.321	521.889	334.466	0.641
22	"13:45:00"	795.882	511.612	328.505	0.642
23	"14:00:00"	777.081	509.453	327.784	0.643
24	"14:15:00"	763.653	514.004	331.243	0.644
25	"14:30:00"	745.748	517.668	333.235	0.644
26	"14:45:00"	724.261	520.408	335.515	0.645
27	"15:00:00"	674.127	504.579	325.33	0.645
28	"15:15:00"	632.05	495.333	319.577	0.645
29	"15:30:00"	598.03	494.383	319.567	0.646
30	"15:45:00"	562.22	494.959	320.975	0.648
31	"16:00:00"	529.991	504.913	327.648	0.649
32	"16:15:00"	465.533	484.333	314.831	0.65
33	"16:30:00"	413.608	481.493	313.132	0.65
34	"16:45:00"	349.15	465.341	302.94	0.651
35	"17:00:00"	301.701	480.104	313.241	0.652
36	"17:15:00"	238.138	478.351	313.856	0.656

$$\tau\alpha_{daily\_ave} := \frac{\sum_{abc=1}^{MN} SRad_{abc,3}}{\sum_{abc=1}^{MN} SRad_{abc,2}} \qquad \tau\alpha_{daily\_ave} = 0.644$$

APPENDIX G

SAMPLE CALCULATIONS

G.1. Calculation of Solar Collector Thermal Efficiency

Date	:	19 September 2005
Time	:	13:00
Fluid	:	Water
Flow Rate	:	0.0077 kg/s
T_a	:	27.3 °C
$T_{c,i}$	:	16.1 °C
$T_{c,o}$	:	26.5 °C
$G_{Tsph}A_T$	:	515.2 W (Calculated using the program in Appendix F)
C_p	:	4180 J/kg°C
A_T	:	1.13 m²

To calculate instantaneous efficiency at specified conditions above, calculation of $\frac{dT_f}{dt}$ is needed. Defining a trend curve for the mean tank temperature, T_f, will be useful. Using the Microsoft Excel program, the trend curve for T_f on 19.09.2005 can be defined as below

$$T_f(t) = -2\ 10^{-9} t^2 + 0.0002t + 19.045 \qquad \text{(G.1)}$$

where T_f is in °C and t is in seconds. Equation of $\frac{dT_f}{dt}$ is

$$\frac{dT_f}{dt} = -4\ 10^{-9} t + 0.0002 \qquad \text{(G.2)}$$

and t at 13:00 is calculated as

$$t_{@13:00} = \left[(13 \text{ hours} + 0 \text{ minutes } \frac{1h}{60\,min}) - (8 \text{ hours} + 30 \text{ minutes } \frac{1h}{60\,min}) \right] \frac{3600s}{1h}$$
$$= 16200 \text{ s}$$

Calculation of Equation (G.2) for t=16200s will give us desired value of $\frac{dT_f}{dt}$ as

$$\frac{dT_f(16200s)}{dt} = 0.000135 \text{ °C/s}$$

Consequently, using specified conditions at previous page and using equation (4.4), instantaneous efficiency at 13:00 is obtained as below

$$\eta = \frac{(0.0077 \text{ kg/s})\ (4180 \text{ J/kg°C})\ (26.5 \text{ °C} - 16.1 \text{ °C}) + (113\text{kg})(4180 \text{ J/kg°C})(0.000135 \text{ °C/s})}{(515.2 \text{ W})}$$
$$= 77 \%$$

In addition, using Equation (4.5) and using the trapezoidal rule to solve integrals in this equation, daily efficiency for the spherical solar collector is found as 75 %.

G.2. Calculation of Collector Efficiency Factor and Heat Transfer Loss Coefficient

The equation of the straight line obtained by plotting the collector instantaneous efficiency values versus $(T_f-T_a)/G_{Tsph}$ in Figure 8.4 is

$$\eta = -1.9265\ (T_f-T_a)/G_{Tsph} + 0.7509 \qquad \text{(G.3)}$$

From Equation (4.11) and Equation (G.3), the values of F' and U_L are calculated.

$F'U_L = 1.9265$ (being the slope)

$F'(\tau\alpha)_{ave} = 0.7509$ (being the y-intercept)

For the present collector, $(\tau\alpha)_{ave}$ was calculated in Appendix F as 0.64. Thus,

$$F' = \frac{0.7509}{0.64} = 1.17$$

$$U_L = \frac{1.9265}{1.17} = 1.65\ \text{W/m}^2\text{°C}$$